Numerical Bifurcation Analysis of Simple Dynamical Systems

Tze Ngon Chan

A Thesis

in

The Department

of

Computer Science

Presented in Partial Fulfillment of the Requirements
for the degree of Master of Computer Science at
Concordia University
Montreal, Quebec, Canada

September 1983

TABLE OF CONTENTS

ABSTRACT

Numerical Bifurcation Analysis of

Simple Dynamical Systems

Tze Ngon Chan

In this thesis, we study the bifurcation behaviour of three 3-dimensional ordinary differential systems. They are the Lorenz system, a transformed Lorenz system and a system arising from biochemistry. The relationship between bifurcation to invariant tori in ordinary differential systems and bifurcation to invariant circles in 2-dimensional diffeomorphisms is also discussed. We introduce a method to compute the fixed point branches and detect Hopf bifurcation points for general 2-dimensional diffeomorphisms. If a Hopf bifurcation is detected, two methods to trace out the invariant circles are presented. Numerical results obtained using these computation methods on the Hénon map and the delay logistic equation are shown.

ACKNOWLEDGEMENT

I would like to take this chance to express my appreciation to Dr. E.J. Doedel for his excellent supervision on the preparation of this thesis. It was he who introduced me to the subject of dynamical systems and chaos. Without his computer program AUTO, part of the work done in this thesis would have been impossible.

Thanks also to Dr. J.McKay for his financial support during my two years of study in the Department of Computer Science, to Dr. W. Byers for the valuable discussions we had and to Dr.A. Buckley for his encouragements in difficult times.

At last, of course never the least, I would like to thank my family and especially my love Ching Kwan for their constant love and understanding.

INTRODUCTION

A large portion of the universe is in a fluid state, but the kind of motion which most fluid flows exhibit has a highly irregular nature called turbulence. Turbulent motion in a fluid flow has long been recognized as an important problem in the theory of fluid dynamics. But, even though it has been extensively studied by scientists from a wide range of disciplines for more than a century, the process by which turbulence develops is still not completely understood.

Difficulties lie in both the experimental and theoretical sides of the problem. As pointed out by H.L. Swinney and J.P. Gollub [37] a major experimental difficulty is the absence of sensitive and quantitative experimental techniques capable of measuring the velocity field, temperature field and vorticity of a fluid flow. On the theoretical side, the basic difficulty is the intractability of the nonlinear Navier-Stokes equations. Also, above all, a convincing definition of turbulence is lacking.

For practical purposes, the structure of strongly turbulent flows is usually characterized using statistical methods including "random initial states" and "time averaging" [28]. The problem of transition to turbulence was mainly left untouched before the past two decades.

In recent years, due to the advances in high speed computer technology, investigation of transition to turbulence has been profoundly active. In laboratories, computers are used in the control of experiments, data collection and analysis. For mathematicians, computers are used to unfold the abundant dynamical behaviour of nonlinear differential equations.

Basically there are two theories about the transition to turbulence. The first one is due to L.D. Landau and E.M. Lifshitz [28] and can also be dated back to E. Hopf [18]. The theory hypothesizes that turbulence is the result of an infinite cascade of loss of stability and bifurcations. In 1971, D. Ruelle and F. Takens introduced the second theory in their well known article "On the Nature of Turbulence" [33]. Their theory is that transition to turbulence need not be a continuous process. Instead, turbulence may occur via the existence of a "strange attractor". The best known example is the Lorenz attractor [24] which appears not through a sequence of bifurcations but under the effect of a homoclinic point in the state space. Dynamics inside the Lorenz attractor are highly irregular and sensitive to initial conditions.

Developments in bifurcation theory and the theory of dynamical systems have also contributed significantly to the understanding of transition to turbulence. Bifurcation theory aims at the classification and characterization of

types of bifurcations (splitting of solutions) that can occur in nonlinear systems. The theory of dynamical systems aims at providing a sound mathematical background for explaining the dynamical behaviour of nonlinear systems.

The purpose of this thesis is to illustrate the bifurcation behaviour of some simple nonlinear systems. Further, numerical techniques for computing some of these bifurcation phenomena are introduced.

In Chapter 1, basic definitions often used in the qualitative theory of differential equations are given as the foundation of discussions in the following chapters. The ideas can mostly be found in [4] and [17]. Emphasis is on the relationships between these definitions and their interpretations in the physical world.

The bifurcation behaviour of three 3-dimensional systems of ordinary differential equations is examined in Chapter 2. They are the well known Lorenz system, a modified Lorenz system and a system arising from biochemistry. The dynamical behaviour of the first system has been studied by a large number of both mathematicians and experimental scientists. Using the computer program AUTO, which uses Keller's pseudo arclength as the continuation technique, several periodic solution branches of the Lorenz system have been traced out. These periodic solution branches lead to the location of periodic solutions inside the Lorenz

attractor. The modified Lorenz system has a cascading sequence of period doubling bifurcations. This sequence of period doubling bifurcations seems to agree with the conjecture due to Feigenbaum. The biochemical system has extremely complicated bifurcation behaviour and contains the essential dynamics of both the Lorenz system and the modified Lorenz system. Detailed descriptions of the dynamical behaviours of these three systems are given along with appropriate bifurcation diagrams. We hope these bifurcation diagrams may give some additional insight into the transition to aperiodicity. The bifurcation diagrams given in Chapter 2 were prepared with extensive use of the computer program AUTO.

From the Hopf bifurcation theorem for diffeomorphisms, we know that if the Jacobian of a diffeomorphism evaluated at a fixed point has a pair of complex conjugate eigenvalues on the unit circle, then invariant circles will generally develop. If these circles are attracting, the local dynamical behaviour of the diffeomorphism is determined by these circles. In Chapter 3, we describe the relationship between bifurcation to invariant tori of a system of ordinary differential equations and bifurcation to invariant circles of two dimensional diffeomorphisms. The relationship is established through the idea of a Poincare map and the center manifold theorem.

A widely used method of computing the bifurcating invariant circles of a two dimensional diffeomorphism is by iterating the map. However, this method fails if the invariant circles are unstable. A numerical method capable of computing the invariant circles for both the stable and unstable cases is introduced in Chapter 4. The method is based on a Fourier series representation of the invariant circles and the pseudo arclength continuation technique. This method has been implemented in a computer program DSYS. Given a 2-dimensional diffeomorphism, DSYS can compute the fixed point branches of the diffeomorphism, and if a Hopf bifurcation point is detected on the branch, DSYS can automatically trace out the invariant circles. Several numerical examples, including the well known Henon map, are used as illustrations in Chapter 6. The numerical results show that for computing the invariant circles, the Fourier series representation has very good performance both in accuracy and efficiency near the Hopf bifurcation point.

The Fourier series representation used in Chapter 4 may not be the most efficient representation for computing the invariant circles when far away from the Hopf bifurcation point. Therefore a representation using cubic B-splines is also discussed in Chapter 4. Also another possible variation in the computation scheme is given in Chapter 5. In this method, some of the conditions required by the method given in Chapter 4 on the diffeomorphism can be

relaxed. However, this method does not have a continuous formulation. The method discussed in Chapter 5 has also been implemented in DSYS.

As mentioned earlier, bifurcation diagrams will be prepared in this thesis so that the dynamical behaviour of the dynamical systems discussed in this thesis can be clearly described. The following conventions are used in all the bifurcation diagrams:

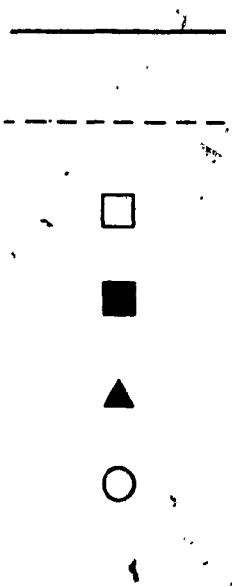

CHAPTER ONE

Basic Ideas in the Theory of Ordinary Differential Equations and Dynamical Systems

1.1 Ordinary differential equations and dynamical systems

Consider an ordinary differential equation

$$u'(t) = f(u(t)) \qquad (1.1)$$

where $f: W \to R^n$ is continuously differentiable (C^1), and W is an open subset of R^n. Since the independent variable t does not appear explicitly in (1.1), the equation is said to be autonomous. A function $\phi: I \to W$, with $I \subset R$, is called a solution of (1.1) if

$$\phi'(t) = f(\phi(t))$$

for all $t \in I$. The well known existence and uniqueness theorem of ordinary differential equations guarantees that given a point u_0 in W, there exists $a>0$ and a function $\phi: (-a,a) \to W$ such that ϕ is a solution of (1.1) satisfying the initial condition

$$\phi(0) = u_0. \qquad (1.2)$$

We denote ϕ satisfying (1.2) by $\phi(u_0)$, and at a particular

t, a point on the solution $\phi(u_0)$ is written as $\phi_t(u_0)$. Therefore $\phi_0(u_0) = u_0$.

Now, let $\Omega \subset RxW$ be

$$\Omega = \{ (t,u) \in RxW \mid t \in I_u \},$$

the function $\phi: \Omega \to W$ with

$$\phi(t,u) = \phi_t(u)$$

is called the <u>flow</u> of equation (1.1). Each $\phi(u)$ is called a <u>trajectory</u> or <u>solution curve</u> in the flow. The flow of equation (1.1) is the collection of all trajectories of equation (1.1). For simplicity we write $\phi(t,u) = \phi_t(u)$. The flow ϕ has the following properties:

(1). $\phi_{s+t}(u) = \phi_s(\phi_t(u))$ in the sense that if one side is defined, so is the other, and they are equal.

(2). ϕ_t is C^1.

(3). $\phi_t \cdot \phi_{-t}$ and $\phi_{-t} \cdot \phi_t$ equal to the identity map.

(4). ϕ_{-t} is C^1.

A differentiable function with a differentiable inverse is called a <u>diffeomorphism</u>. Thus ϕ is a diffeomorphism.

To each $u_0 \in W$, we can associate a vector $X(u_0) = f(u_0)$ in R^n with the initial point at u_0. Therefore, f defines a vector field X. Since f is C^1, we call X a C^1 vector field, and for any point v on a solution curve $\phi(u_0)$, the tangent

To each $u_0 \in W$, and for every v on the trajectory $\phi(u_0)$ we can associate a vector $X(v) = f(v)$ in R^n with the initial point at v. Therefore, f defines a vector field X. Since f is C^1, we call X a C^1 vector field, and for any point v on a solution curve $\phi(u_0)$, the tangent of the curve is the vector X(v). See Figure 1.1 for an illustration in R^3.

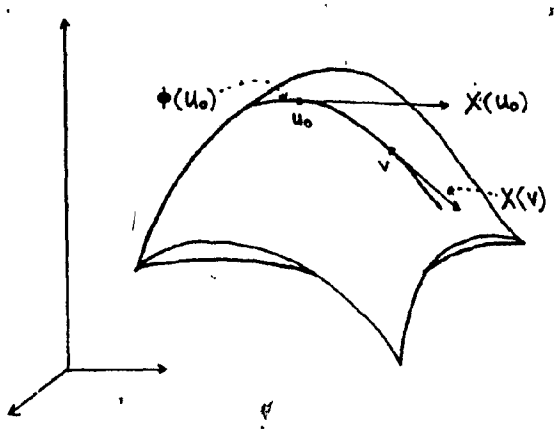

FIGURE 1.1

When equation (1.1) is used to model a system in some physical situation, the space filled with trajectories $\phi(u)$ in ϕ is called the phase portrait or state space of equation (1.1). Each point $\phi_t(u)$ represents a state of the system at a certain "time" t. The vector X(u) of a point u is the rate of change of u along the unique trajectory on which u lies. We assume X is C^1, so that all rates of change of the flow are smooth. By looking at the phase portrait at different discrete time steps, equation (1.1)

describes the change of states of the real system, and thus gives rise to a dynamical system.

More formally we can define a dynamical system as a C^1 map ϕ: $R \times W \to W$, where W is an open subset of R^n, and if we define $\phi_t : W \to W$ by $\phi_t(u) = \phi(t,u)$, ϕ_t satisfies

(1) ϕ_0: $W \to W$ is the identity map.

(2) $\phi_t \cdot \phi_s = \phi_{s+t}$.

We note that this definition implies that the map ϕ_t: $W \to W$ is C^1 for each t and has a C^1 inverse ϕ_{-t}. Hence ϕ_t is a diffeomorphism.

On the other hand, given a dynamical system ϕ, if we define

$$f(u) = \frac{d}{dt} \phi(t,u)|_{t=0}, \qquad (1.3)$$

for every $u \in W$ and write $\phi(u) = \phi(u)$, then (1.3) is a differential equation equivalent to $\phi' = f(\phi)$. Thus every dynamical system is also associated with a differential equation.

A solution $\phi(u) = \bar{u}$ (for all t) in W with $f(\bar{u}) = 0$ is called a steady state solution (or an equilibrium point or fixed point) of equation (1.1). In the state space, if the system described by (1.1) is at $\bar{u}$, it will always be (and always was) at $\bar{u}$. A solution $\phi(u)$ of equation (1.1) is called a periodic solution if there exists ρ positive in R

such that $\phi_t(u) = \phi_{t+\rho}(u)$ for all t. The smallest such number ρ is called the <u>period</u> of $\phi(u)$. The study of these types of solutions plays a central role in the theory of ordinary differential equations as well as in dynamical systems.

1.2 <u>Stability definitions of a dynamical system</u>

While studying the dynamics of a dynamical system, it is essential to know whether the qualitative behaviour of a solution remains unchanged under slight <u>perturbations</u>. In other words, we wish to know whether the trajectories "near" to one particular trajectory stay nearby and display a similar qualitative behaviour. This is because measurements are never one hundred percent accurate, and one can only pinpoint a state of the system approximately. Therefore the system under consideration when applied in physical situations is always perturbed.

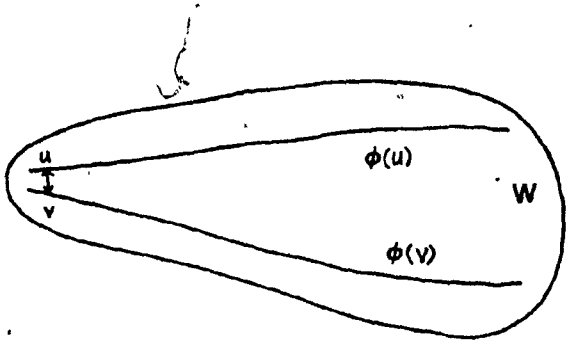

FIGURE 1.2

More precisely, a set A is said to be invariant under a mapping T if $T(A) \subset A$. The trajectories of steady state solutions and periodic solutions are all invariant sets under ϕ. An invariant set $A \subset W$ of the flow ϕ is said to be stable if given any neighbourhood U of A there is a neighbourhood V of A such that every trajectory $\phi(v)$ with $\phi_0(v)$ in V is defined and in U for all $t>0$. If in addition, $\bigcap_{t\geq 0} \phi(V) = A$, then A is said to be asymptotically stable or an attractor in ϕ. Further, A is said to be unstable if it is not stable. Thus, A is stable when trajectories with initial state slightly perturbed from A remains near A and A is asymptotically stable or attracting when trajectories with initial state slightly perturbed from A tend towards A. If at least one nearby trajectories go away from A, A is unstable.

Steady state solutions and periodic solutions correspond to "observable" phenomena in a dynamical system, since they represent states which are unchanging or which repeat themselves. However, besides steady state behaviour and periodic behaviour, other kinds of dynamical behaviour are also observed in nature. The most well known one is turbulence in a fluid flow. Recently, due to the advances in electronic computers, many models from every discipline of science have been carefully examined. These examinations have revealed an abundance of dynamical behaviours in many systems. They all lead to the conclusion that even very

simple systems can have complicated dynamics.

In the following, we further classify the points in the state space of a dynamical system according to their dynamical behaviour.

A point u_0 in W is called a non-wandering point in the flow ϕ if given any neighbourhood U of u_0, there exists a neighbourhood V of u_0 such that for sufficiently large t, $\phi(V) \cap U \neq \phi$. We denote the set of all non-wandering points of W by $\Omega(\phi)$. A point u_* is called a wandering point if it is not a non-wandering point. In more plain language, if u_0 is non-wandering then for any point u_1, which is arbitrarily close to u_0, the trajectory through u_1 returns infinitely often to any neighbourhood of u_0. Obviously, recurrent behaviour of this kind may also be associated with some kind of observable phenomenon although it could have a rather irregular character.

Wandering points only correspond to some transient behaviour in a dynamical system. In order to understand their long-term behaviour we need to know what these wandering points approach asymptotically as t tends to infinity. For any point u_0, a point v_0 is called an ω-limit point of u_0 if there exists a sequence $\{t_n\}$ with $t_n \to \infty$ $\phi(t_n,u_0) \to v_0$ as $n \to \infty$. The set of all ω-limit point of u_0 is called the ω-limit set of u_0, which is denoted by $L_\omega(u_0)$. Replacing the condition $t_n \to \infty$ in the definition of

ω-limit point and ω-limit set by $t_n \to -\infty$, we can define <u>α-limit points</u> and the <u>α-limit set</u> $L_\alpha(u_0)$ of u_0.

If $\bar{u}$ is an asymptotically stable steady state solution, it is the ω-limit set of points which are sufficiently close. Of course any steady state solution is the ω-limit set and α-limit set of itself. A periodic solution is the ω-limit set and α-limit set of every point on its trajectory. Further if the periodic solution is asymptotically stable, then it is the ω-limit set of the points on the trajectories which are sufficiently close to the solution curve. See Figure 1.3.

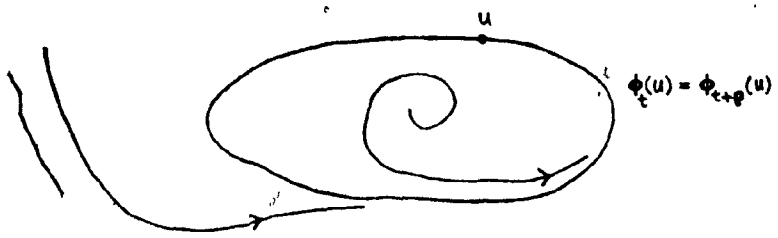

FIGURE 1.3

There are examples of limit sets which are neither periodic solutions nor steady state solutions. A typical example in R^2 is the figure 8 curve in Figure 1.4. In Figure 1.4 , there are three unstable steady state solutions and the figure 8 curve is the ω-limit set of all points

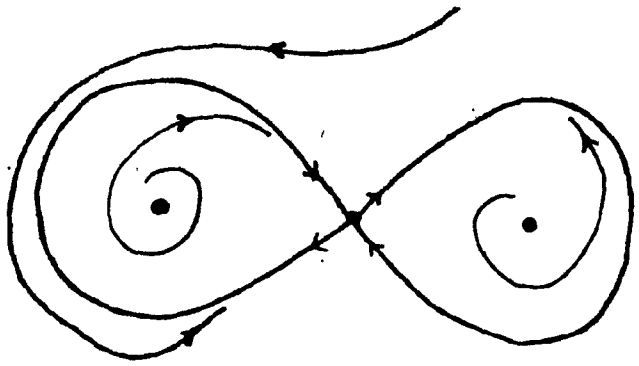

FIGURE 1.4

outside it. The right half of the 8 is the ω-limit set of all points inside it except the steady state, and similarly for the left half. In R^3 or higher dimensional spaces, there are extremely complicated examples of limit sets, for example the Lorenz attractor which we shall describe in Chapter 2. See Figure 1.5 for a three dimensional limit set which appears as a torus.

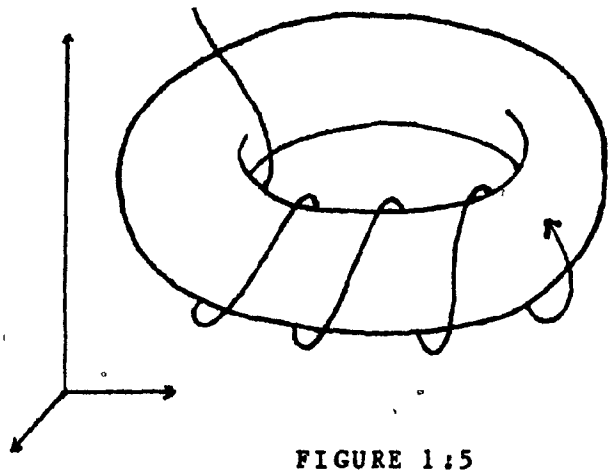

FIGURE 1.5

In Chapter 2 and Chapter 3 we shall analyze the change in some of the behaviours we just described when a parameter

in the system is varied. The parameter usually is a coefficient in the associated differential equation.

1.3 Discrete dynamical systems

A differential equation is not the only way to study the dynamics of a system. Let $W \subset R^n$ again be open. A C^1 map $g: W \to R^n$ is called a discrete dynamical system if $g(u)$ is the state of the system one unit of time after it is in the state u. After two units of time, the system will be in state $g^2(u) = g(g(u))$ and $g^{-1}(u)$ is the state of the system one unit of time before it is in state u. Thus instead of a continuous family of states $\{\phi_t(u) \mid t \in R\}$ we have a discrete family of states $\{g^n(u) \mid n \in Z\}$, where Z is the set of integers.

The definitions we discussed in the previous sections about a continuous dynamical system all have their analogues in the discrete case. The analogues can be obtained simply by replacing the flow ϕ by the map g and the real number t by some integer n. We state them again briefly in the following.

A point $\bar{u}$ W is called a fixed point if $g(\bar{u}) = \bar{u}$ and $u_0 \in W$ is called periodic if there exists some integer n such that $g^n(u_0) = u_0$. The least such positive n is called the period of u_0.

An invariant set A is said to be <u>stable</u> if given any neighbourhood U of A there is a neighbourhood V of A such that $g^n(V) \subset U$, for all $n>0$. Also, a is said to be <u>asymptotically stable</u> if in addition to being stable, $\bigcap_{n\geq 0} g^n(V)=A$; A is said to be <u>unstable</u> if it is not stable.

A point $u_0 \in W$ is called <u>non-wandering</u> if given any neighbourhood U of u_0, there exists $v_0 \in U$ and $n\geq 1$ such that $g^n(v_0) \in U$. The set of all non-wandering points of g is denoted by $\Omega(g)$.

A point v_0 is called an <u>ω-limit point</u> of u_0 if there exists a sequence $\{n_i\}$ with $n_i \to \infty$ and $g^{n_i}(u_0) \to v_0$ as $i \to \infty$. The set of all ω-limit points of u_0 is called the <u>ω-limit set</u> of u_0, which is denoted by $L_\omega(u_0)$. If the sequence $\{n_i\}$ has the property $n_i \to -\infty$ instead, then v_0 is called the <u>α-limit point</u> of u_0 and the set of all α-limit points of u_0 is called the <u>α-limit set</u> of u_0 and denoted by $L_\alpha(u_0)$.

Examples of discrete dynamical systems arise mostly from population dynamics. The one that has attracted much attention recently is the map $f: [0,1] \to [0,1]$ with $f(x) = \lambda x(1-x)$. Here λ is a parameter in the interval $[0,4]$, x is the population of some species at one generation and $f(x)$ is the population of the next generation. When λ lies in $[3.5,4]$, f has extremely complicated dynamics [13],[30].

1.4 Bifurcations and bifurcation diagrams

In many cases, free parameters are involved in the equation of a dynamical system. For example, in the discrete logistic equation

$$f(x) = \lambda x(1-x), \qquad (1.5)$$

λ is a free parameter, which could for example be the birth rate of a particular species. With different choices of λ, the above system could then represent the population dynamics of the species assuming different birth rates.

In general, if we express the free parameter, say λ, explicitly, we can rewrite equation (1.1) as

$$u'(t) = f_\lambda(u(t)) \qquad (1.6)$$

with λ in R. In the discrete case we write g as g_λ. We further suppose f_λ and g_λ are differentiable in λ. As λ varies, the phase portrait of (1.6) changes. A value λ_0 at which there is a basic structural change in this phase portrait is called a bifurcation point. For instance, as λ varies, a stable steady state solution may lose its stability and new steady state solutions may develop. Such a bifurcation phenomenon is called a steady state bifurcation.

For each system, if we prepare a two dimensional diagram with the vertical axis representing $||u(t)||$, where $||\ ||$

denotes a norm, (or some other measure of u(t)) and the horizontal axis representing λ, then each u(t) appears as a point in the diagram. This diagram is called a <u>bifurcation diagram</u> of the system. As λ varies, we have a branch or branches of solutions. At each bifurcation point, since there are basic structural changes in the system; other branches of solutions are expected to "bifurcate" from the original branch. A bifurcation diagram is a helpful representation in the analysis of the global dynamical behaviour of a system.

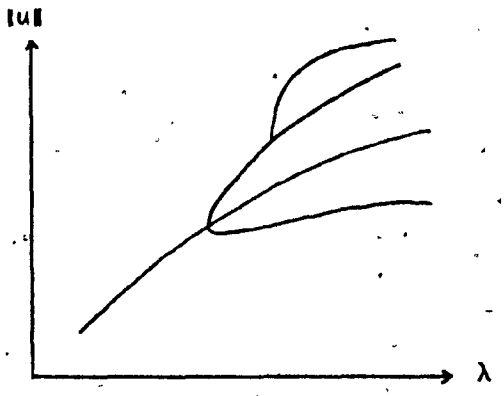

FIGURE 1.6

A large number of different bifurcating structures have been found in applied problems . In this thesis, we are mainly interested in three kinds of bifurcation behaviour, namely the Hopf bifurcation, period doubling bifurcation and the bifurcation to invariant tori.

1.5 Stability of steady state solutions

When analyzing the dynamics of a system, the local dynamical behaviour of the system is determined by a solution if it is attracting. Also, as mentioned in the previous section, when a parameter of the system reaches a critical value, a stable solution may lose its stability and some interesting bifurcations may occur. Thus it is very desirable to know whether a solution is asymptotically stable.

Let $T : R^n \to R^n$ be a linear transformation and

$$p(z) = \text{Determinant } (T - zI)$$

where I is the identity map. Now, p(z) is a polynomial and the roots of p(z) are called the eigenvalues of T. A vector ξ in R^n is said to be an eigenvector of T if

$$T(\xi) = z\xi$$

where z is an eigenvalue of T. In this and the following section we shall show the usefulness of eigenvalues in determining the stability of steady state and periodic solutions.

Let $\bar{u}$ be a steady state solution of the equation

$$u'(t) = f_\lambda(u(t)) \qquad u \in R^n,$$

i.e. $f_\lambda(\bar{u})=0$. Consider a solution v(t) slightly perturbed

from $\bar{u}$, with $v(0) = \bar{u}+\varepsilon$ where ε in R^n, and let $b(t)=v(t)-\bar{u}$. Then we have

$$\begin{aligned} b'(t) &= v'(t) \\ &= f_\lambda(v(t)) \\ &= f_\lambda(b(t) + \bar{u}). \end{aligned}$$

By Taylor's theorem, we have

$$b'(t) = f_\lambda(\bar{u})+b(t)f_\lambda'(\bar{u})+ O(|b(t)|^2).$$

Since $f_\lambda(\bar{u})=0$, $b(t)$ approximately satisfies

$$\begin{cases} b'(t) = A\, b(t) \\ b(0) = \varepsilon \end{cases} \tag{1.7}$$

where $A = f_\lambda'(\bar{u})$. Since system (1.7) is linear and A is a constant matrix, its solution can be written as

$$\begin{aligned} b(t) &= e^{tA}\,\varepsilon \\ &= (I+\sum_{k=1}^{\infty} \frac{t^k}{k!}A^k)\,\varepsilon \\ &= \sum_{j=1}^{n} (c_j e^{tz_j}\,\xi_j), \end{aligned} \tag{1.8}$$

where z_j, $j=1,2,\ldots,n$, are the eigenvalues of A (here we assume all eigenvalues are simple) and ξ_j are the corresponding eigenvectors. The coefficients c_j, $j=1,2,\ldots,n$, are determined from

$$\epsilon = c_1\xi_1 + c_2\xi_2 + \ldots + c_n\xi_n.$$

We know that $\bar{u}$ is asymptotically stable if and only if

$$b(t) \to 0 \qquad \text{as } t \to \infty. \qquad (1.9)$$

From (1.8), the sufficient condition for (1.9) is

$$\text{Re } z_j < 0 \text{ for } j=1,2,\ldots,n.$$

Theorem (1.1) Let $W \subset R^n$ be open and let $f_\lambda: W \to R^n$ be continuously differentiable. Suppose $f_\lambda(\bar{u}) = 0$. If the eigenvalues of $f_\lambda'(\bar{u})$ all have negative real parts then $\bar{u}$ is asymptotically stable.

Obviously when λ varies, a steady state solution can change its stability in one of the following two ways:

(1) A real eigenvalue crosses the imaginary axis.

(2) A pair of complex conjugate eigenvalues cross the imaginary axis.

If a steady state solution changes its stability via (1), then one or more new stable steady state solutions may branch off [21]. However, if the change of stability is via (2), then stable periodic solutions may develop. This is the well known Hopf bifurcation theorem [18] [29]. In the physical world, when a system is in a steady state, the system is "dead" and remains unchanged for all time. The Hopf bifurcation theorem thus implies that when a parameter of the system reaches a critical value, the system may

become "alive".

Theorem (1.2) Hopf bifurcation theorem for differential equations

Let $W \subset R^n$ be open and $f_\lambda: W \to R^n$ be continuously differentiable. Consider the one parameter family of ordinary differential equations

$$u'(t) = f_\lambda(u(t))$$

with λ in R. Suppose that $f_\lambda(\bar{u}) = 0$ and $f'_{\lambda_0}(\bar{u})$ has a single pair of simple complex conjugate eigenvalues $z(\lambda)$ and $\bar{z}(\lambda)$ such that

$$\frac{d}{d\lambda}(\text{Re } z(\lambda_0)) \neq 0, \text{ Re } z(\lambda_0) = 0 \text{ and Im } z(\lambda_0) \neq 0. \quad (1.10)$$

Then at $\lambda=\lambda_0$ there are periodic solutions bifurcating from the steady state solution $\bar{u}$ with period close to $\frac{2\pi}{\text{Im } z(\lambda_0)}$.

Conditions (1.10) in the above theorem simply mean that a pair of eigenvalues crosses the imaginary axis at an acute angle.

1.6 Stability of periodic solutions

Let $u(t)$ be a periodic solution of the equation

$$u'(t) = f_\lambda(u(t)) \qquad u \in R^n,$$

with $u(t) = u(t+\rho)$ for all $t \geq 0$. Consider a slightly perturbed solution $v(t)$ from $u(t)$ satisfying

$$\begin{cases} v'(t) = f_\lambda(v(t)) \\ v(0) = u(0) + b_0. \end{cases}$$

We define a function $b(t) = v(t) - u(t)$; then

$$\begin{aligned} b'(t) &= v'(t) - u'(t) \\ &= f_\lambda(v(t)) - f_\lambda(u(t)) \\ &= \frac{f_\lambda(v(t)) - f_\lambda(u(t))}{(v(t)-u(t))} \, (v(t)-u(t)) \\ &= f'_\lambda(u(t))\, b(t). \end{aligned}$$

Therefore $b(t)$ approximately satisfies the following system

$$\begin{aligned} b'(t) &= A(t)b(t) \\ b(0) &= b_0, \end{aligned} \qquad (1.20)$$

where $A(t) = f'_\lambda(u(t))$. $A(t)$ is ρ-periodic because $u(t)$ is ρ-periodic. Since (1.20) is linear, there is a fundamental solution matrix $M(t)$ of (1.20) satisfying

$$\begin{cases} M'(t) = A(t)M(t) \\ \\ M(0) = I, \end{cases} \tag{1.21}$$

where I is the identity matrix. Therefore we have $b(t) = M(t)b_0$ and this implies

$$b(\rho) = M(\rho)b_0. \tag{1.22}$$

Let $c(t) = b(\rho+t)$, so we have

$$\begin{aligned} c'(t) &= A(\rho+t)c(t) \\ &= A(t)c(t). \end{aligned}$$

Hence

$$\begin{aligned} c(t) &= M(t)c(0) \\ &= M(t)b(\rho) \\ &= M(t)M(\rho)b_0, \end{aligned}$$

which implies

$$\begin{aligned} c(\rho) &= b(2\rho) \\ &= (M(\rho))^2 b_0. \end{aligned}$$

Repeating this process m times we get

$$b(m\rho) = (M(\rho))^m b_0,$$

and

$$b(m\rho+t) = M(t)(M(\rho))^m b_0, \quad t \in [0,\rho],$$

which implies

$$||b(m\rho+t)|| \leq \max||M(t)||\ ||(M(\rho))^m||\ ||b_0||.$$

We can see that the perturbation function b(t) is bounded if there exists a constant $N > 0$ such that

$$||(M(\rho))^m|| \leq N \text{ for all } m>0. \qquad (1.23)$$

A sufficient condition for (1.23) is

$$|z_j|<1, \qquad j=1,2,\ldots,n,$$

where z_j, $j=1,2,\ldots,n$ are the eigenvalues of matrix $M(\rho)$.

In fact we have the following more general and stronger result:

Theorem (1.3) Let $f_\lambda: W \to R^n$ be a C^1 vector field on an open set $W \subset R^n$, λ in R; the flow of the equation

$$u'(t) = f_\lambda(u(t)) \qquad (1.24)$$

is denoted by ϕ. Let u(t) be a periodic solution of equation (1.24) with period ρ and u_0 u(t). Suppose that n-1 eigenvalues of the linear map

$$\phi'(u_0) : R^n \to R^n$$

are less than 1 in absolute value. Then u(t) is asymptotically stable.

Before we proceed, we make several notes about Theorem (1.3).

(1) $\phi'(u_0)$ is independent of $u_0 \in u(t)$. For if $v_0 \in u(t)$ is a different point, let $r \in R$ be such that $\phi_r(u_0) = v_0$. Then

$$\phi'(u_0) = (\phi_{-r}\phi\phi_r)'(u_0)$$

$$= \phi'_r(u_0)^{-1}\,\phi'(v_0)\,\phi'_r(u_0)$$

this shows that $\phi'(u_0)$ is similar to $\phi'(v_0)$.

(2) 1 is always an eigenvalue of $\phi'(u_0)$ since

$$\phi'(u_0)\, f_\lambda(u_0) = f_\lambda(u_0).$$

(3) Theorem (1.3) is not as convenient to use as Theorem (1.1) and Theorem (1.2) since it requires information about the flow of the equation, not merely the vector field.

From Theorem (1.3) we can see that a periodic solution can change its stability in one of the following three ways:

(1) an eigenvalue crosses the unit circle at z=1.

(2) an eigenvalue crosses the unit circle at z=-1.

(3) a pair of complex conjugate eigenvalues cross the unit circle.

If a periodic solution changes its stability via (2), a period doubling bifurcation may occur [21] (i.e a periodic solution on the bifurcating branch close to the bifurcation

point has period approximately double the period of a periodic solution on the original branch which is close to the bifurcation point), see Figure 1.7

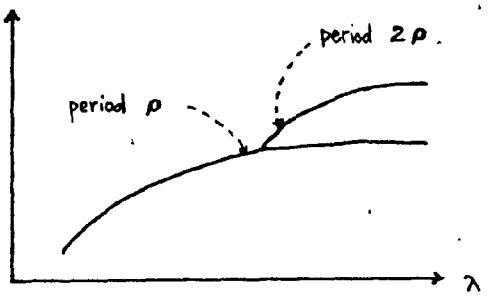

FIGURE 1.7

The case when a periodic solution changes its stability via (3) is discussed in more detail in Chapter 3.

From Theorem (1.1) to (1.3) we know that by monitoring the eigenvalues of the "linearized" part of the vector field and the flow (i.e. $f'_\lambda(u)$ and $\phi'(u_0)$) we can obtain much information about the stability of a solution of the system. This idea was implemented in a computer program AUTO by E. Doedel [7] for the so called "automatic bifurcation analysis". In Chapter 2, we use AUTO to analyze the bifurcation behaviour of three ordinary differential equations in R^3, including the well known Lorenz system. In the following chapters, when an eigenvalue z is discussed with a steady state solution $\bar{u}$, it is understood that z is an eigenvalue of $f'_\lambda(\bar{u})$. When z is discussed with a periodic solution u(t), it is also understood that z is an eigenvalue of $\phi'(u_0)$ where u_0 u(t).

CHAPTER TWO

Bifurcation behavior of three 3-dimensional Ordinary Differential Equations

For a long time, it was believed that the classification of the dynamical behaviour of differential equations discussed in Chapter 1 was quite sufficient. But recently, driven by the fact that highly irregular motions are so often observed in physical systems, the following question was naturally raised: can deterministic differential equations, which are often used to model physical systems, have aperiodic dynamics ? If the answer to this question were to be negative, then using differential equations to model physical systems might be completely irrelevant. Fortunately, the answer is affirmative and to many people's surprise even simple looking systems can exhibit very complicated dynamics. One of the well known examples of such systems is the Lorenz system. This 3-dimensional system of ordinary differential equations has an attractor which has aperiodic dynamical behavior even inside the attractor. The mechanism which leads to the existence of such attractors is not yet fully understood.

2.1 AUTO

Recently, a computer program AUTO for the numerical analysis of autonomous systems of the form

$$u'(t) = f_\lambda(u(t)); \qquad t \geq 0,\ u \in R^n,$$

was developed by E. Doedel [7]. Here λ is a free parameter. Given f, the Jacobian of f, the derivative $\frac{\partial f}{\partial \lambda}$, a steady state solution for some value of λ and a number of control parameters, AUTO has the following basic capabilities:

(1) Trace out branches of steady state solutions.

(2) Accurately locate steady state bifurcation points.

(3) Switch automatically onto bifurcating branches of steady states.

(4) Accurately locate Hopf bifurcation points.

(5) Switch automatically onto branches of periodic solutions and trace out such branches.

(6) Compute past turning points without added difficulty, both on branches of steady state solutions and on branches of periodic solutions.

(7) Compute stable as well as unstable branches. For periodic solutions this is made possible by reformulating the problem as a boundary value problem on $[0,2\pi]$.

(8) Compute the Floquet multipliers of steady state

and periodic solutions.

(9) Adapt the mesh to the solution. The discretization used is the method of orthogonal collocation with 2, 3 or 4 collocation points per mesh interval.

(10) Adaptive stepsize along branches of periodic solutions.

(11) Automatic restarting at certain points.

(12) Continuation of curves of limit points of steady state branches in two parameters .

(13) Continuation of curves of limit points of periodic solution branches in two parameters .

(14) Continuation of curves of Hopf bifurcation points in two parameters .

(15) Store plotting information in files. These files can be investigated by an interactive graphics program.

Fruitful results in bifurcation analysis have been obtained using AUTO on several models from different disciplines including chemical reactions, coupled oscillators and population dynamics [8],[2].

Since chaotic dynamical behaviour was found in the Lorenz system in 1963, the dynamical behaviour of simple 3-dimensional ordinary differential systems has attracted the attention of many scientists. Due to the existence and

uniqueness theorem of ordinary differential equations, we know that 2-dimensional ordinary differential systems cannot have chaotic dynamics (because the solution curves cannot intersect). Therefore 3-dimensional ordinary differential systems are bound to be the simplest models for studying stochasticity in deterministic systems.

In the following sections, with the aid of AUTO, we analyse the bifurcation behaviour of the Lorenz system and two other 3-dimensional systems of ordinary differential equations. We hope that these analyses can contribute to the understanding of transition to stochasticity in deterministic systems. The results show that complicated bifurcation behaviour also exists in simple-looking differential equations.

2.2 Bifurcation behaviour of the Lorenz system

In the 1950's, there were basically two approaches for numerical weather prediction. The first approach followed the dynamical method which performed weather forecasting by numerically integrating atmospheric equations. The second approach favoured the statistical method using linear regression with large numbers of predictors. Also, the idea was presented that the statistical method could duplicate the performance of the dynamical method. In 1963, being skeptical about this idea, E. Lorenz tried to find "non-predictable" dynamics in a system of twelve variables. The search was successful and when he compared the results generated by both methods Lorenz observed that the statistical method cannot duplicate the performance of the dynamical method. In order to better understand the problem, he further eliminated nine variables, and a simpler system which still possessed aperiodic dynamics was obtained. The system is as follows:

$$\begin{cases} x' = -\sigma(x-y) & (2.2a) \\ y' = -x(z-r)-y & (2.2b) \\ z' = xy-bz\ , & (2.2c) \end{cases}$$

where σ and r are related to the Prandtl number and the Rayleigh number respectively, and b is a positive parameter. This is now generally called the Lorenz system [25],[35].

System (2.2) is not quite realistic in the sense of modelling weather prediction; however, as many people have pointed out, these equations can be used to model a laboratory water wheel or irregular laser spiking [25],[32].

Since the divergence of the flow represented by (2.2), $\frac{\partial x'}{\partial x} + \frac{\partial y'}{\partial y} + \frac{\partial z'}{\partial z}$, equals $-(\sigma+b+1)$, system (2.2) is dissipative [35]. A volume element, V, is contracted by the flow into a volume element $Ve^{-(\sigma+b+1)t}$ in a time t. Lorenz has also shown that there is a bounded ellipsoid in R^3 which all trajectories eventually enter [24]. These two remarks, taken together, imply that all trajectories tend towards some bounded non-wandering set of volume zero. Also, no invariant tori can exist. Notice that system (2.2) contains no noisy or stochastic terms, so one would expect that the dynamical behaviour of system (2.2) would be quite simple.

At $\sigma=10$, $b=\frac{8}{3}$ and $r=28$, the non-wandering set of system (2.2) is as shown in Figure 2.1. Inside the attractor, the trajectories continue to wander back and forth in a random manner and they never intersect if we consider the full three dimensional picture. This attractor is now called the Lorenz attractor. Lorenz also argued that if one uses a line which is parallel to the y-axis to cut through the attractor, the resulting intersection is a cantor set. It is this complicated dynamical behaviour that has generated so much interest in the Lorenz system. It initiated the suggestion that complicated turbulent

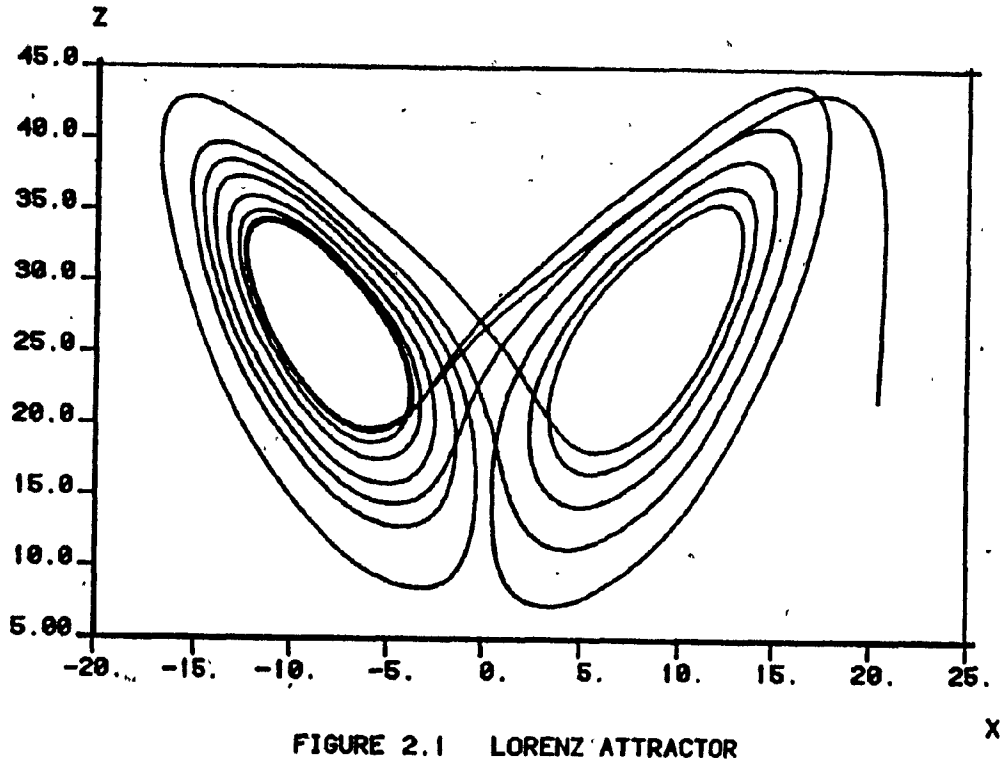

FIGURE 2.1 LORENZ ATTRACTOR

behaviour in systems with an infinite number of degrees of freedom might be modelled by simple deterministic finite-dimensional systems.

The Lorenz attractor is sometimes called a strange attractor due to its strange dynamics. However, in the literature, the term "strange attractor" is also frequently used for other attracting sets with different dynamical natures [32]. In this thesis, the term "strange attractor" is used in its most general sense to mean any attractor with aperiodic dynamics.

So much has been said about the Lorenz system that it is not possible to survey all available results. For an extensive analysis and survey on the system, see [35]. In

the following, we concentrate on some bifurcation behaviour of the Lorenz system. The choice of the parameter values $\sigma=10$, $b=\frac{8}{3}$ and r varying between zero and infinity is conventional.

We write system (2.2) in the form of (2.1), i.e.

$$u' = f(u;\ \sigma,r,b), \quad u^T = (x,y,z) \qquad (2.3)$$

where

$$f(u;\ \sigma,r,b) = \begin{cases} -\sigma(x-y) \\ -x(z-r)-y \\ xy-bz \end{cases} .$$

Clearly, the right hand side of (2.3) vanishes at $0^T=(0,0,0)$; therefore 0 is a steady state solution of (2.3). The Jacobian matrix of f is

$$f'(u;\ \sigma,r,b) = \begin{bmatrix} -\sigma & \sigma & 0 \\ -z+r & -1 & -x \\ y & x & -b \end{bmatrix} .$$

Evaluating the Jacobian matrix at 0 we have

$$f'(0;\sigma,r,b) = \begin{matrix} -\sigma & \sigma & 0 \\ r & -1 & 0 \\ 0 & 0 & -b \end{matrix}$$

and the characteristic polynomial of $f'(0;\sigma,r,b)$ is

$$\lambda^3 + (1+\sigma+b)\lambda^2 + (b\sigma+b+\sigma-r\sigma)\lambda + b\sigma(1-r) = 0.$$

This implies

$$(\lambda+b)[\lambda^2+(\sigma+1)\lambda+\sigma(1-r)] = 0$$

or

$$\lambda = -b,$$

$$\lambda = \frac{-(\sigma+1) \pm \sqrt{(\sigma+1)^2-4\sigma(1-r)}}{2}$$

If $r < 1$, all three eigenvalues of $f'(0;\sigma,r,b)$ are negative real numbers. If $r>1$, one of the three eigenvalues, namely

$$\lambda = \frac{-(\sigma+1)+\sqrt{(\sigma+1)^2-4\sigma(1-r)}}{2}$$

becomes positive. Hence we know that for $r < 1$, $u=0$ is an attracting steady state solution of (2.3). When r becomes greater than 1, $u=0$ loses its attraction and there exists two new steady state solutions:

$$v^T = (\sqrt{b(r-1)}, \sqrt{b(r-1)}, r-1),$$

and

$$\bar{v}^T = (-\sqrt{b(r-1)}, -\sqrt{b(r-1)}, r-1).$$

To determine the stability of v and $\bar{v}$, we consider

$$f'(v;\sigma,r,b) = \begin{bmatrix} -\sigma & \sigma & 0 \\ 1 & -1 & -\sqrt{b(r-1)} \\ \sqrt{b(r-1)} & \sqrt{b(r-1)} & -b \end{bmatrix}$$

and its characteristic polynomial

$$\lambda^3 + (\sigma+b+1)\lambda^2 + (r+\sigma)b + 2\sigma b(r-1) = 0. \quad (2.4)$$

We can see that all three coefficients of polynomial (2.4) are positive. Hence one of the roots of (2.4) must be a negative real. The other two roots are initially negative reals, then become a pair of complex conjugates which become purely imaginary when

$$r = \frac{\sigma(\sigma+b+3)}{\sigma-b-1}.$$

This is the critical value of r for the instability of the two new steady state solutions v and $\bar{v}$. From Theorem (1.2), we know that periodic solutions appear. Figure 2.2 shows the bifurcation diagram of the Lorenz system.

In Figure 2.2, branch 1 is the zero steady state. When $r \leq 1$, branch 1 is stable. At r=1, one of the eigenvalues becomes positive and two new steady state solutions

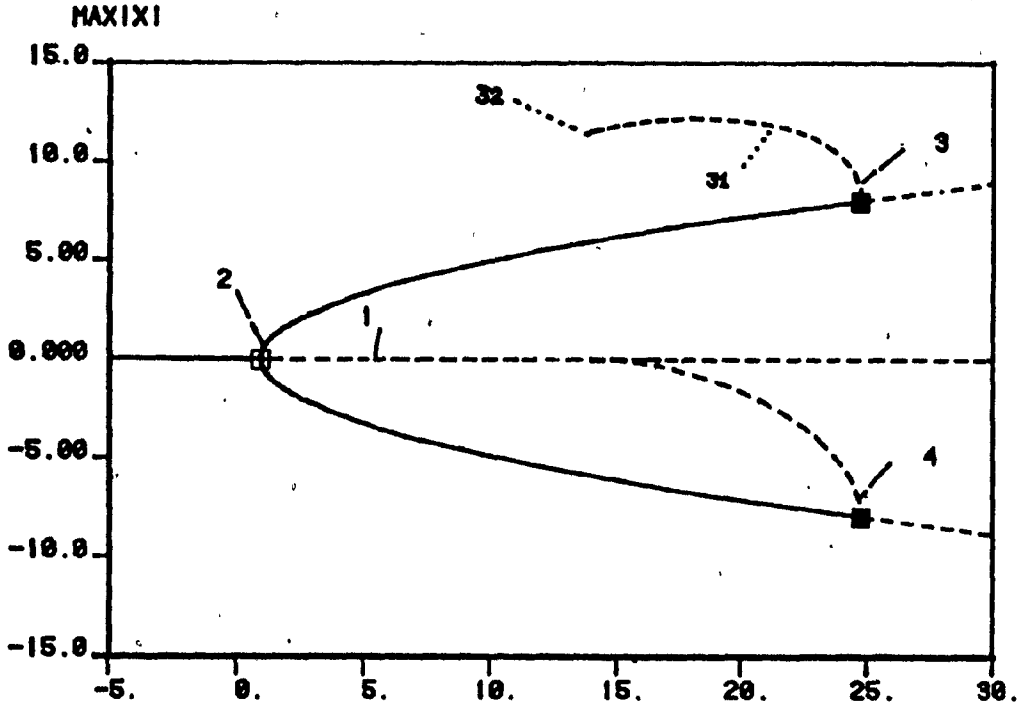

FIGURE 2.2 (BIFUR DIA OF LORENZ SYS)

bifurcate from branch 1. These two new steady state solutions are stable when $r \leq 24.74$. In Figure 2.2, these two steady state solutions are both named branch 2. From here on, unless otherwise specified, we only discuss the branch on the upper half plane.

At r=24.74, a pair of complex eigenvalues crosses the imaginary axis of the complex plane (Hopf bifurcation). Branch 2 becomes unstable at this point. The bifurcating branch of periodic solutions goes backward and the periodic solutions on this branch are unstable. This type of bifurcation is usually called subcritical (in contrast to supercritical bifurcations which generally lead to a forward and stable bifurcating branch).

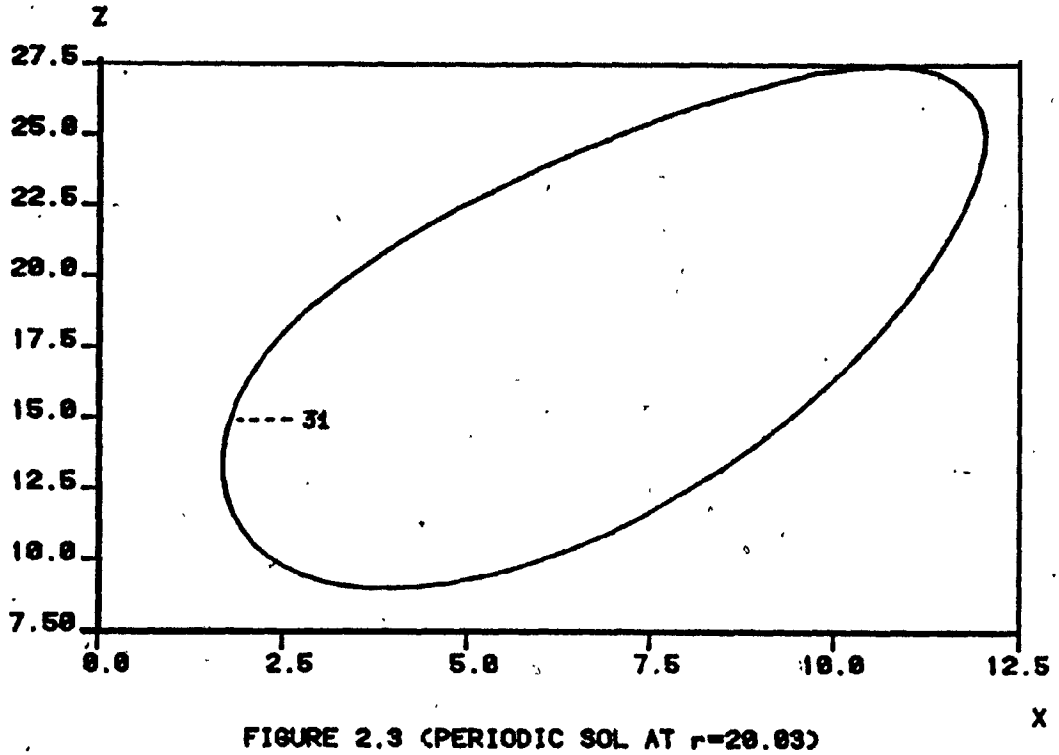

FIGURE 2.3 (PERIODIC SOL AT r=20.03)

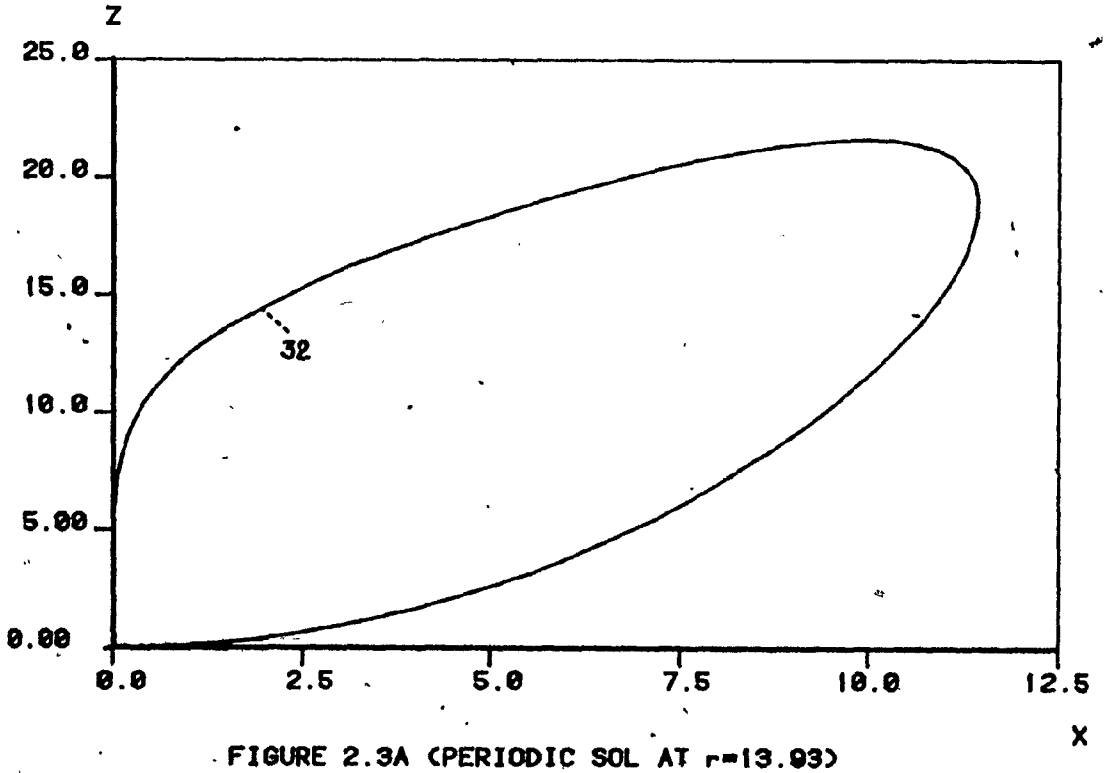

FIGURE 2.3A (PERIODIC SOL AT r=13.93)

In Figure 2.2, branch 3 is the periodic solution branch bifurcating from branch 2 in the upper half plane and branch 4 is the periodic solution branch bifurcating from branch 2 in the lower half plane. Their symmetry is not apparent because of the choice of the vertical axis.

For a periodic solution on branch 3, see Figure 2.3. Along branch 3, the period of the periodic solutions increases very rapidly as r decreases. The computation terminates at the solution labelled 32 where r=13.93 and the period is very high (see Figure 2.3A). This matches the observation by C. Sparrow [35]. Sparrow also argued that these periodic solutions with high period are "generated" from a homoclinic orbit of the unstable zero steady state (a homoclinic orbit is an orbit that tends, in both forward and backward time, towards an unstable steady state).

Other periodic solutions have been observed by some authors when r is around 100 or greater [34], [35]. See Figure 2.4 for one given by Sparrow at r=100.5. Using this periodic solution as a starting point, we traced out a periodic solution branch. This branch is named branch 9 in Figure 2.5, which shows the global bifurcation diagram of the Lorenz system on the upper half plane. Using a second periodic solution located by ourselves at r=200.87, we traced out another periodic solution branch named branch 5 in Figure 2.5. See Figure 2.6 for the starting periodic solution of branch 5.

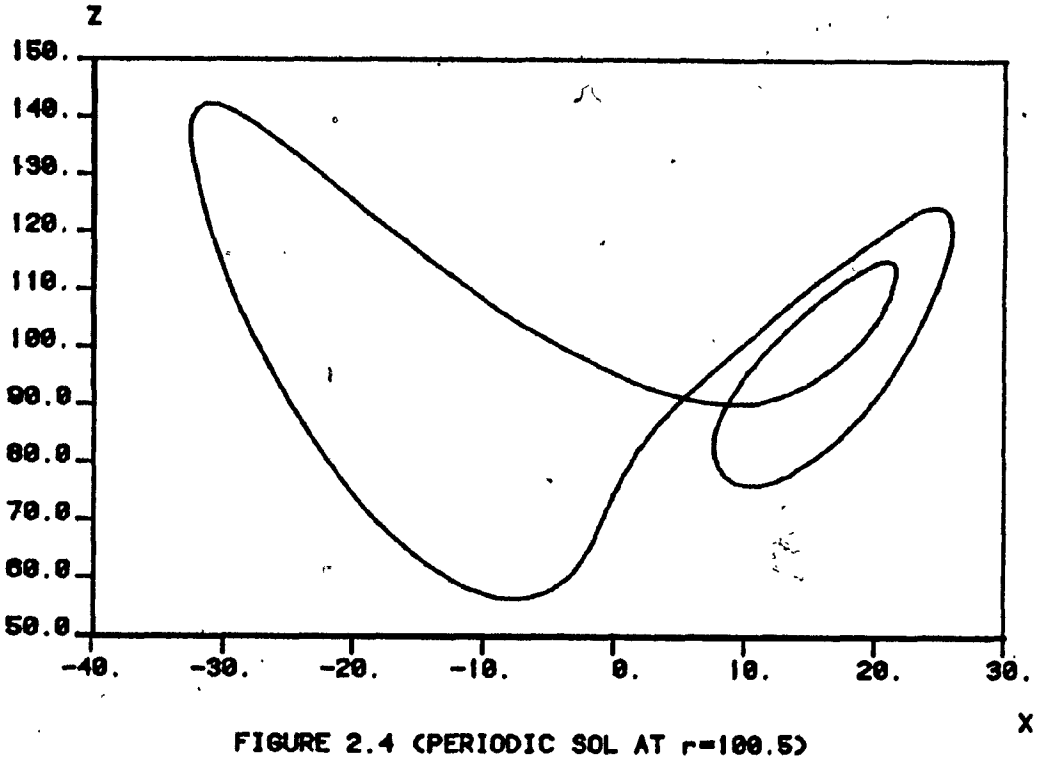

FIGURE 2.4 (PERIODIC SOL AT r=100.5)

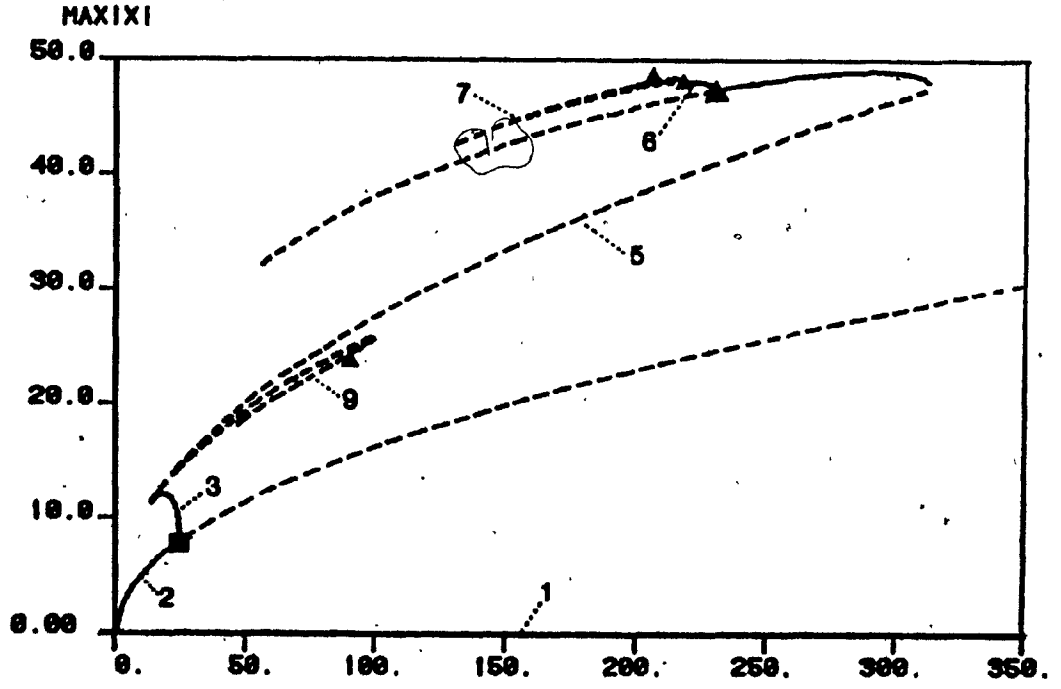

FIGURE 2.5 (BIFUR DIA OF LORENZ SYS)

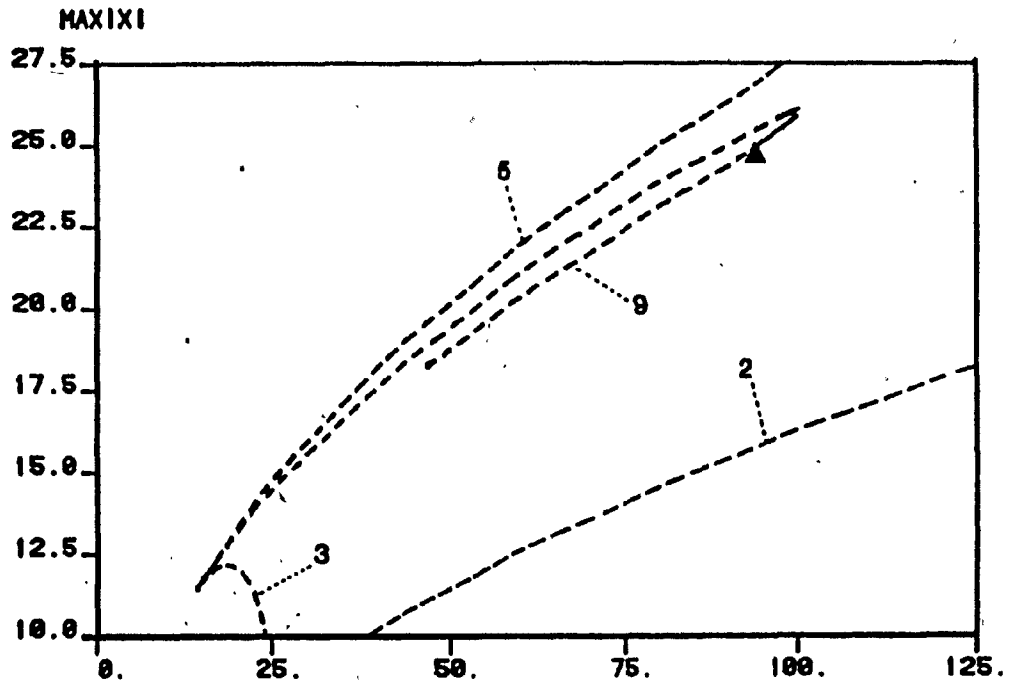

FIGURE 2.5A (LOCAL ENLARGEMENT OF 2.5)

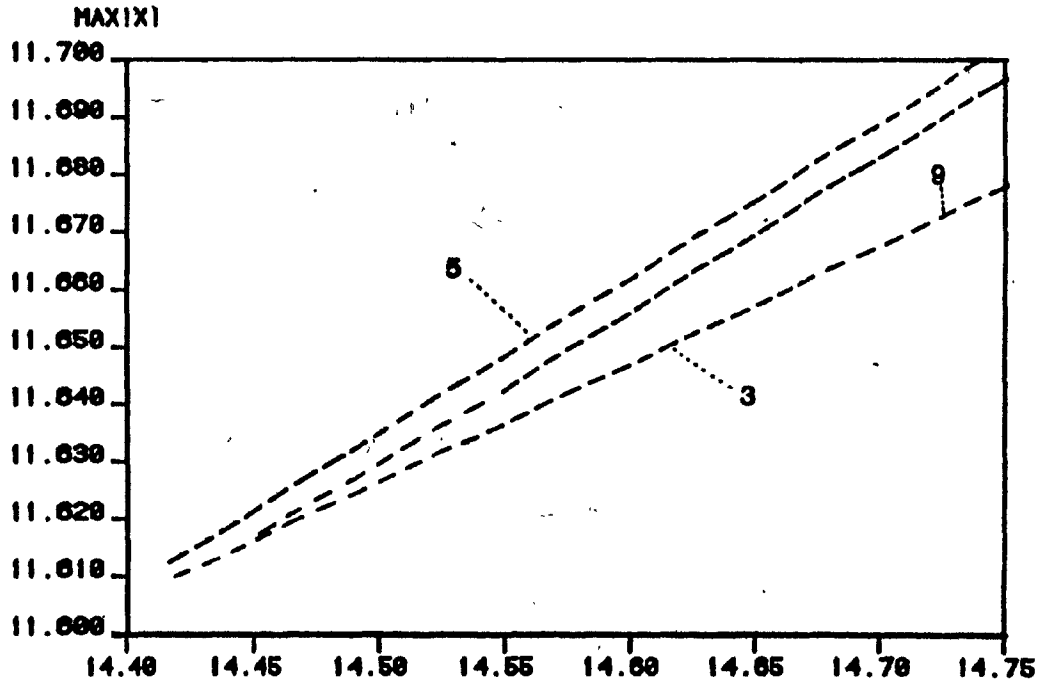

FIGURE 2.5B (LOCAL ENLARGEMENT OF 2.5)

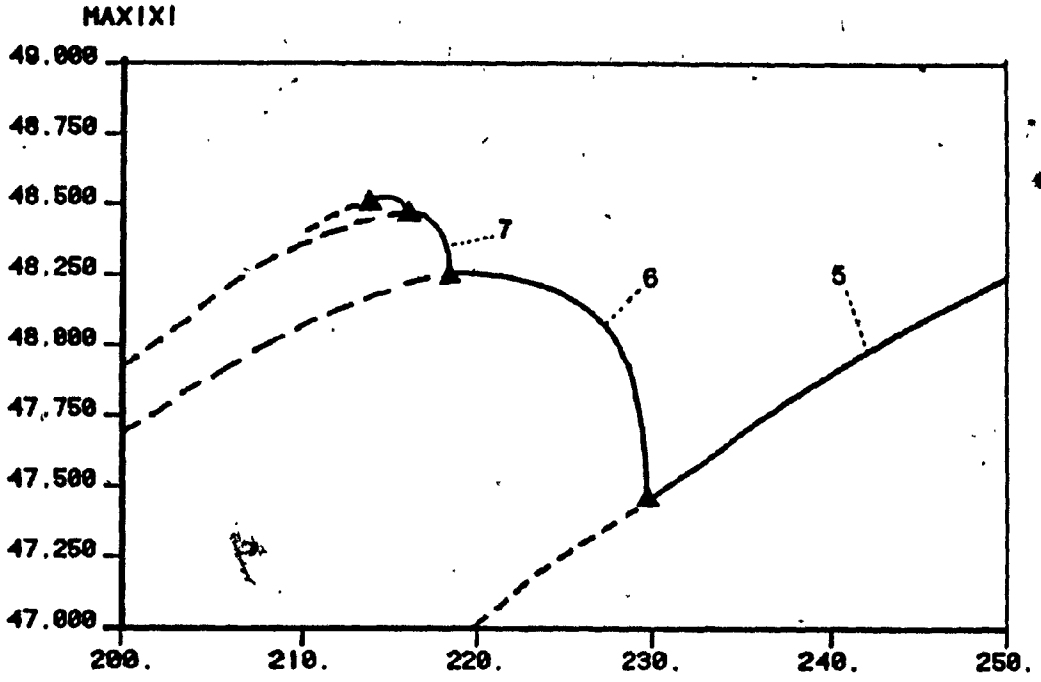

FIGURE 2.5C (CASCADING SEQ OF PD BIF)

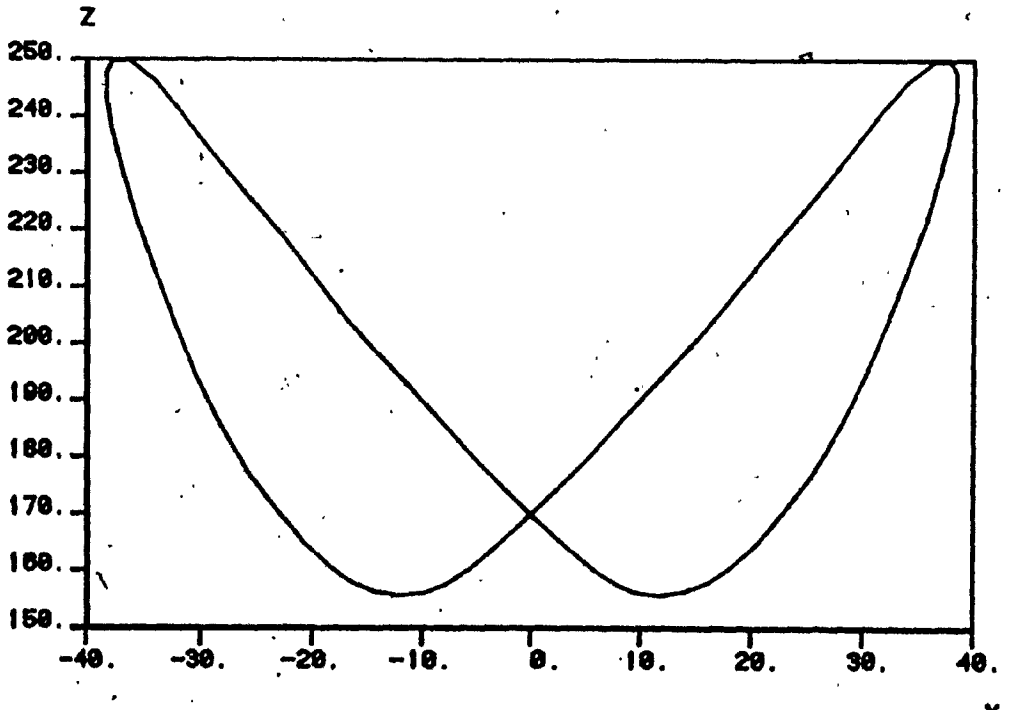

FIGURE 2.6 (PERIODIC SOL AT r=200.87)

Let us examine branch 5 more carefully. Three local blow-ups of Figure 2.5 are given in Figure 2.5A, 2.5B and 2.5C starting from low values of r, solutions on branch 5 are high period unstable periodic solutions. As r increases, the period of the periodic solutions decreases. Some periodic solutions on branch 5 are shown in Figure 2.7. At r=325, one of the eigenvalues becomes real and enters the unit circle through positive one. This corresponds to a turning point on the branch. Now all three eigenvalues of the linearized flow are inside the unit circle and therefore the periodic solutions on the branch are stable. Stable periodic solutions exist until a period doubling bifurcation is detected. Starting from the period doubling bifurcation point, another periodic solution branch (branch 6) is traced. The bifurcation direction is towards low values of r. At first, periodic solutions on this new branch are stable and stability changes when another period doubling bifurcation point is found on this branch. When the bifurcating branch of periodic solutions (branch 7) is again traced out, another period doubling bifurcation is located at the point where the periodic solutions lose stability. See Figure 2.5C for a bifurcation diagram for this cascading sequence of period doubling bifurcations. Some of the corresponding periodic solutions are shown in Figure 2.8. Branch 5 continues with decreasing values of r and the computation terminates when the periodic solution branch approaches the homoclinic orbit. Since the homoclinic orbit

has an infinite period, the computation gets into difficulty at this point.

Starting at r=100.5, branch 9 is traced in both directions. The behaviour of branch 9 is almost the same as described above for branch 5 except it is on a smaller scale. At low values of r, branches 3, 5 and 9 are very close to each other; see Figure 2.5B. However, we emphasize that this is not a bifurcation and that periodic solutions on branches 3, 5 and 9 have entirely different shapes, as shown in Figures 2.3B, 2.9 and 2.10.

In the other direction, when r=100.77, one of the eigenvalues enters the unit circle through positive one at the turning point on the branch. As on branch 5, after the turning point, the periodic solutions become stable until a period doubling bifurcation point is detected at r=100. From this bifurcation point we again expect a cascading sequence of period doubling bifurcation branches to be found. The period doubling phenomenon in this parameter region is also reported by Sparrow ([35],p.56). After r=100, branch 9 becomes unstable. Again the computation terminates when the periodic solution branch approaches the homoclinic orbit.

The bifurcation diagram given in Figure 2.5 may not be complete. Other periodic solution branches are likely to exist. From our computation, several unstable periodic

solutions have been observed in the parameter range where the Lorenz attractor exists. See Figure 2.9 and Figure 2.10 for two of these orbits. These unstable periodic solutions exist and are very close to each other in a certain region in the state space. We suspect that the interesting dynamical behaviour inside the Lorenz attractor is caused by the fact that many unstable periodic solutions are packed very close to each other in this area. When a trajectory enters the Lorenz attractor, due to the unstable character of the periodic solutions, the trajectory is forced to wander around without settling down.

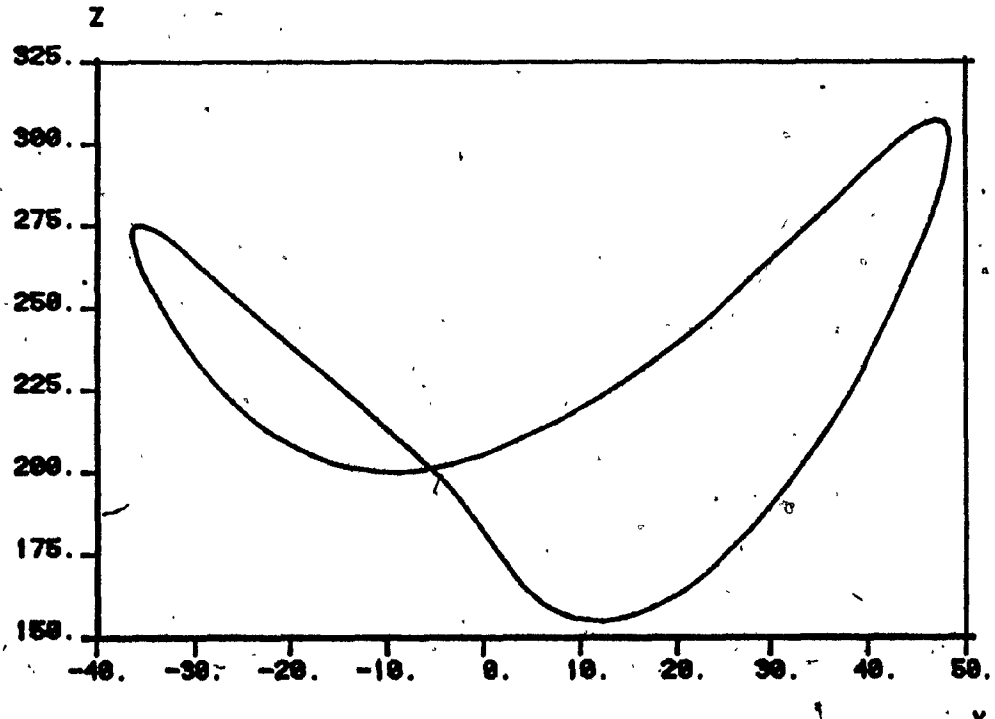

FIGURE 2.7 (PERIODIC SOL AT r=220.41)

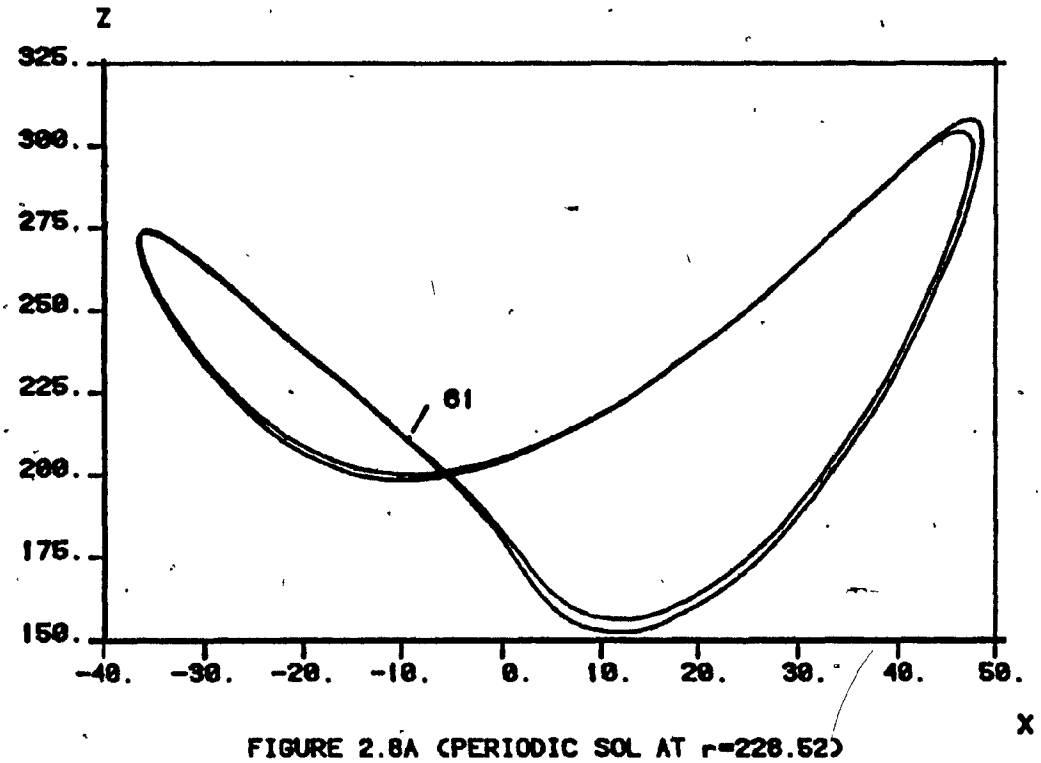

FIGURE 2.8A (PERIODIC SOL AT r=228.52)

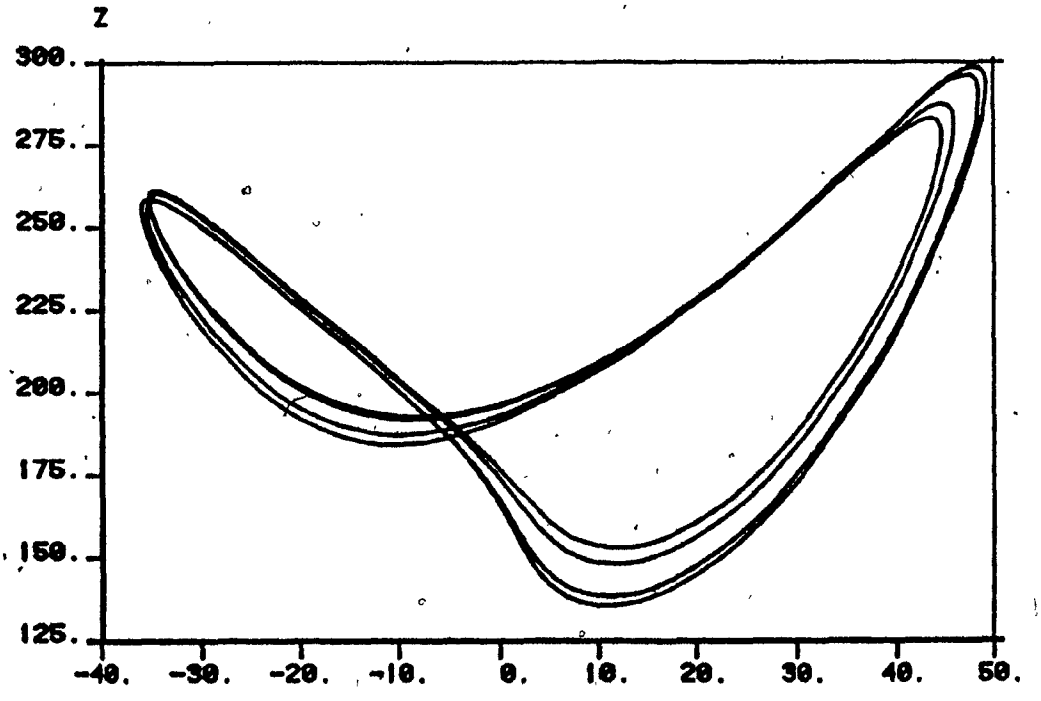

FIGURE 2.8B (PERIODIC SOL AT r=215.97)

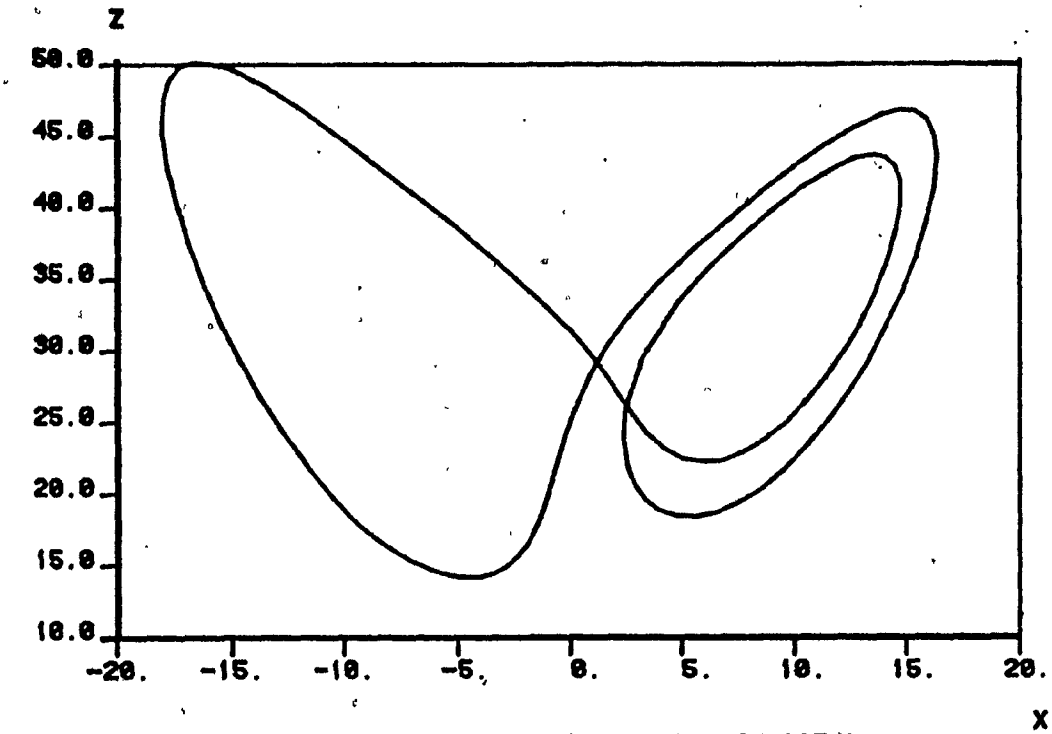

FIGURE 2.9 (PERIODIC SOL AT r=34.0674)

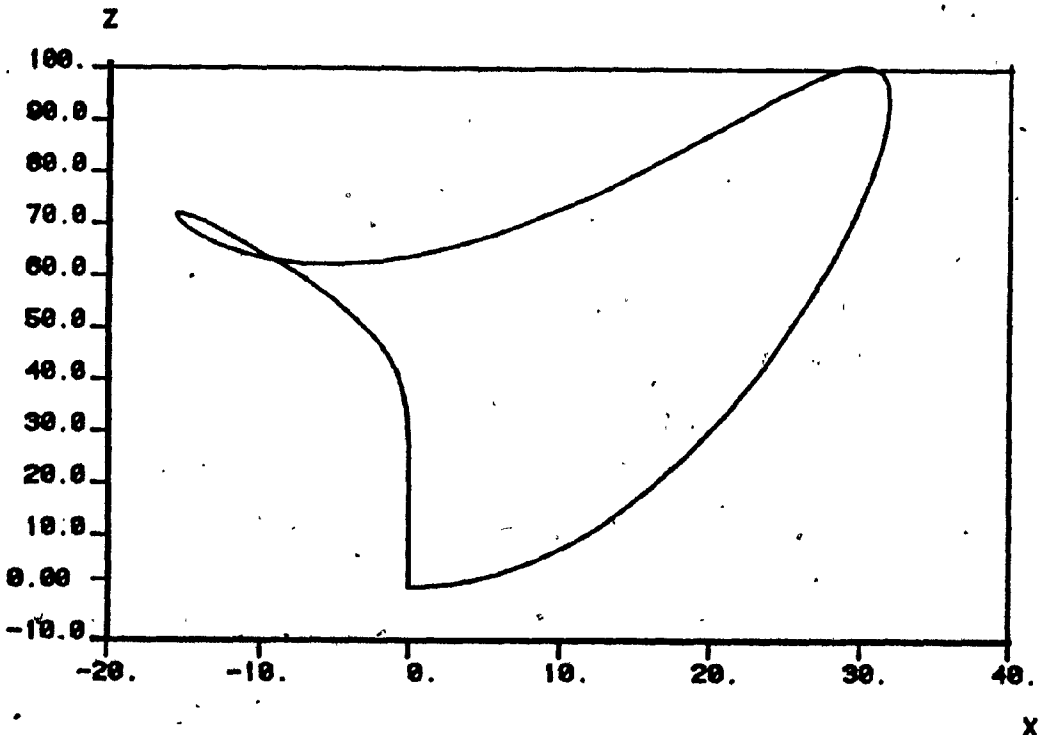

FIGURE 2.10 (PERIODIC SOL AT r=54.64)

2.3 Bifurcation behaviour of the transformed Lorenz system

In 1978, T. Shimizu and N. Morioka [34],[5] proposed a new direction for studying the Lorenz system. By change of variables, they transformed the Lorenz system into a differential system describing a particle in some potential depending on a varying parameter:

$$\begin{cases} u'' + \beta u' + \dfrac{\partial V(u,\eta)}{\partial u} = 0, \\ \\ \eta' = f(\eta,u), \quad V(u,\eta) = au^4 + c(\eta)u^2 , \end{cases} \tag{2.5}$$

where $\beta, a, c(\eta)$ and $f(\eta,u)$ are functions of the parameters σ, b, r of the Lorenz system.

The change of variables is as follows: from (2.2a) and (2.2b) we have

$$\begin{aligned} x'' &= -\sigma(x' - y') \\ &= -\sigma[x' - (-xz + rx - y)] \\ &= -\sigma[x' - x(r-z) + y]. \end{aligned} \tag{2.6}$$

From (2.2a) again we have

$$y = \frac{x' + \sigma x}{\sigma}. \tag{2.7}$$

Substituting (2.7) into (2.6) we have

$$\begin{aligned} x'' &= -\sigma\left[x' - x(r-z) + \frac{x' + \sigma x}{\sigma}\right] \\ &= -\sigma x' + \sigma x(r-z) - x' - \sigma x \end{aligned}$$

or

$$x'' + (\sigma+1)x' = \sigma x(r-z-1). \qquad (2.8)$$

Dividing both sides of (2.8) by $\sqrt{2\sigma(r-1)}$ and letting $u = \frac{x}{\sqrt{2\sigma(r-1)}}$ we have

$$\begin{aligned} u'' + (\sigma+1)u' &= \sigma u(r-z-1) \\ &= -\sigma(r-1)u\left(\frac{z-r+1}{r-1}\right) \\ &= -\sigma(r-1)u\left(\frac{z}{r-1} - 1 + u^2 - u^2\right), \end{aligned}$$

or

$$\begin{cases} u'' + (\sigma+1)u' = -\sigma(r-1)u(u^2-1+m) \\ m = \frac{z}{r-1} - u^2 \end{cases} \qquad (2.9)$$

where

$$m' = -b\left[m - \left(\frac{2\sigma}{b} - 1\right)u^2 \right].$$

if we write $\beta=\sigma+1$ and $\frac{\partial V(u,m)}{\partial u} = \sigma(r-1)u\,(u^2-1+m)$ then (2.9) corresponds to (2.5).

A very wide class of differential systems may be expressed in the form of (2.5) with different choice of V and f. In 1979, P.Coullet, C.Tresser and A.Arneodo [5] proposed to study a particularly simple choice, namely

$$\begin{cases} V = u - \eta, \\ \\ \eta' = -u(b+a(1-u)). \end{cases} \tag{2.10}$$

Their prime motive is that it is easier to understand the transition to stochasticity in a simple system than in a complex system if stochasticity exists. Using the special V and f given in (2.10), (2.5) can be written as

$$u''' + \beta u'' + u' = -u(b+a(1-u))$$

or

$$\begin{cases} u' = v \\ v' = -u-w \\ w' = au(1-u)-bw \end{cases}$$

or

$$\begin{cases} x' = -y-z \\ y' = x \\ z' = ay(1-y)-bz. \end{cases} \tag{2.11}$$

System (2.11) has two parameters which is one less than the Lorenz system. It is also slightly simpler than the Lorenz system. In order to analyze the bifurcation behaviour of (2.11), we again express (2.11) in the form of (2.1), i.e.

$$u' = f(u;a,b), \quad u^T = (x,y,z) \tag{2.12}$$

where

$$f(u;a,b) = \begin{cases} -y-z \\ x \\ ay(1-y)-bz \end{cases},$$

with the Jacobian matrix

$$f'(u;a,b) = \begin{bmatrix} 0 & -1 & -1 \\ 1 & 0 & 0 \\ 0 & a(1-2y) & -b \end{bmatrix}$$

The characteristic polynomial of $f'(u;a,b)$ is

$$\lambda^3 + b\lambda^2 + b + (a-2ay) = 0. \qquad (2.13)$$

Obviously $0^T = (0,0,0)$ is a steady state solution of (2.11). When evaluated at 0, characteristic polynomial (2.13) becomes

$$\lambda^3 + b\lambda^2 + \lambda + b + a = 0. \qquad (2.14)$$

At $b=-a$, one of the eigenvalues crosses the imaginary axis and causes a steady state bifurcation to a new steady state solution $u^T = (0, \frac{a+b}{a}, -\frac{a+b}{a})$. Then the characteristic polynomial evaluated at u is

$$\lambda^3 + b\lambda^2 + \lambda - (b+a) = 0 \qquad (2.15)$$

The discriminant of (2.15) can be written as

$$Q = (\frac{p}{3})^3 + (\frac{q}{2})^2$$

where $p = -\frac{b^2}{3}+1$ and $q = 2(\frac{b}{3})^3 - \frac{b}{3} - (b+a)$. When b is small, Q is positive and we know that (2.15) has one real root and

two complex conjugate roots. The two complex conjugate roots are pure imaginary if

$$b = -(a+b)$$

or

$$b = -\frac{a}{2}.$$

See Figure 2.11 for the bifurcation diagram of system (2.12) with a=0.375 and b as a free parameter. Again, branch 1 is the zero steady state which is unstable for the entire branch. The computation starts at b=-5. At first, all three eigenvalues have positive real parts. At b=-0.375, one real eigenvalue crosses the imaginary axis when a steady state bifurcation occurs. The new steady state solution is named branch 2 and is also unstable.

Along branch 2, a Hopf bifurcation point is located at b=-0.1875 (which matches the argument given above). At this point, a pair of complex eigenvalues cross the imaginary axis and go into the left half plane. A periodic solution branch results and is named branch 3.

When first bifurcating from the steady state branch 2, branch 3 is unstable. Branch 3 is unstable until a bifurcation to invariant tori is found at $b=6.569939\times10^{-8}$. At this point, a pair of complex conjugate eigenvalue enter the unit circle. The branch remains stable for a while and turns unstable again at b=0.09529 where a period doubling bifurcation is encountered. Then branch 3 turns stable at

b=0.6458 where another period doubling bifurcation is detected. A schematic diagram of the sequence of period doubling bifurcations is shown in Figure 2.12 and two solutions indicating the period doubling are shown in Figure 2.13A and Figure 2.13B.

The existence of a cascading sequence of period doubling bifurcations in the one dimensional discrete logistic equation

$$f(x) = \lambda x(1-x)$$

is well known (see section 1.3). If $\{\lambda_n\}$ denotes the corresponding parameter sequence, then the limit

$$\delta = \lim \frac{\lambda_n - \lambda_{n-1}}{\lambda_{n+1} - \lambda_n}$$

is called the Feigenbaum's constant [12]. However, although cascading sequences of period doubling bifurcations have been found in many models of higher dimensions, they have not been clearly described. From the computation in the transformed lorenz system. If we let

$$\delta_n = \frac{b_n - b_{n-1}}{b_{n+1} - b_n}$$

then

$$\delta_1 = \frac{0.1671 - 0.0953}{0.1933 - 0.1671} = 2.740458$$

$$\delta_2 = \frac{0.1933 - 0.1671}{0.2010 - 0.1933} = 3.4025974$$

It is not clear yet that $\delta_n \to 4.6692...$ (the Feigenbaum's constant). But further information can be obtained if we trace out more doubling branches.

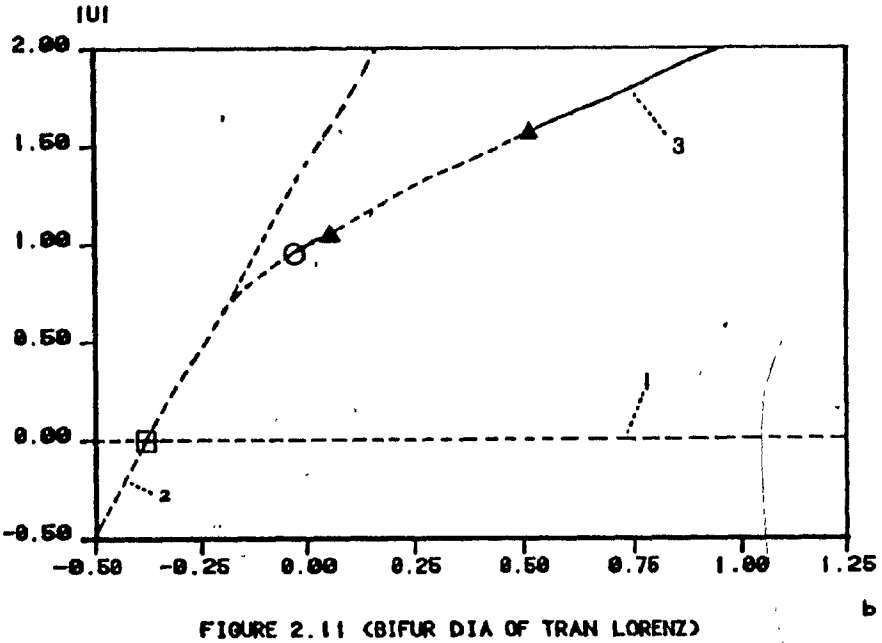

FIGURE 2.11 (BIFUR DIA OF TRAN LORENZ)

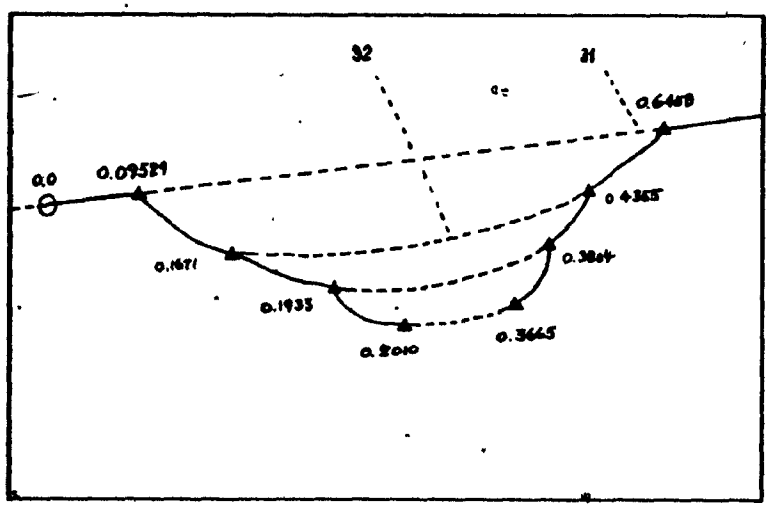

FIGURE 2.12 SCHEMATIC DIAGRAM

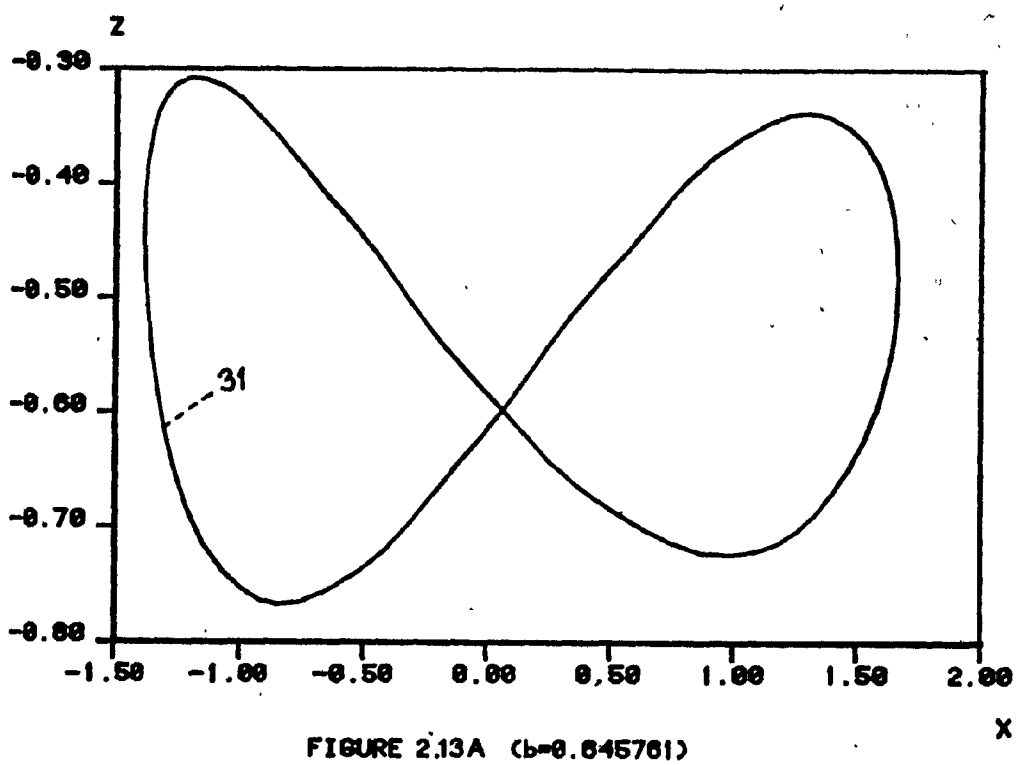

FIGURE 2.13A (b=0.845761)

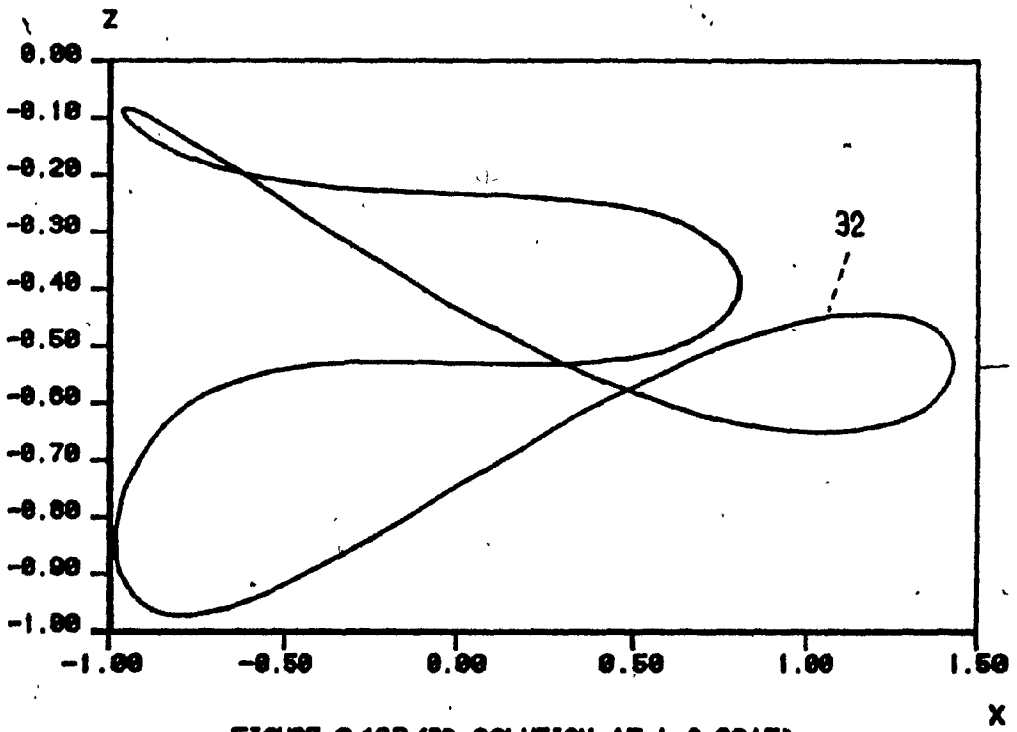

FIGURE 2.13B (PD SOLUTION AT b=0.3015)

2.4 Bifurcation behaviour of a biochemical system

The following model may not be directly related to turbulence in a fluid flow, however it is an example that shows chaotic behaviour of a dynamical system can occur via a sequence of bifurcations and loss of stability. Also this model exhibits a bifurcation behaviour which is very complicated and on the other hand very interesting.

Rhythmic behaviour is a property of living systems that is encountered at all levels of biological organizations. Most biological oscillations have a stable period and amplitude but in some cases complicated oscillations are also observed. Finding the mechanism of periodic behaviour sometimes can be reduced to finding the mechanism producing instability. A question therefore arises as to what happens when two instability-generating mechanisms are operating in the same system?

Among oscillations in biology, enzymatic periodicities are best understood at the molecular level. These oscillations, which have a period of several minutes, are of interest both for their role in metabolic pathways and as general models for biological rhythms. In 1982, O.Decroly and A.Goldbeter [6] considered a biochemical system with two allosteric enzymes for the study of biorhythmic behaviour. The two allosteric enzymes are coupled in series and each of them can be activated by their respective products. In [6],

they showed that the variety of possible types of dynamical behaviour is greatly increased.

Allosteric enzymes are key metabolic enzymes. They have dependent substrate binding sites, i.e the binding of one substrate molecule induces structural or electronic changes that result in altered affinities for the vacant sites. This can affect the way that the next substrate molecule is bound with the enzyme. In other words, the catalysis rate of the enzyme on the reaction between the substrates can be modified by the catalysis itself. The reaction rate of an allosteric enzyme can also be modulated by its allosteric effectors (positive effector or allosteric activator for increasing the rate; negative effector or allosteric inhibitor for decreasing the rate).

The system can be written as

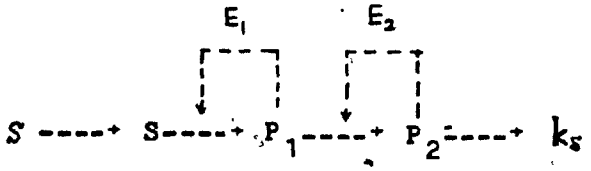

where S, P_1 and P_2 represent the original substrate, product 1 and product 2 respectively. E_1, E_2 stand for the two allosteric enzymes. s is the injection rate of substrate S and k is the rate of removal of product 2. The feedback loops of the two allosteric enzymes E_1, E_2 create two

instability generating mechanisms in the system and lead to a wide variety of dynamical behaviours.

O.Decroly and A.Goldbeter write the time evolution of the metabolite concentrations as

$$\begin{cases} \frac{du}{dt} = \frac{s}{k_{m1}} - \sigma_1 A \\ \frac{dv}{dt} = q_1\sigma_1 A - \sigma_2 B \\ \frac{dw}{dt} = q_2\sigma_2 B - kw \end{cases} \qquad (2.16)$$

with

$$A = \frac{u(1+u)(1+v)^2}{L_1+((1+u)(1+v))^2}$$

and

$$B = \frac{v(1+w)^2}{L_2+(1+w)^2}.$$

In system (2.16),

$$u = \frac{\bar{u}}{K},\ v = \frac{\bar{v}}{K},\ w = \frac{\bar{w}}{K}$$

with $\bar{u}$, $\bar{v}$ and $\bar{w}$ denote the concentration of S, P_1 and P_2 respectively. $K=K_{p1}K_{p2}$, where K_{p1} is the dissociation constant of P_1 for E_1 and K_{p2} is the dissociation constant of P_2 for E_2 (i.e. the ways that E_1 and E_2 affect the reaction $S\dashrightarrow P_1$ and $P_1\dashrightarrow P_2$). Also in system (2.16), s is the rate of input of the substrate S, k is the rate of removal of the substrate P_2 and $q_1=K_{p1}^{-1}$, $q_2=K_{p1}K_{p2}^{-1}$. Finally L_1, L_2 are the allosteric constants of enzymes E_1, E_2

respectively and they regulate the allosteric effect that E_1, E_2 can have on the substrates. With a small value of the allosteric constant L, the reaction between substrates regulated by the corresponding enzyme is more favoured. For example, in (2.16) a small value of L_1 implies that the value of A is large and thus the rate of increase of u is small. In other words, the reaction $S \rightarrow P_1$ is favoured and more of S is consumed in the reaction.

The reaction rates A and B follow the assumption that E_1 and E_2 are both dimers, i.e. the exclusive binding of ligands create more active conformational state and thus increases the rate of the reaction further. This can be seen from the quadratic terms in the expressions of A and B. For example, in the expression of B, the dominate quadratic term only involves the concentration of P_2 which is w. The difference in the expressions of A and B implies that the two reactions activated by the enzymes E_1 and E_2 are different. This feature is essential for the complicated dynamics in the system.

The formulation of system (2.16) is straight-forward the rate of change in the concentration of substrate S ($\frac{du}{dt}$) is the input rate of S subtracting the reaction rate that leads from S to P_1. This reaction is activated by the enzyme E_1 and therefore the maximum activity σ_1 of E_1 is involved. The rate of change in the concentration of product P_1 ($\frac{dv}{dt}$) is the rate that P_1 is produced subtracting the rate that P_1

is used to produce P_2. The reaction from P_1 to P_2 is activated by E_2 and therefore the maximum activity σ_2 of E_2 is involved. The rate of change in the concentration of product P_2 ($\frac{dw}{dt}$) is the rate that P_2 is produced subtracting the rate that P_2 is removed from the reaction.

In their computations, O.Decroly and A.Goldbeter relied heavily on the traditionally used initial value methods. However, initial value methods often encounter difficulties in locating unstable solutions. Furthermore, if two asymptotically stable solutions exist simultaneously and are quite close to each other in the phase portrait, it would be quite difficult to locate both of them using initial value methods. Since AUTO can overcome these problems quite easily, we use AUTO to re-examine system (2.16). Before we proceed we note that system (2.16) can be simplified considerably by applying some linear transformations and scaling out some of the parameters.

From the simulation in [6] we observe that the maximum activities σ_1, σ_2 of the two enyzmes E_1, E_2 can be set to be equal. Also, we can set $k_{p1}=1$ and thus $q_1= \frac{1}{q_2}$. Therefore system (2.16) can be written as

$$\begin{cases} \dfrac{du}{dt} = \dfrac{s}{\sigma_1} - A \\ \dfrac{dv}{dt} = q_1 A - B \\ \dfrac{dw}{dt} = \dfrac{1}{q_1} B - \dfrac{k}{\sigma_1} w \end{cases} \qquad (2.17)$$

with

$$A = \frac{u(1+u)(1+v)^2}{L_1+((1+u)(1+v))^2}$$

and

$$B = \frac{v(1+w)^2}{L_2+(1+w)^2}.$$

With the transformations $x=1+u$, $y=1+v$, $z=1+w$ we can write system (2.17) as

$$\begin{cases} \dfrac{dx}{dt} = s_k - \dfrac{(x-1)xy^2}{L_1+(xy)^2} \\ \dfrac{dy}{dt} = q\,\dfrac{(x-1)xy^2}{L_1+(xy)^2} - \dfrac{(y-1)z^2}{L_2+z^2} \\ \dfrac{dz}{dt} = \dfrac{1}{q}\,\dfrac{(y-1)z^2}{L_2+z^2} - k_s(z-1) \end{cases} \qquad (2.18)$$

where $s_k = \frac{s}{\sigma_1}$, $q=q_1$ and $k_s = \frac{k}{\sigma_1}$.

System (2.18) has three parameters less than system (2.16) and is considerably simpler. A global bifurcation diagram using k_s as a free parameter is given in Figure 2.14. The other four parameters have the following values

$s_k = 0.045$

$q = 50$

$L_1 = 5 \times 10^8$

$L_2 = 100.$

There are three basic solution branches in the bifurcation diagram shown in Figure 2.14, namely one steady state branch (branch 1) and two periodic solution branches (branch 2, branch 3). At low values of k_s, branch 1 is unstable. Branch 1 changes its stability at $k_s = 0.7906$ and a Hopf bifurcation is detected. As branch 1 becomes stable, branch 2 is developed from this Hopf bifurcation point. At $k_s = 1.585$, branch 1 changes its stability again and another Hopf bifurcation point is detected. From this second Hopf bifurcation, branch 3 is developed. When first bifurcating from branch 1, branch 2 is unstable. However, at $k_s = 1.821$, one eigenvalue enters the unit circle through positive one. Branch 2 changes its stability and turns backward.

In the parameter range $0 \leq k_s \leq 0.7906$, since the steady state branch 1 is unstable, the dynamics of the system are dominated by the periodic solutions on branch 2. In range $0.7906 \leq k_s \leq 1.585$, the steady state branch 1 becomes stable. As the periodic solution branch 2 keeps its stability, given a value of k_s, the system can either reside on the steady state solution on branch 1 or the periodic solution on branch 2 depending on the initial conditions. Although another segment of branch 2 also exists in this range, it

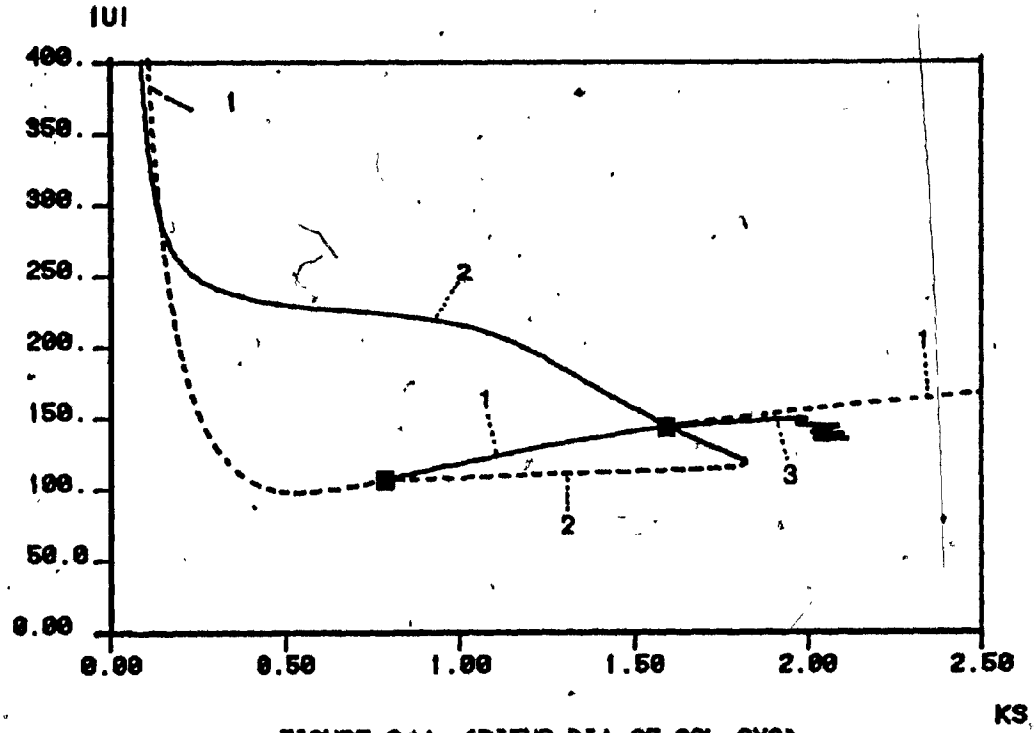

FIGURE 2.14 (BIFUR DIA OF GOL SYS)

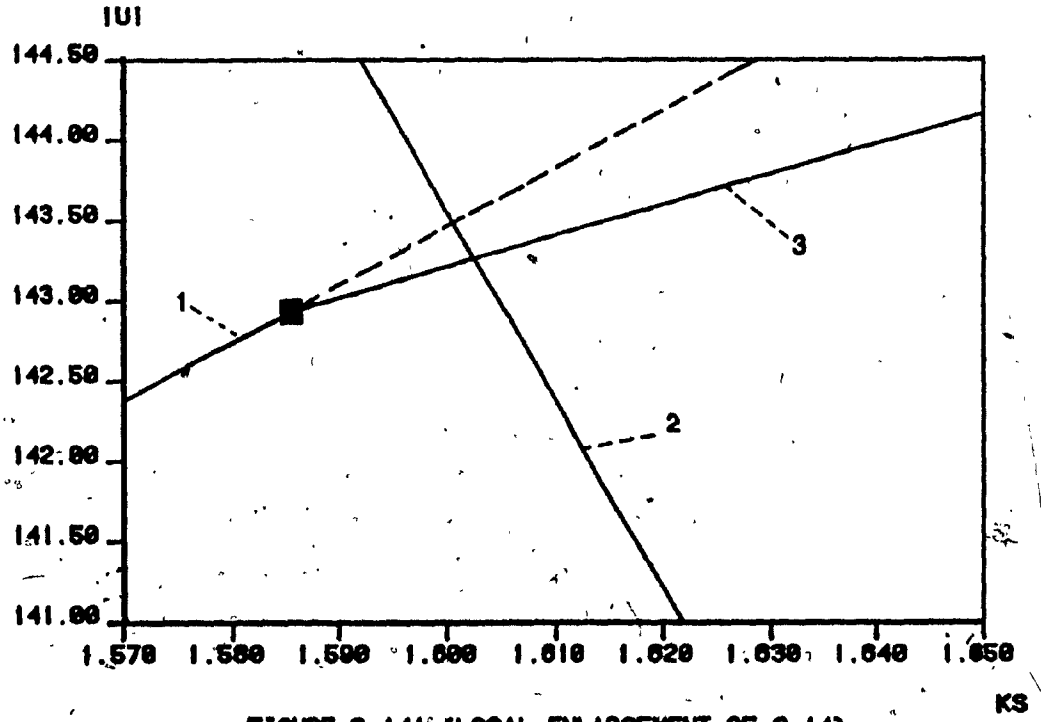

FIGURE 2.14A (LOCAL ENLARGEMENT OF 2.14)

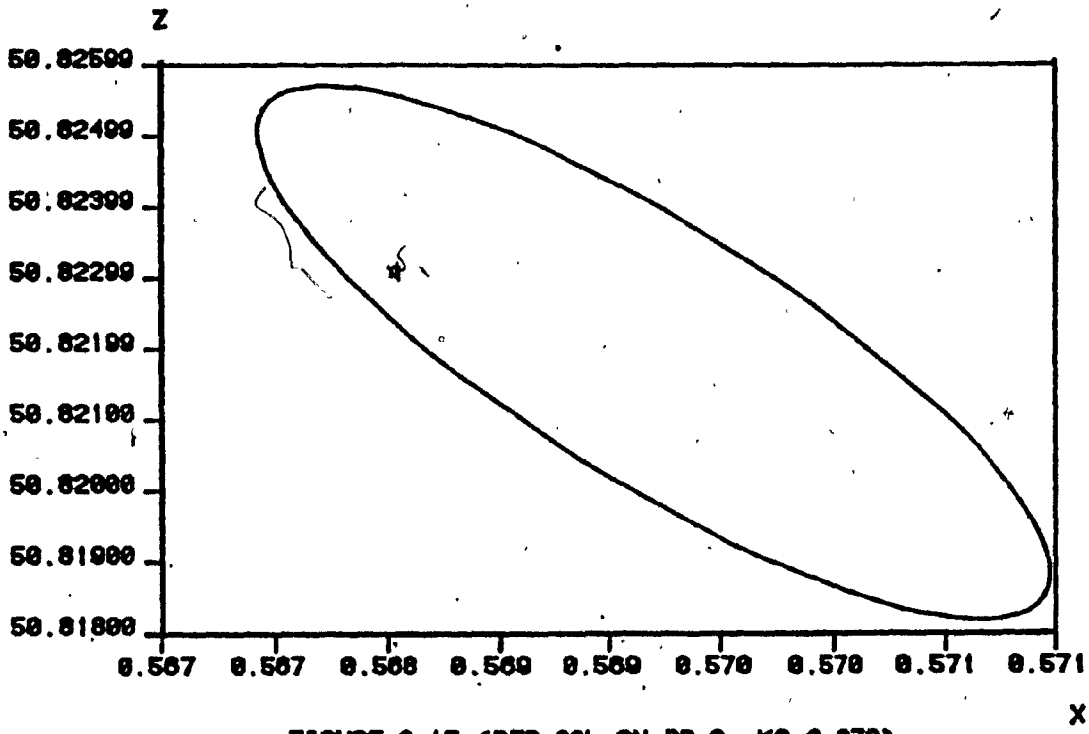

FIGURE 2.15 (PER SOL ON BR 2, KS=0.079)

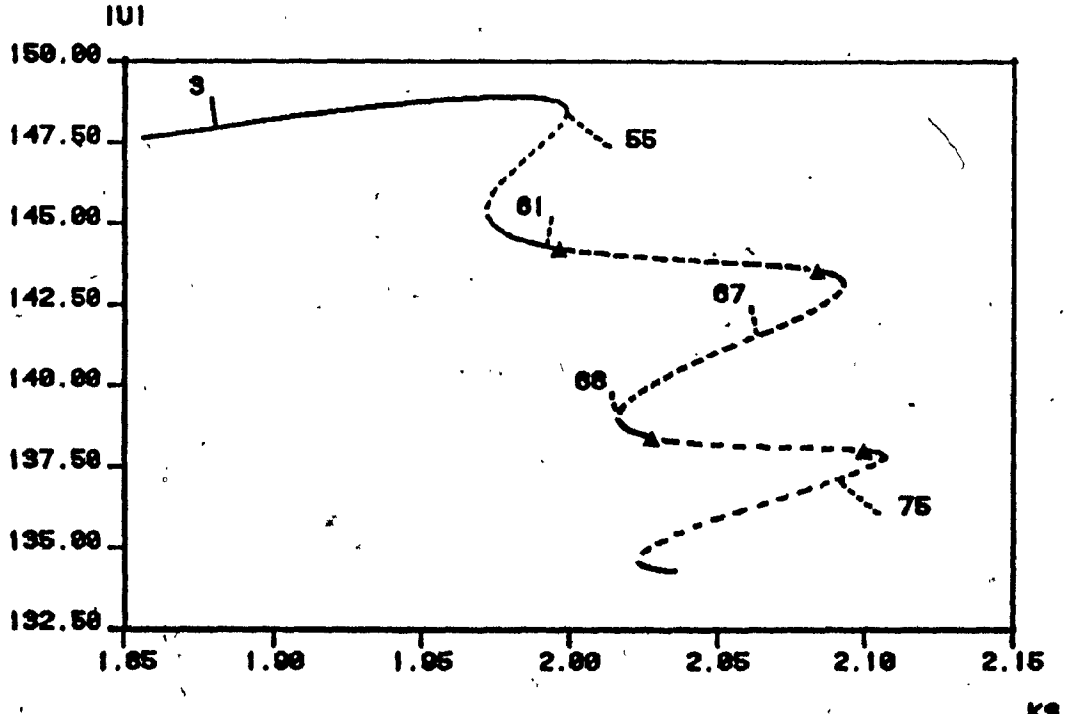

FIGURE 2.16 (LOCAL ENLARGEMENT OF 2.10)

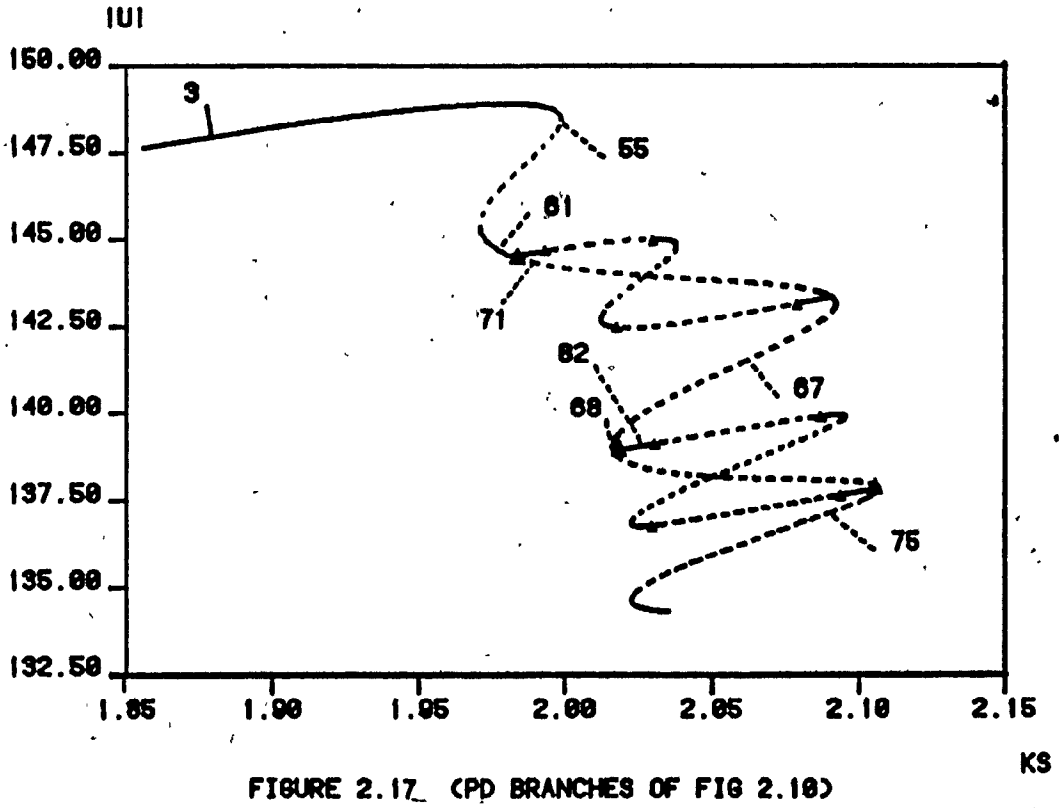

FIGURE 2.17 (PD BRANCHES OF FIG 2.16)

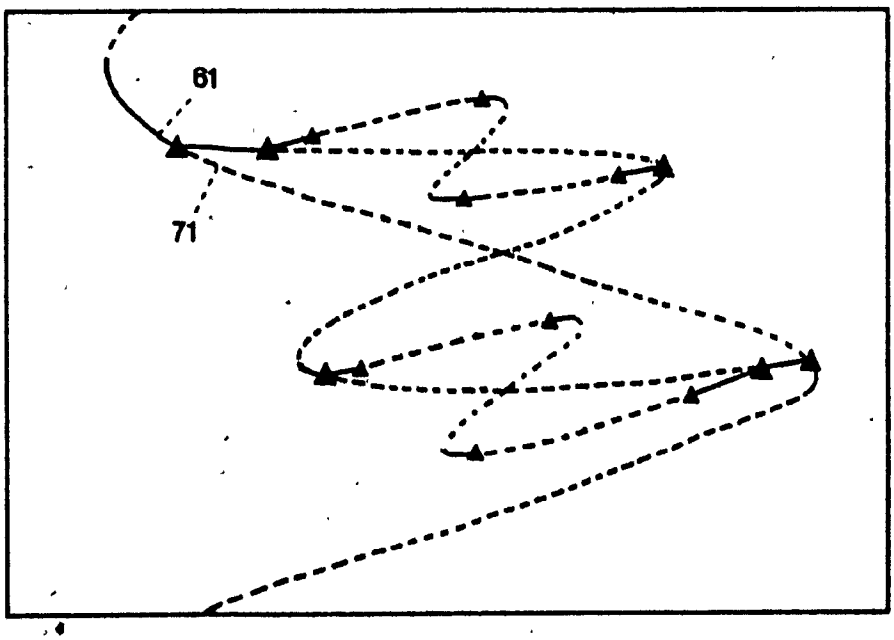

FIGURE 2.18 SCHEMATIC DIAGRAM

does not affect the periodic behaviour of the system due to its unstable character. In the range $1.585 \leq k_s \leq 1.821$, branch 1 becomes unstable and the periodic solution branch 3 appears. In this parameter range, given a value of k_s, the system can reside on either the periodic solution on branch 2 or the periodic solution on branch 3 depending on the initial conditions. We note that the periodic solutions on branch 2 and 3 differ significantly in period and amplitude. For a periodic solution on branch 2, see Figure 2.15. After $k_s = 1.821$, the dynamics of the system follows branch 3.

The bifurcation behaviour of branch 3 is extremely interesting. A local enlargement of branch 3 is given in Figure 2.16. Note the many turning points and period doubling bifurcations. The stability of the branch changes each time when a turning point or a period doubling bifurcation point is encountered. Restarting the computation at these period doubling bifurcation points, we obtain other short branches of periodic solutions. See Figure 2.17. On each of these new periodic solution branches, four period doubling bifurcations are found again. In fact, we expect these cascading bifurcations will continue. See Figure 2.18 for a schematic diagram. The orbit of some of the periodic solutions on branch 3 is given in Figure 2.19 - 2.23.

Due to the cascading phenomenon of branch 3, we note that in certain small intervals in the parameter range $1.974 \leq k_s \leq 2.1$ there may exist many stable periodic solutions of the system. Whether the dynamics of the system is attracted by any of these stable periodic solutions depends on the initial conditions. Therefore, in these k_s-intervals, the system is highly sensitive to initial conditions and exhibits complicated dynamical behaviour.

Complicated dynamical behaviour often comes with strange attractors. In [6], the existence of strange attractors in the parameter region $2.0 < k_s < 2.034$ is reported. See Figure 2.24 for a strange attractor found at $k_s = 2.0$. Once again, according to our computation, we know that many unstable periodic solutions exist and are very close to each other in this region. When a trajectory enters this attracting area, it is "pushed around" by the unstable periodic solutions and causes the complicated dynamical behaviour of a strange attractor. This "pushed around" effect can be easily seen by comparing Figure 2.24A, 2.24B and Figure 2.19-2.23. Periodic solutions shown in Figure 2.19-2.23 are found in the parameter range $1.95 < k_s < 2.1$ (see Figure 2.16 and Figure 2.17). We note that the parameter value at which the strange attractor exists also lies in this parameter range. From Figure 2.24 we see that this strange attractor has a "layered" structure. The shape of each layer is very similar to the shape of the

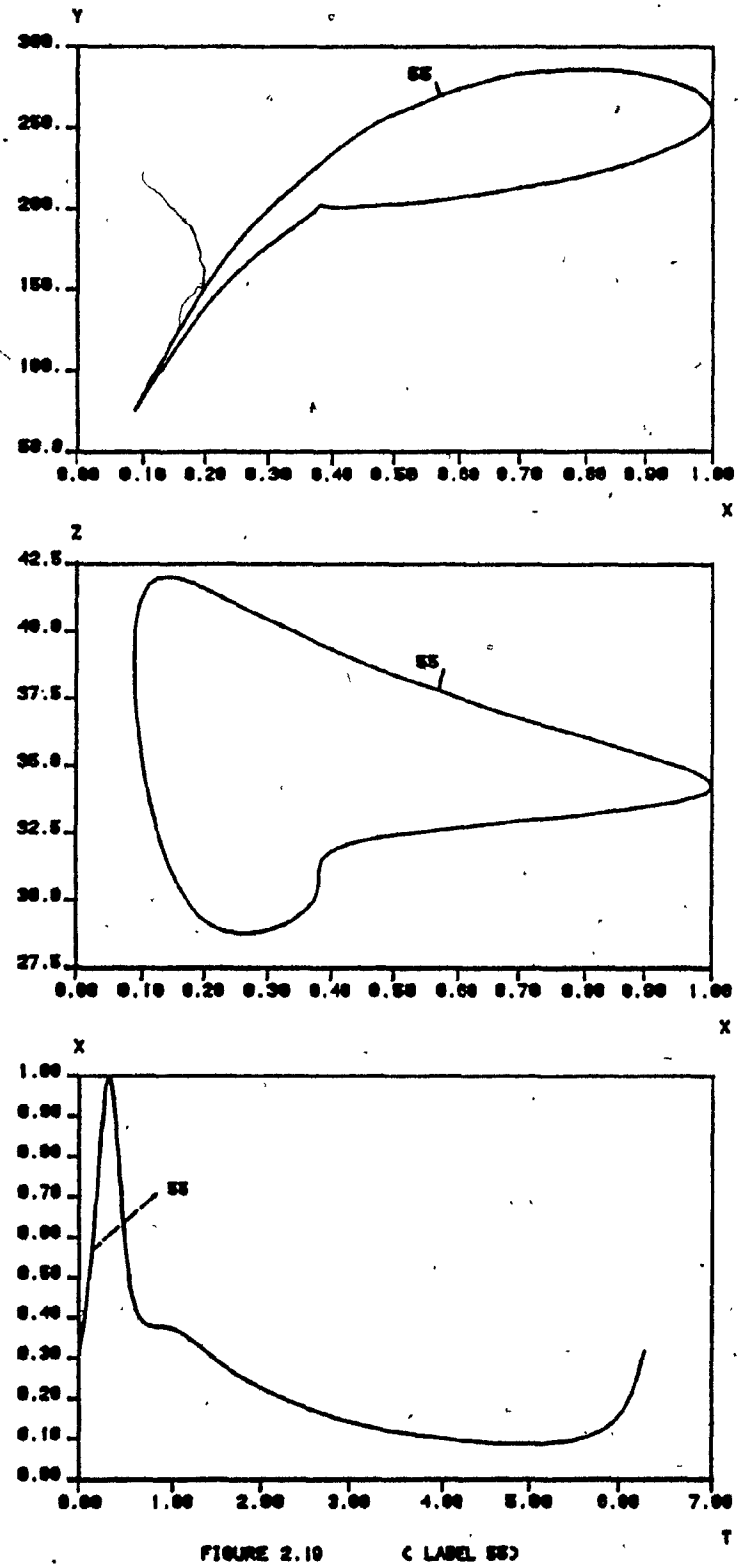

FIGURE 2.10 (LABEL SS)

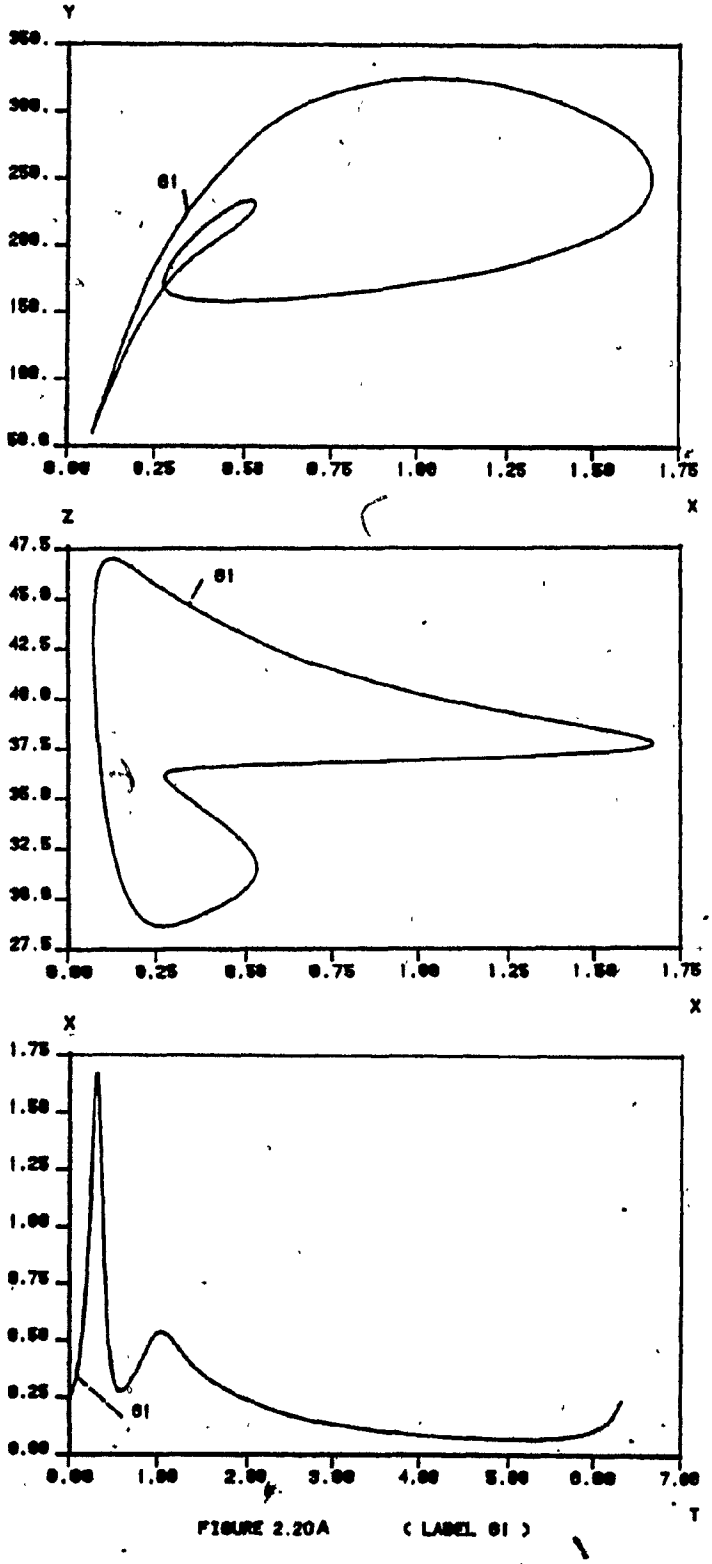

FIGURE 2.20A (LABEL 61)

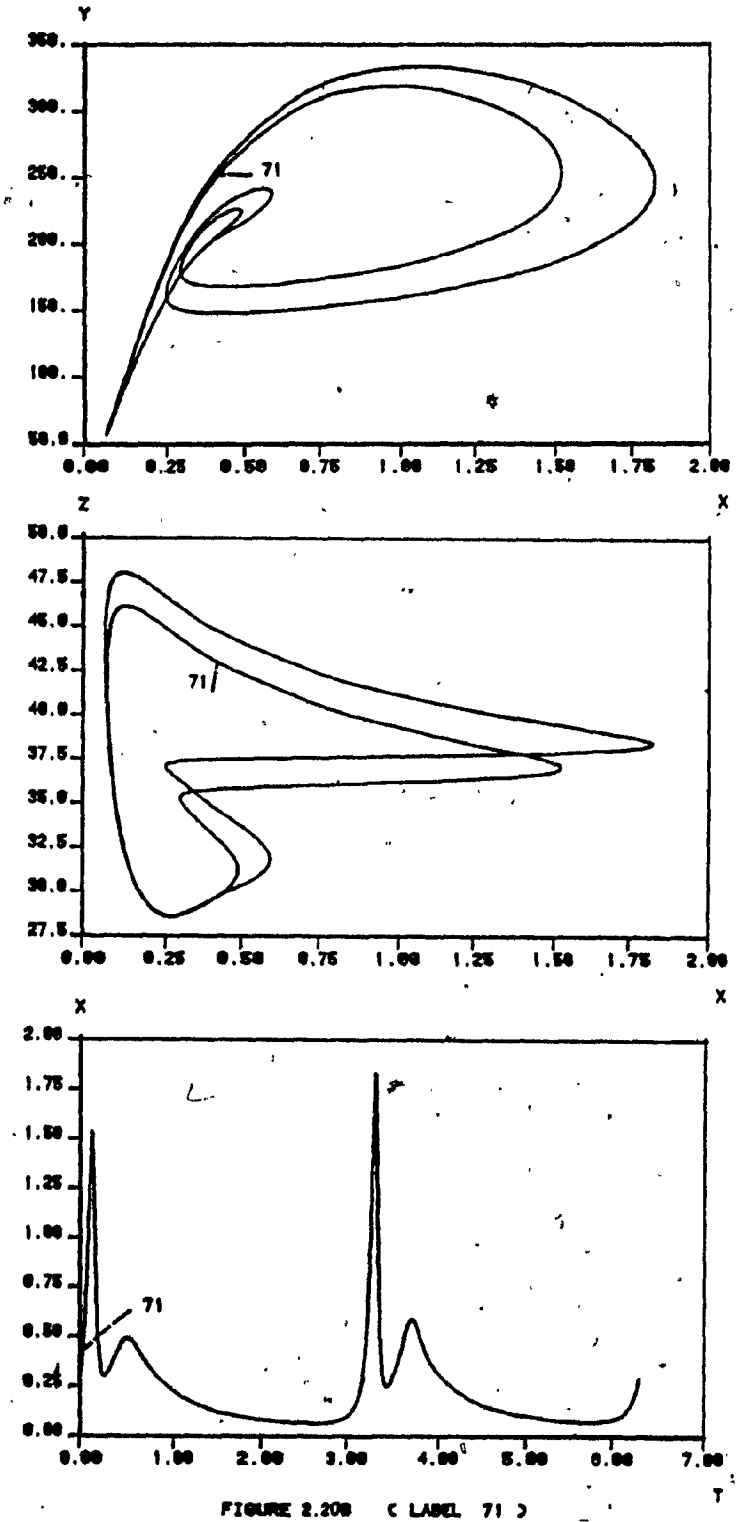

FIGURE 2.208 (LABEL 71)

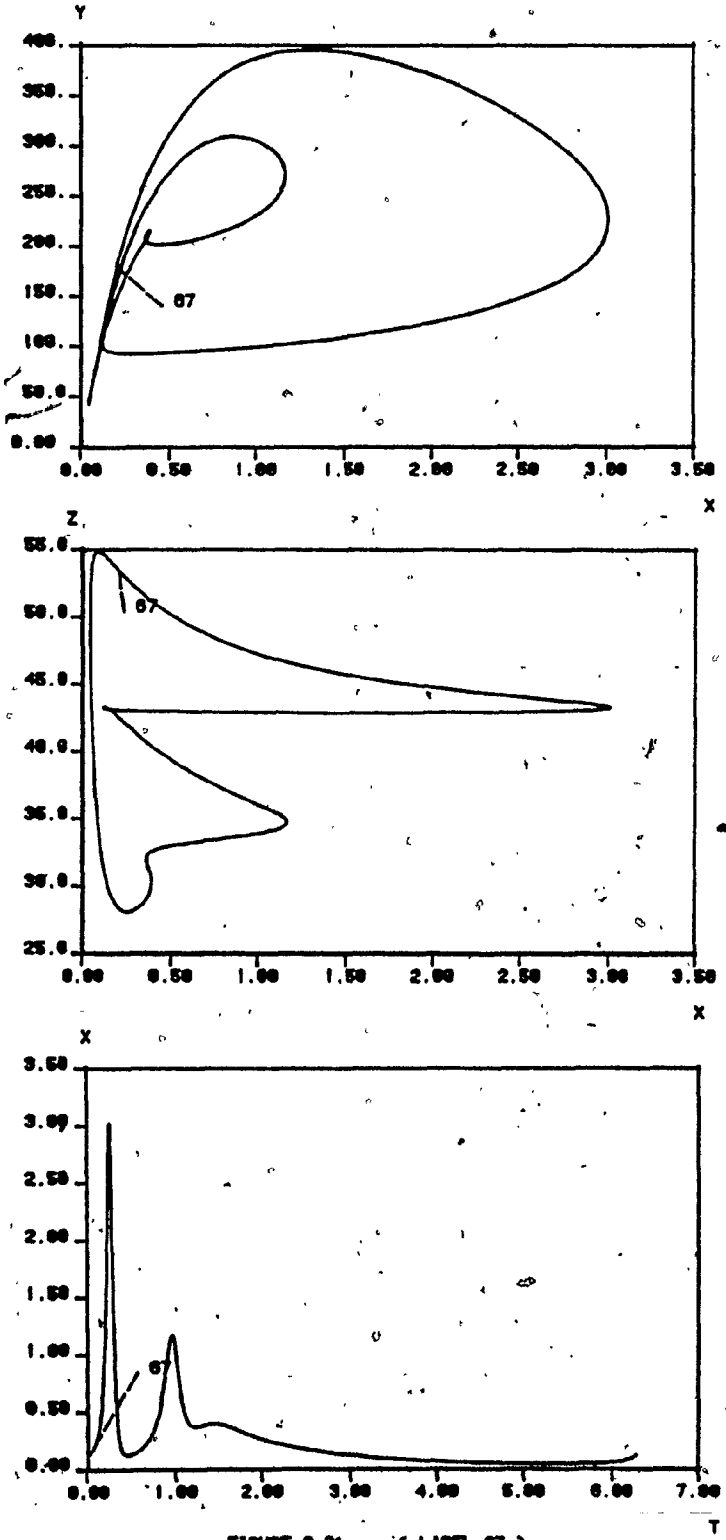

FIGURE 2.21 (LABEL 67)

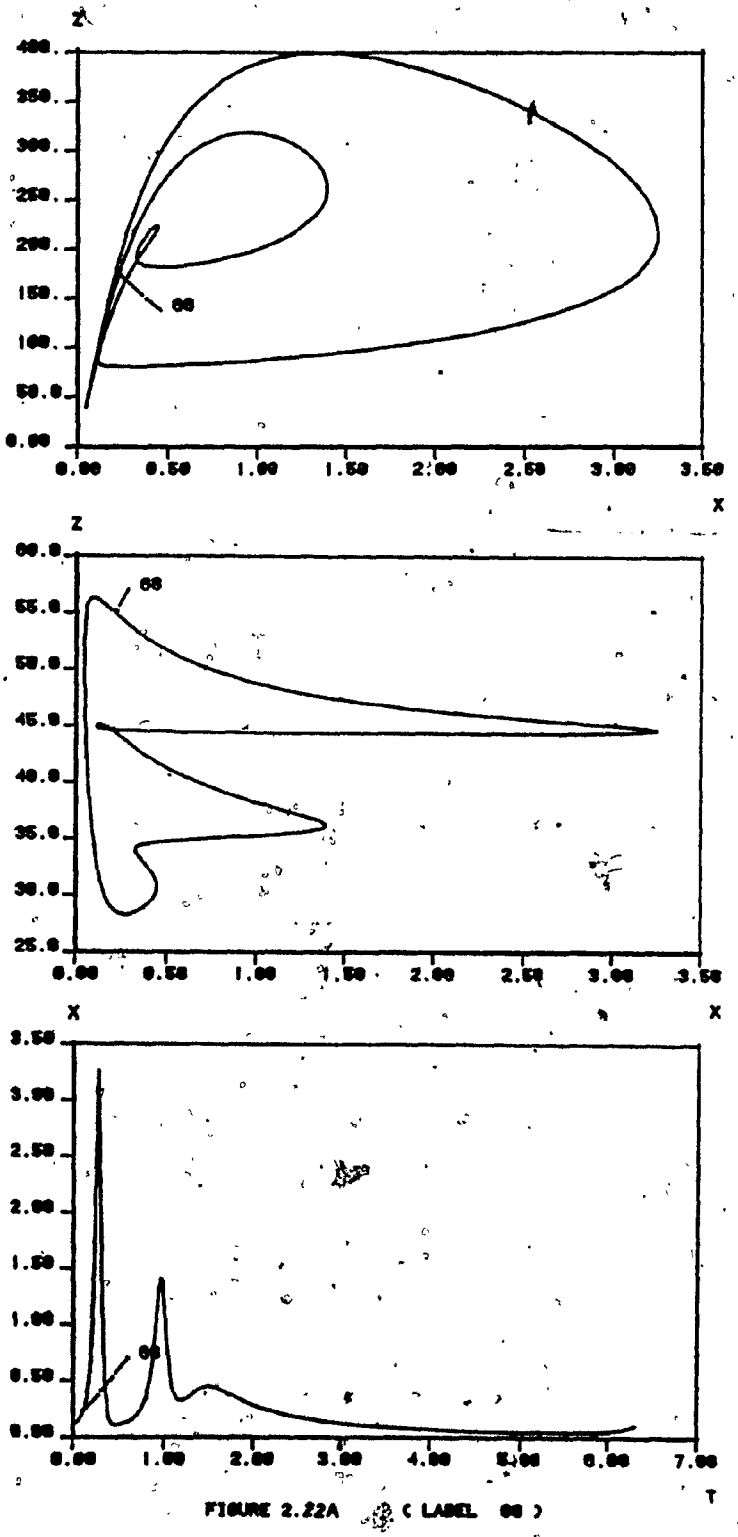

FIGURE 2.22A (LABEL 66)

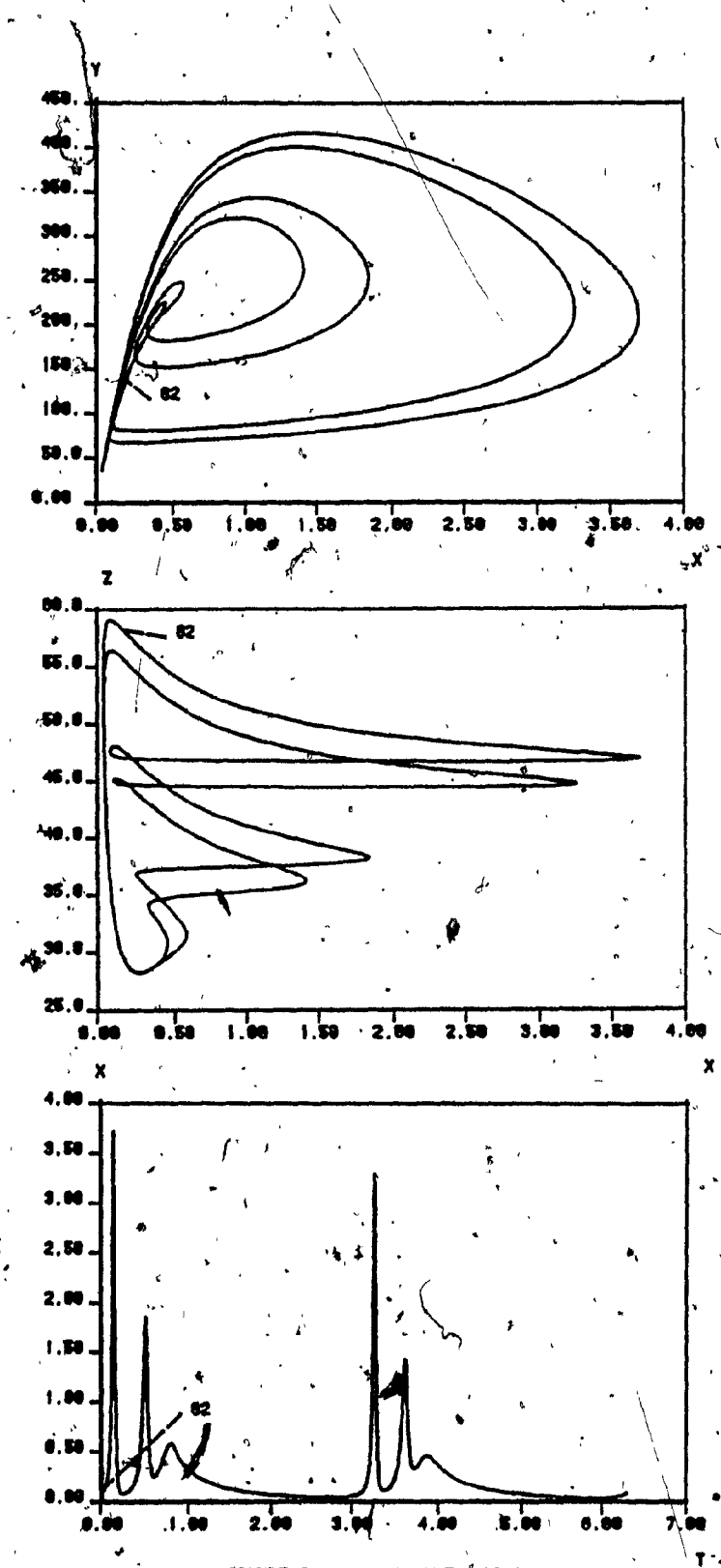

FIGURE 2.22B (LABEL '82)

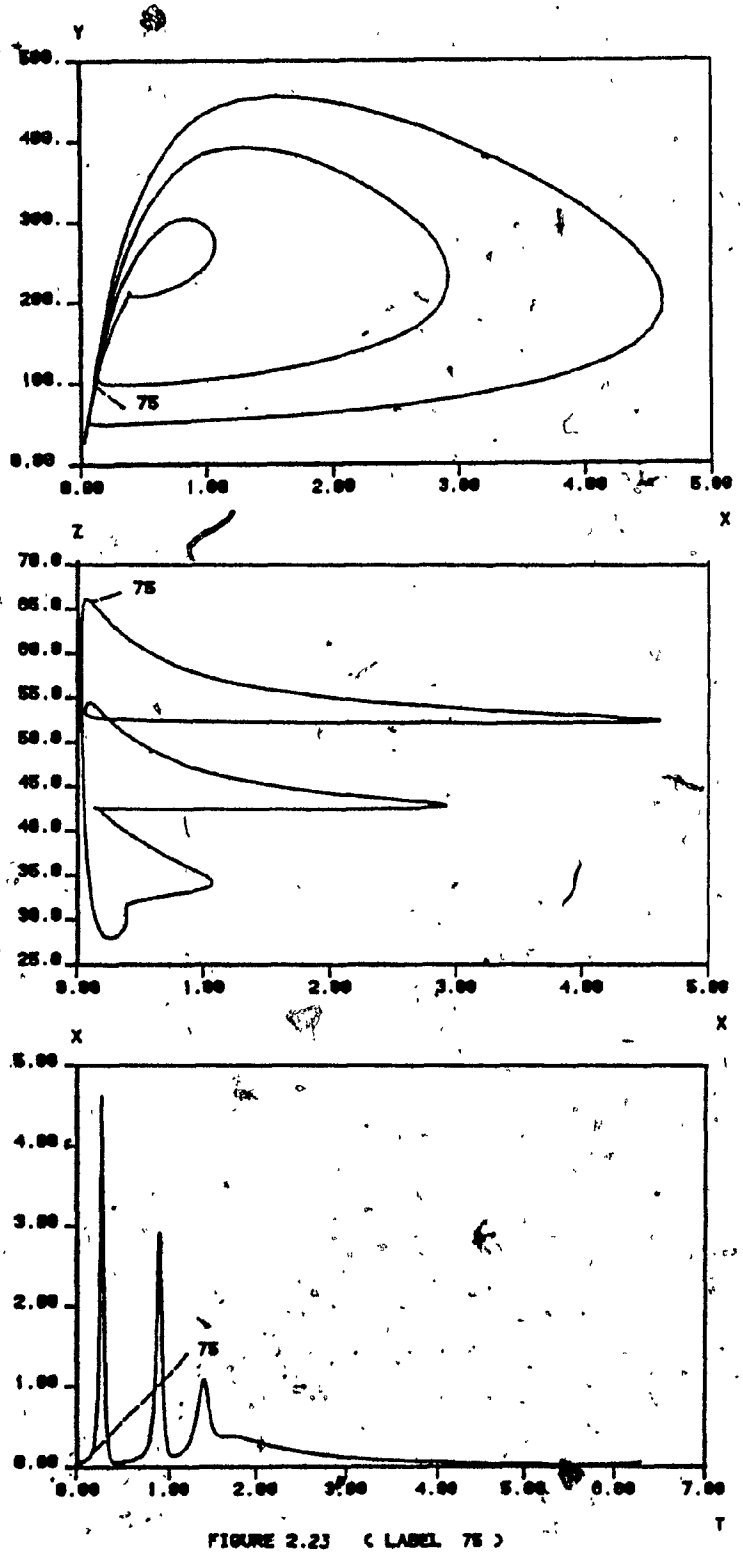

FIGURE 2.23 (LABEL 75)

periodic solutions shown in Figure 2.19-2.23.

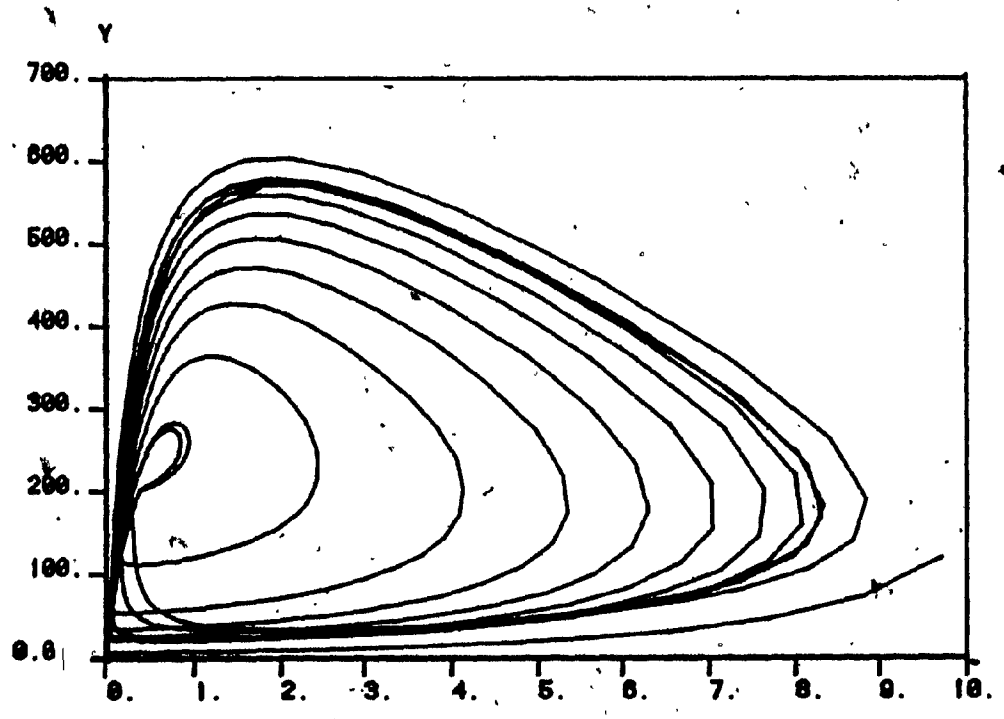

FIGURE 2.24A (STRANGE ATTRACTOR KS=2.0)

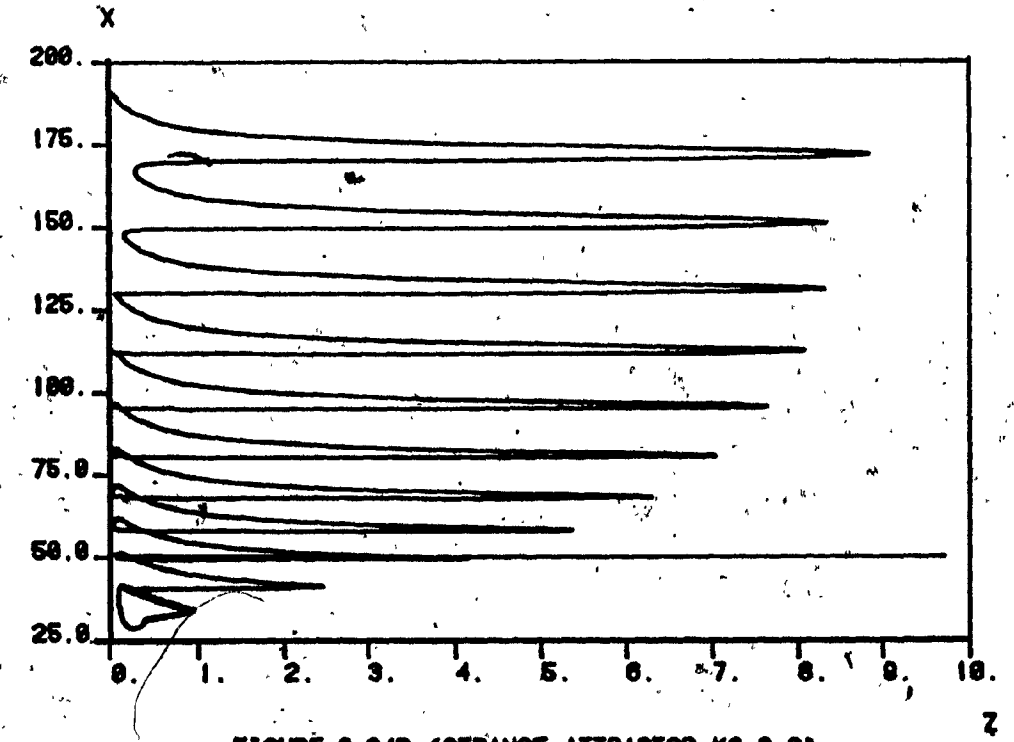

FIGURE 2.24B (STRANGE ATTRACTOR KS=2.0)

2.5 Summary

All three models discussed in this chapter deserve more detailed studies and computations. A more complete bifurcation diagram (i.e. with more periodic solution branches) for the Lorenz system could be revealing. The fact that in $14.5<r<50$, many unstable periodic solutions exist and are close to each other might explain the dynamical nature of the Lorenz attractor. Once a trajectory enters the Lorenz attractor, it wanders between unstable periodic solutions and can never settle down because of the unstable character of the solutions.

The reason we also chose to consider the transformed Lorenz system is that it is simpler than the Lorenz system and also exhibits chaotic dynamics. The cascading sequence of period-doubling bifurcation branches in this model can be seen and described more clearly. A cascading sequence of period doubling bifurcations is observed in many systems including the Lorenz system. The particular sequence in the transformed model also makes clear that a cascading sequence of period doubling bifurcations can occur in both directions and possibly lead to a common chaotic region.

In the enzyme model, multiple cascading sequences of period doubling bifurcations are found. They presumably lead to the existence of many chaotic regions. The chaotic dynamical behaviour in each of these regions is similar to

the chaotic behaviour found in the transformed Lorenz system. It is caused by the existence of stable periodic solutions of arbitrarily high period and also the simultaneous existence of many stable periodic solutions in the same parameter region. High sensitivity to initial conditions in this area is the result. Strange attractors are also found in this model. We believe that the chaotic dynamical behaviour inside these attractors is the result of the boundedness of the flow and the existence of many unstable periodic solutions.

CHAPTER THREE

The Poincare Map and

The Centre Manifold Theorem

Consider a differential equation

$$u'(t) = f_\lambda(u(t)) \qquad (3.1)$$

where $f_\lambda : W \to R^n$, $W \in R^n$ is open and λ is a parameter in R. We suppose f_λ is C^1. As mentioned in Chapter 1, a steady state solution $\bar{u}$ is stable if all the eigenvalues of $f'_\lambda(\bar{u})$ have negative real parts. For a periodic solution u(t), it is stable if all the eigenvalues of $\Phi'(u_0)$ have absolute value less than one, where $u_0 \in u(t)$ and Φ is the flow of equation (3.1). When λ changes, the Hopf bifurcation theorem gives sufficient conditions for the loss of stability of a steady state solution and the bifurcation to periodic solutions. Thus a very natural question to ask is : what is the next kind of bifurcation behaviour that can possibly occur when a periodic solution loses its stability ? In fact, under certain conditions, invariant tori can result.

3.1 Poincare map

One way to study the dynamics of (3.1) is to study the Poincare map induced by the flow Φ defined by f_λ. The

phenomenon of bifurcation to invariant tori can be clearly explained using the idea of a Poincare map. The following ideas can be found in [4] and [17].

To illustrate the concept of a Poincare map, we start by recalling that a hyperplane of R^n is an (n-1)-dimensional linear subspace of R^n. Consider the flow ϕ of the C^1 vector field f_λ and let $\phi(u_0) \subset W$ be a closed orbit. Suppose S is an open subset of a hyperplane H of R^n, which is transverse to the vector field f_λ at u_0, i.e. $f_\lambda(u) \notin H$ for any u in S. If ρ is the period of $\phi(u_0)$, then as time increases past ρ, the solution curve $\phi(u_0)$ crosses S again at u_0. If u_1 is sufficiently close to u_0, there will be a time $\gamma(u_1)$ near ρ when $\phi_{\gamma(u_1)}(u_1)$ crosses S. Therefore a map

$$g: U \to S$$

with

$$g(u) = \phi_{\gamma(u)}(u)$$

is in obtained, where u is a neighbourhood U of u_0.

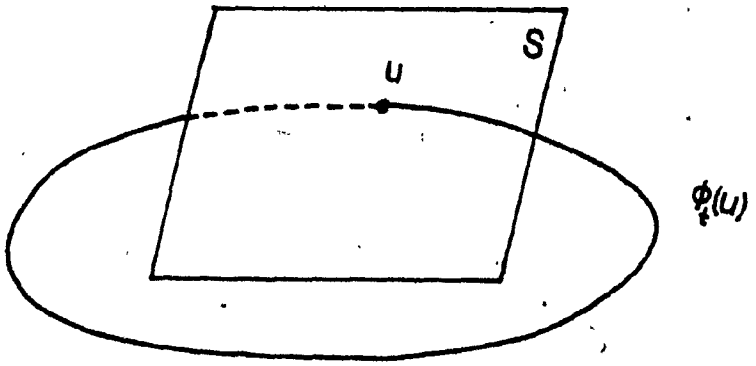

FIGURE 3.1

However g will not be well defined if the time map τ is not unique. This can be easily seen from the fact that if there exists another time map $\bar{\tau}$ such that $\phi_{\bar{\tau}(u_1)}(u_1)$ crosses S, then

$$\bar{\tau}(u_1) \neq \tau(u_1)$$

implies that

$$\phi_{\bar{\tau}(u_1)}(u_1) \neq \phi_{\tau(u_1)}(u_1).$$

Fortunately, the following Theorem (3.1) guarantees the uniqueness of the time map τ.

Theorem (3.1)

Let S be an open subset of the hyperplane $H \subset R^n$ transverse to a C^1 vector field $f:W \to R^n$. Suppose $u_0 \in S$ and $\phi_{t_*}(u_*) = u_0$. Then, there exists an open set $U \subset W$ containing u_* and a unique C^1 map $\tau:U \to R$ such that

$$\tau(u_*) = t_*$$

and

$$\phi_{\tau(u)}(u) \in S$$

for all u in U.

A proof of Theorem (3.1) can be found in [17]. Let u_* be a point in the state space and u_0 be a point lying on a hyperplane S transverse to the vector field f_λ of a flow ϕ. In simple words, Theorem (3.1) tells us that, if the flow brings u_* to u_0 in time t_* then the flow also brings the

neighbouring points of u_* to points on S in uniquely defined times subject to t_*. See Figure 3.2.

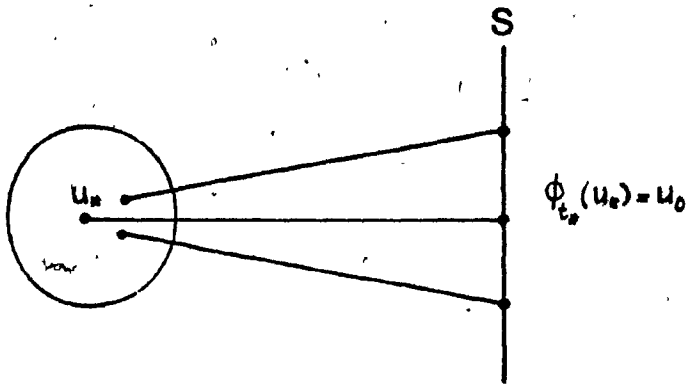

FIGURE 3.2

Now if we put $S_0 = S \cap U$ (S and U are as defined in Theorem (3.1)) and define a C^1 map

$$p: S_0 \to S$$

such that

$$p(u) = \phi_{\gamma(\Omega)}(u),$$

then p is called a <u>Poincaré map</u> of $\phi(u_0)$. In order to indicate that p also depends on λ, we write p as p_λ. See Figure 3.3. From theorem (3.1) we know that given any vector field f_λ, a point u_0 on a periodic orbit ϕ in the flow defined by f_λ, and a hyperplane H transverse f_λ at u_0, a Poincaré map is uniquely determined. We also note that, since ϕ is a diffeomorphism, p_λ is a diffeomorphism, and p_λ is itself a discrete dynamical system with a fixed point u_0.

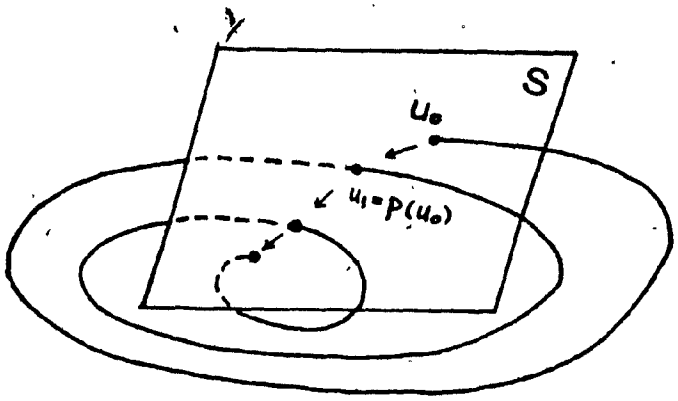

FIGURE 3.3

For example if ϕ lies in R^3, then the corresponding Poincaré map p_λ is a diffeomorphism in R^2.

The Poincaré map p_λ provides a powerful tool for analyzing the qualitative behaviour of the solution curves of the differential equation near $\phi(u_0)$. For example, if p_λ has a fixed point v_0 in addition to u_0, then the solution curve $\phi(v_0)$ is again periodic. More generally, if v_0 is a periodic point of period n for p_λ, the solution curve $\phi(v_0)$ is again periodic but crosses S_0 n times before it comes back to v_0 again. Therefore, if v_0 is asymptotically stable, so is $\phi(v_0)$. Further, suppose there is a circle $\Gamma \subset S_0$ which is invariant under p_λ, then $\bigcup_t \phi(\Gamma)$ is an invariant torus for the flow ϕ. We have the following analogue of Theorem (1.3) given in section 1.6.

Theorem (3.2)

Let v_0 be a fixed point of a discrete dynamical system $p_\lambda : U \dashrightarrow R^n$, $U \subset R^n$. If the eigenvalues of $p_\lambda'(v_0)$ are less than 1 in absolute value, v_0 is asymptotically stable.

In order to apply the above idea of a Poincaré map, we need to compute all the eigenvalues of p_λ' because the stability of the fixed point v_0 is determined by the absolute value of the eigenvalues. However, it is often very difficult, if not impossible, to find an explicit expression of p_λ given a flow ϕ of some vector field f_λ. Therefore it is very desirable if we can establish some association between the set of all eigenvalues of $\phi'(v_0)$ and the set of all eigenvalues of $p_\lambda'(v_0)$.

We let $\sigma(T)$ be the set of all eigenvalues of a linear transformation $T: R^n \to R^n$. $\sigma(T)$ is called the spectrum of T. The following theorem gives the relationship between $\sigma(\phi'(v_0))$ and $\sigma(p_\lambda'(v_0))$.

Theorem (3.3)

Let $f_\lambda : W \to R^n$ be a C^1 vector field defined on an open subset $W \subset R^n$, and ϕ be the corresponding flow of the equation

$$u'(t) = f_\lambda(u(t)) \qquad u, f \in R^n.$$

Let $\phi(v_0)$ be a periodic solution and p_λ be the Poincaré map

with a fixed point at v_0 induced by $\phi(v_0)$. Then

$$\sigma(\phi'(v_0)) = \sigma(p_\lambda'(v_0))U(1)$$

3.2 The Hopf bifurcation theorem for diffeomorphisms

In 1971 D.Ruelle and F.Takens [33] gave an extension of the Hopf bifurcation theorem for differential equations. Their result gives the conditions under which bifurcation to invariant tori may be expected after the loss of stability of a periodic solution. This result is called the Hopf bifurcation theorem for diffeomorphisms by J.E.Marsden and M.McCracken [29]. We state without proof the theorem in the following. A proof of the theorem can be found in [26] [29] and [33].

For simplicity of notation we shall assume the stable periodic solution $u(t)$ for inducing the Poincaré map goes through the origin, and that the critical value for the loss of stability of $u(t)$ is occuring at $\lambda=0$.

Theorem (3.4) Hopf bifurcation theorem for diffeomorphisms

Let $\Psi_\lambda : R^2 \to R^2$ be a one parameter family of C^k $(k \geq 5)$ diffeomorphisms satisfying:

(1) $\Psi_\lambda(0) = 0$ for all $\lambda \in R$.

(2) For $\lambda = 0$, $\Psi'_\lambda(0)$ has two isolated, simple, complex conjugate eigenvalues $z(\lambda)$ and $\bar{z}(\lambda)$ such that

$$|z(\lambda)| = 1.$$

(3) $$\frac{d|z(\lambda)|}{d\lambda}\Big|_{\lambda=0} > 0.$$

(4) As one can always reparametrize so that the eigenvalues of $\Psi'_\lambda(0)$ have the form

$$(1+\lambda)e^{i\theta}\lambda,$$

one further assumes $e^{im\theta(0)} \neq 1$ for $m = 1,2,3,4,5$.

(5) Subject to (4), one can make a smooth λ-dependent change of coordinates such that

$$\Psi_\lambda = N\Psi_\lambda(u) + o(|u|^5)$$

where in polar coordinates

$$N\Psi_\lambda : (r,\rho) \to ((1+\lambda)r - f_1(\lambda)r^3, \rho + \theta_\lambda + f_3(\lambda)r^2).$$

If $f_1(0) > 0$, then for all sufficiently small positive λ, Ψ_λ has a family of attracting invariant circles. If $f_1(0) < 0$, then for all sufficiently small negative λ, Ψ_λ has a family of repelling invariant circles.

Now suppose the flow Φ lies in R^3. If at $\lambda=0$ $\Phi'(0)$ has a pair of complex conjugate eigenvalues cross the unit circle, by Theorem (3.2) and Theorem (3.3) we know that at $\lambda=0$ u(t) changes its stability and bifurcates into an invariant torus.

3.3 The centre manifold theorem

Although the diffeomorphism Ψ_λ considered in Theorem (3.4) is only two dimensional, the description of bifurcation to invariant tori implied in Theorem (3.4) via a Poincare map is still valid for flows of dimension higher than three. This is due to the virtue of a technical result called the center manifold theorem [3]

Theorem (3.5) Center manifold theorem

Let h be a mapping of a neighbourhood of zero in a Banach space B into B. Assume h is C^{k+1} and $h(0)=0$. Further, assume that the spectrum of $h'(0)$ is contained in the unit circle and the spectrum of $h'(0)$ splits into a part on the unit circle and the remaining part is at a nonzero distance from the unit circle. Let Y denote the generalized eigenspace of $h'(0)$ belonging to the part of the spectrum on the unit circle. Assume that Y has dimension $d<\infty$. Then there exists a neighbourhood V of 0 in B and a C^k submanifold M of V of dimension d, passing through 0 and tangent to Y at 0, such that

(1) (Local invariance): If $x \in M$ and $h(x) \in V$, then $h(x) \in M$.

(2) (Local attractivity): If $h^n(x) \in V$ for all $n=0,1,2,\ldots$ Then $d(h^n(x),M) \to 0$ as $n \to \infty$.

The main function of the center manifold theorem is to enable one to reduce an infinite dimensional problem to a finite dimensional one. In the case of bifurcation to invariant tori, it enables us to reduce the study of the Poincaré map to the study of a two dimensional diffeomorphism from which the Hopf bifurcation theorem for diffeomorphisms can be applied. Before we proceed to discuss how the reduction is actually made, we first recall that:

A subset S of a normed linear space E is called a submanifold of E if S has the following property:

For each $x \in S$, there is a neighbourhood U of x in E and a diffeomorphism $\varphi: U \to U'$, where U' is an open set in E such that

$$\varphi(S \cap U) = L \cap U'$$

where L is some affine subspace of E. φ is called a chart of S.

Informally, we can think of S as being glued together using pieces of a linear subspace of E (by changing φ we can take L to be the same for all x). The diffeomorphism φ also

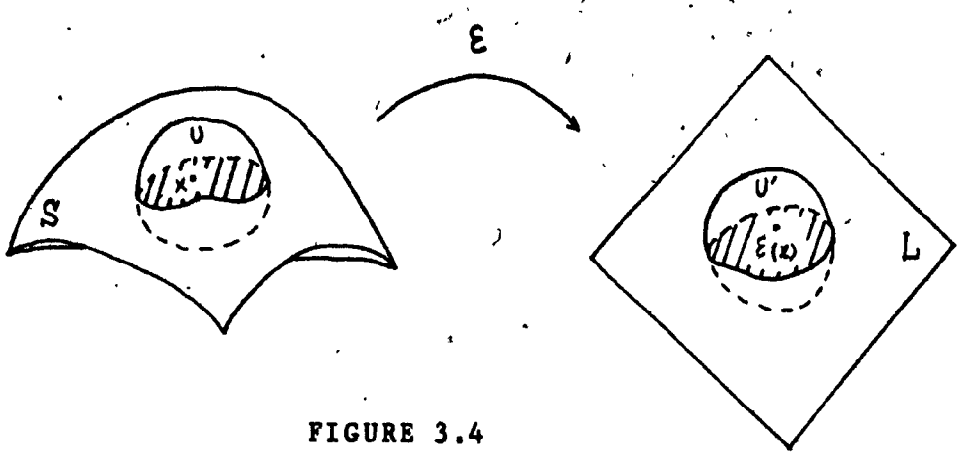

FIGURE 3.4

ensures that S has no 'corners'.

Now we come to the crucial step. We apply the center manifold theorem not to p_λ', but to the mapping

$$h: (u,\lambda) \to (p_\lambda(u),\lambda)$$

If $p_\lambda'(u_0)$ has two simple complex conjugate eigenvalues on the unit circle, then the generalized eigenspace Y for h' is three dimensional with one of the dimension in the λ direction. Thus the theorem asserts the existence of a three dimensional manifold M. If we hold λ fixed and sufficiently small, we obtain a two dimensional section M_λ of M which is locally invariant and attracting for p_λ. Since we are looking for reccurrent behavior, we can restrict p_λ to M_λ. M_λ is itself a two dimensional manifold and therefore can be equipped with certain coordinate charts. Now, the study is reduced to a smooth one parameter family of mappings ψ_λ defined in a neighbourhood of the

origin by p_λ together with a chart map of M_λ, having the property that $\psi_\lambda(0)=0$ and $\psi_\lambda'(0)$ has two distinct complex eigenvalues on the unit circle. Therefore the Hopf bifurcation theorem for diffeomorphisms can be applied.

CHAPTER FOUR

Computation of the Invariant Circles

The significance of the Hopf bifurcation theorem for diffeomorphisms does not only lie in the fact that it gives conditions for bifurcation to invariant tori for a differential equation. It is also important in the study of diffeomorphisms, which are often encountered in the modelling of population dynamics. One typical diffeomorphism that has been employed in modelling population dynamics is the delay logistic equation

$$N_{t+1} = \lambda N_t(1-N_{t-1}), \qquad (4.1)$$

where N_t stands for the population of the species at the t-th generation [1]. If we let $x_t=N_{t-1}$ and $y_t=N_t$ then equation (4.1) can be transformed into a two dimensional system

$$u_{t+1} = g_\lambda(u_t) \qquad (4.2)$$

where $u^T_t=(x_t,y_t)$ and

$$g_\lambda \begin{bmatrix} x \\ y \end{bmatrix} = \begin{bmatrix} y \\ \lambda y(1-x) \end{bmatrix} .$$

Here g_λ is a two dimensional diffeomorphism with a fixed

point at $x_2=y_2=\frac{\lambda-1}{\lambda}$. The Jacobian matrix of g_λ is :

$$g_\lambda' = \begin{bmatrix} 0 & 1 \\ -\lambda y & \lambda(1-x) \end{bmatrix}$$

Evaluating $g_\lambda'-\alpha I$ at $x_2=y_2=\frac{\lambda-1}{\lambda}$, where I is the identity matrix, we have the following characteristic equation :

$$\alpha^2 - \alpha + (\lambda - 1) = 0,$$

which has roots $\alpha = \frac{1\pm\sqrt{1-4(\lambda-1)}}{2}$. Therefore, we know that the fixed point is stable for $1<\lambda\leq 2$. As λ passes through the value 2, the fixed point loses its stability and from the Hopf bifurcation theorem for diffeomorphisms we know that invariant circles are developed [1]. In this case, the invariant circles are attracting and the local dynamics of g_λ is determined by these invariant circles.

Attempts have been made to compute these bifurcating invariant circles. In [1], the direct iteration of the map is used. This method is not very desirable because it fails if the invariant circles are repelling. Also the result is heavily influenced by the dynamics of the diffeomorphism on the circle. In [20], G. Iooss, A. Arneodo, P. Coullet and C. Tresser tried to obtain an explicit analytic expression of the invariant circles for general two dimensional diffeomorphisms. The expression turned out to be very

complicated.

In the following, we propose a numerical method to compute the invariant circles for a general two dimensional diffeomorphism $\psi_\lambda : R^2 \to R^2$. In order to efficiently compute the invariant circles, we utilize some dynamical properties of ψ_λ on these invariant circles. Therefore before we proceed to describe the numerical method, we first recall some properties of ψ_λ on the invariant cirles. These results are classical in the theory of diffeomorphisms [31].

4.1 Dynamics on the invariant circles

In this section, we introduce the definition of a rotation number of a diffeomorphism ψ_λ. Many interesting dynamical properties of ψ_λ on an invariant circle can be described in terms of its rotation number.

Denote an invariant circle by S^1. Due to the invariance property, we can restrict the diffeomorphism ψ_λ to S^1 as

$$\psi_\lambda : S^1 \to S^1.$$

If we assume ψ_λ is orientation preserving, it can be "lifted" to a map $F:R \to R$ which covers ψ_λ via the covering projection $\exp: t \to e^{2\pi i t}$. Any two lifts of ψ_λ differ only by a translation [31]. The limit

$$\tau(\psi_\lambda) = \lim_{n\to\infty} \frac{F^n(x)}{n},$$

where $x\in R$, $F^n(x)=\overbrace{F(F(\ldots F}^{n}(x)\ldots))$ and F any lift of ψ_λ, is called the rotation number of ψ_λ. $\tau(\psi_\lambda)$ measures the average rotation of ψ_λ on S_1. $\tau(\psi_\lambda)$ has the following properties:

(1). $\tau(\psi_\lambda)$ is unique and independent of x.

(2). $\tau(\psi_\lambda)$ is irrational if and only if ψ_λ has no periodic points.

(3). Let $\omega(x)$ be the set of all accumulation points of

$$\{\psi_\lambda{}^n(x): n \text{ is any positive integer}\}.$$

Irrationality of $\tau(\psi_\lambda)$ implies $\omega(x)$ is independent of x. Also, either $\omega(x)$ is perfect and nowhere dense or $\omega(x)=S^1$.

(4). If conditions of the Hopf bifurcation theorem for diffeomorphisms are satisfied, $\tau(\psi_\lambda)$ is a continuous function of λ.[19]

If $\omega(x)=S^1$, ψ_λ is said to be transitive. Roughly speaking, the image of a transitive ψ_λ has no gaps. We also have the following two theorems [31]:

Theorem (4.1) If ψ_λ is a diffeomorphism of S^1, with ψ_λ' continuous and of bounded variation, and $\tau(\psi_\lambda)$ irrational, then ψ_λ is transitive.

Theorem (4.2) If ψ_λ is transitive, then ψ_λ is topologically conjugate to a rotation through $\tau(\psi_\lambda)$.

The main idea of Theorem (4.2) is that under certain assumptions, we can always find a parametrisation of u(t) such that ψ_λ is a rotation on the circle u(t). Theorem (4.2) is a very desirable result for our scheme of computation because with the assumption that the conditions in Theorem (4.2) are met, we only need the following equation

$$\psi_\lambda(u(t)) = u(t+\tau)$$

to enforce the invariance property of an invariant circle.

4.2 The pseudo arclength Continuation Method

The main framework of the method we propose is H.B. Keller's pseudo arclength continuation technique [23]. This technique has been used by various authors [8], [9], [10] [22]. It can be used, for example, to compute solution branches of ordinary and delay differential equations with turning points.

We first recall the basic features of the pseudo arclength method. Consider the operator equation

$$G(u,\lambda) = 0 \qquad (4.3)$$

where λ is a parameter and G a nonlinear map from one

Hilbert space into another. Let $w=(u,\lambda)$, if there exists some parametrized solution branch $w(s)$ of (4.3) then under appropriate smoothness assumptions we have

$$G'(w(s))w'(s) = 0.$$

Thus the derivative G' always has a null space along the branch. Assume now that we have a solution w_0 of (4.3), i.e. $G(w_0) = 0$, and that in addition the null space of $G'(w_0)$ is spanned by a vector w_0'. Thus the null space is one dimensional. Let $w_0'^*$ be the adjoint element such that $w_0'^* w_0' = 1$. Then the inflated problem

$$G(w) = 0 \qquad (4.4a)$$

$$w_0'^*(w-w_0)-s = 0 \qquad (4.4b)$$

which we write more compactly as

$$H(w,s) = 0,$$

has the solution $w=w_0$ when $s=0$. Further the derivative

$$\frac{\partial H}{\partial w}(w_0,0) = \begin{bmatrix} G'(w_0) \\ \\ w'^*_0 \end{bmatrix}$$

is nonsingular since $\frac{\partial H}{\partial w}(w_0,0)v=0$ if and only if $G'(w_0)v=0$ and $w_0'^* v=0$; but $w_0'^* \neq 0$, hence $v=0$. Thus the implicit mapping theorem as stated below guarantees the existence of a branch of solution $w(s)$ for small s.

Theorem (4.3) (Implicit mapping theorem)

Let B_1 and B_2 be Banach spaces and let H be a continuously differentiable transformation from an open set $D \subset B_1 \times B_2$ with values in B_1. Let (w_0, s_0) be a point in D for which $H(w_0, s_0)=0$ and for which $\frac{\partial H}{\partial w}(w_0, s_0)$ is nonsingular. Then there is a neighbourhood N of s_0 and a continuous function w mapping N into B_1 such that $w(s_0)=w_0$ and $H(w(s), s)=0$ for all s in N.

We note that the pseudo arclength method can be applied in a very general setting.

4.3 Computation of a branch of fixed points

In order to compute the invariant circles of ψ_λ, we must first determine the fixed points of ψ_λ and their stability as λ varies. We can find the fixed points of ψ_λ by considering the map $h_\lambda : R^2 \to R^2$ with

$$h_\lambda(u) = u - \psi_\lambda(u).$$

The fixed points of ψ_λ corresponds to the solutions of the algebraic equation

$$h_\lambda(u) = 0.$$

As λ varies $h_\lambda(u)$ has solution branches and thus fixed point branches for $\psi_\lambda(u)$. We consider this transformation because solution branches of $h_\lambda(u)=0$ can also be viewed as the

steady state branches of an ordinary differential equation with vector field h_λ, and computing steady state branches is exactly one of the capabilities of AUTO. Therefore, we can use AUTO to compute the fixed point branches of ψ_λ. In the following, we briefly recall the method which AUTO uses to compute solution branches of $h_\lambda(x)=0$. The basic scheme is again Keller's pseudo arclength continuation technique.

To compute a solution branch of $h_\lambda(u)$ we let (u_{k-1},λ_{k-1}) be a point, but not a singular point, on the branch. Let $(\dot{u}_{k-1},\dot{\lambda}_{k-1})$ be a vector which spans the null space of $h'(u_{k-1},\lambda_{k-1})$. Then the inflated system solving for the k-th solution (4.4) can be written as

$$\begin{cases} h(u_k\ ;\ \lambda_k)=0 & (4.5a) \\ M(u_k,\lambda\ ;\delta s)= (u_k-u_{k-1})^T\dot{u}_{k-1} & \\ \qquad +(\lambda_k-\lambda_{k-1})\dot{\lambda}_{k-1}-\delta s=0. & (4.5b) \end{cases}$$

Here δs is a fixed number called a <u>step size</u>, see Figure 4.1.

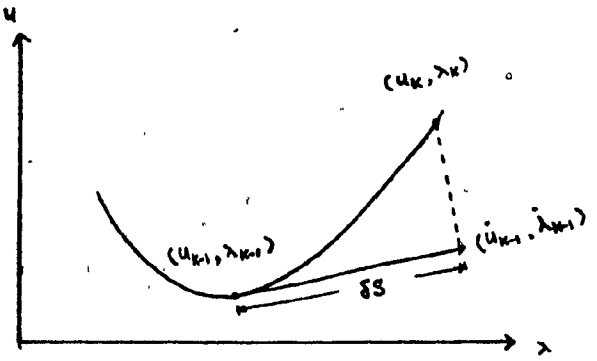

FIGURE 4.1

To determine the initial direction vector $(\dot{u}_0,\dot{\lambda}_0)$ at the starting point (u_0,λ_0), we compute the null vector of $h'(u_0,\lambda_0)$ by Gauss elimination with complete pivoting, if necessary, and back substitution. The direction vector $(\dot{u}_k,\dot{\lambda}_k)$ at (u_k,λ_k) for $k\geq 1$ can be approximated by

$$\dot{u}_k = (u_k - u_{k-1})/\delta s$$

and

$$\dot{\lambda} = (\lambda_k - \lambda_{k-1})/\delta s.$$

To obtain the k-th point on the branch, we solve (4.5) by Newton's method.

4.4 Computation of the Invariant circles

Given a two dimensional diffeomorphism ψ_λ, using the method described in section 4.3 we can trace out the fixed point branches of ψ_λ. Along a fixed point branch the change of stability can be detected by monitoring the eigenvalues of ψ_λ' and the eigenvalues of ψ_λ' can be computed using the IMSL subroutine EIGRF. In this section and the following section 4.5, we introduce a numerical method to automatically trace out the invariant circles after a Hopf bifurcation is detected. All these functions have been implemented in a computer program DSYS. Therefore given certain information about ψ_λ, DSYS can trace out fixed point branches of ψ_λ, detect Hopf bifurcations and automatically trace out the invariant circles if a Hopf bifurcation is

detected.

In the computation, an invariant circle can be represented by a truncated Fourier series

$$u(t) = a_0 + \sum_{k=1}^{m} (a_k \sin kt + b_k \cos kt) \quad (4.6)$$

with a_0, a_k, b_k in R^2, $k=1,\ldots,m$. From Theorem (4.2) we know that for $u(t)$ to satisfy the invariance property, we can require that

$$\psi_\lambda(u(t)) = u(t+\tau).$$

In other words, every point on the circle must again lie on the circle after the action of the diffeomorphism ψ_λ and by reparametrisation of $u(t)$, ψ_λ is a rotation on $u(t)$. The discrete system is then obtained by collocation using $2m+1$ equally spaced time steps $t_i = i\delta t$ where $\delta t = \frac{2\pi}{2m+1}$, $i=1,\ldots,2m+1$. The discrete system is as follows

$$\psi_\lambda(u(t_i)) - u(t_i+\tau) = 0. \quad (4.7)$$

Equation (4.7) has $2(2m+1)$ equations and $2(2m+1)+1$ unknowns. Due to the indeterminacy in the system, one more equation is required.

Note that an invariant circle can be translated freely in time; that is, if $u(t)=v(t)$ is an invariant circle, then so is $u(t)=v(t+r)$, for any r. Therefore $u(t)$ must also be "anchored". There are many ways to solve this inherent

non-uniqueness problem of u(t). One is to simply fix one of the components of u at t=0 to some constant c where min u(t) < c < max u(t) [10]. This method requires knowledge of the bounds of u(t) in advance which is usually difficult to obtain. Another method which is suggested by [7] is to seek a circle v(t) that minimizes the distance

$$\int_0^{2\pi}(v(t+r) - \hat{u}(t))^2 dt \qquad (4.8)$$

over r. Here $\hat{u}(t)$ denotes the previous circle that has been computed. This method forces peaks of v and $\hat{u}$ (with respect to t) to remain approximately in the same place. The minimizing r^* is obtained by setting the derivative of (4.8) with respect to r equal to zero. That is

$$\int_0^{2\pi}(v(t+r^*) - \hat{u}(t))^T v'(t+r^*)dt = 0.$$

Letting $u(t) = v(t+r^*)$, we have

$$\int_0^{2\pi}(u(t) - \hat{u}(t))^T u'(t)dt = 0. \qquad (4.9)$$

It is shown in [10] that (4.9) is equivalent to

$$\int_0^{2\pi}(u(t) - \hat{u}(t))^T \hat{u}'(t)dt = 0 \qquad (4.10)$$

Expressing (4.10) in terms of the truncated Fourier series (4.6) we get

$$\int_0^{2\pi}((a_0-\hat{a}_0)+\sum_{k=1}^{m}((a_k-\hat{a}_k)\sin kt+(b_k-\hat{b}_k)\cos kt))^T$$

$$(\sum_{k=1}^{m}k(\hat{a}_k\cos kt-\hat{b}_k\sin kt))dt=0 \qquad (4.11)$$

Since

$$\int_0^{2\pi}\sin mx \sin nxdx = 0 \quad \text{for } m\neq n,$$

$$\int_0^{2\pi}\cos mx \cos nxdx = 0 \quad \text{for } m\neq n,$$

$$\int_0^{2\pi}\sin mx \cos nxdx=0 \quad \text{for all integer } m,$$

$$\int_0^{2\pi}\sin^2 xdx = \pi,$$

and

$$\int_0^{2\pi}\cos^2 xdx = \pi,$$

it follows that (4.11) equals

$$\sum_{k=1}^{m}k(\hat{a}_k^T b_k - a_k^T\hat{b}_k) = 0. \qquad (4.12)$$

The next consideration is the continuation method. To fully specify a solution in Keller's general psuedo arclength continuation, we require the psuedo arclength between two consecutive solutions be equal to a prespecified increment δs. Let $w=(u(t),\tau,\lambda)$ and $\hat{w}=(\hat{u}(t),\hat{\tau},\hat{\lambda})$, if we approximate w' by

$$w' = \frac{w-\hat{w}}{\delta s},$$

then the psuedo arclength equation in (4.4b) becomes

$$(w - \hat{w})^T(w - \hat{w}) - \delta s^2 = 0$$

or

$$|w - \hat{w}|^2 = \delta s^2$$

or

$$|u-\hat{u}|^2 + (\tau - \hat{\tau})^2 + (\lambda - \hat{\lambda})^2 = \delta s^2$$

or

$$\int_0^{2\pi}(u(t)-\hat{u}(t))^2dt + (\tau-\hat{\tau})^2 + +(\lambda-\hat{\lambda})^2 = \delta s^2.$$

Now suppose we have the (l-1)-th invariant circle, to compute the l-th invariant circle we need to solve the following (2m+1)2+2 equations for the unknowns a_0^l, $a_1^l,\ldots,a_m^l,b_1^l,\ldots,b_m^l,\tau^l,\lambda^l$:

$$\psi_\lambda(a_0^l+\sum_{k=1}^{m}(a_k^l\sin kt_i+b_k^l\cos kt_i)) -$$

$$(a_0^l+\sum_{k=1}^{m}(a_k^l\sin k(t_i+\tau)+b_k^l\cos k(t_i+\tau)))=0; \qquad (4.13a)$$

$$\sum_{k=1}^{m} k((a_k^{l-1})^T b_k^l - (b_k^{l-1})^T a_k^l) = 0 \qquad (4.13b)$$

$$2\pi(a_0^l-a_0^{l-1})^T(a_0^l-a_0^{l-1}) +$$

$$\pi\sum_{k=1}^{m}((a_k^l-a_k^{l-1})^T(a_k^l-a_k^{l-1}) + (b_k^l-b_k^{l-1})^T(b_k^l-b_k^{l-1})) +$$

$$(\tau^l-\tau^{l-1})^2 + (\lambda^l-\lambda^{l-1})^2 - \delta s^2 = 0. \qquad (4.13c)$$

System (4.13) can be solved using the Newton-Chord method, and the initial approximation to the next invariant circle $w^1=(u^1(t),\tau^1, \lambda^1)$ is obtained by extrapolation from the two preceeding invariant circles. If we write system (4.13) in the compact form as

$$H(w)=0,$$

then the algorithm is as follows:

Algorithm 4.1

(step 1). Set j=0;

(step 2). $w_k^{(j)} = w_{k-1} + \delta s w_{k-1}$

(step 3). If NOT CHORD evaluate $\frac{\partial H}{\partial w}$ with $w_k^{(j)}$

(step 4). Apply Gauss elimination method to solve

$$\frac{\partial H}{\partial w}(w_k^{(j)})\ (\delta w) = -H(w_k^{(j)})$$

(step 5). j=j+1

(step 6). If $|\delta w|$ is less than the prespecified tolerance or j is greater than the maximum number of iterations allowed then stop

else

(step 7). $w_k^{(j)} = w_k^{(j-1)} + \delta w$; go to (step 3).

4.5 Asymptotic Estimate at the Hopf bifurcation point

The general procedure described in section 4.4 requires two known circles to find the initial approximation of the third one. Since when starting at the Hopf bifurcation point, only the Hopf point is known, we use an asymptotic estimate to be the initial approximation to the first circle. Consider the linearization of the diffeomorphism ψ_λ:

$$u_{k+1} = A\, u_k \qquad (4.14)$$

where $A=\psi_\lambda'(u_k)$. Since A has a pair of complex conjugate eigenvalues on the unit circle, we have

$$A\xi = e^{i\theta}\xi$$

$$A\,\bar{\xi} = e^{-i\theta}\,\bar{\xi}$$

where $e^{i\theta}$ is the eigenvalue and ξ is the corresponding eigenvector. The general solution of (4.14) can be written as

$$u_k = \alpha e^{ik\theta}\xi + \beta e^{-ik\theta}\,\bar{\xi} \qquad (4.15)$$

where α,β are complex numbers. Since we are only interested in real solutions, we consider

$$u_k = \bar{u}_k$$

for every k, which implies

$$\alpha e^{ik\theta}\xi + \beta e^{-ik\theta}\bar{\xi} = \bar{\alpha} e^{-ik\theta}\bar{\xi} + \bar{\beta} e^{ik\theta}\xi$$

for every k, or

$$(\alpha - \bar{\beta}) e^{ik\theta}\xi + (\beta - \bar{\alpha}) e^{-ik\theta}\bar{\xi} = 0,$$

for every k, which further implies

$$\bar{\beta} = \alpha. \tag{4.16}$$

Substituting (4.16) into (4.15) we have

$$\begin{aligned} u_k &= \alpha e^{ik\theta}\xi + \bar{\alpha} e^{-ik\theta}\bar{\xi} \\ &= \alpha e^{ik\theta}\xi + \alpha \overline{e^{ik\theta}\xi} \\ &= 2\mathrm{Re}(\alpha e^{ik\theta}\xi) \\ &= 2\mathrm{Re}((\alpha_R + i\alpha_I)(\cos k\theta + i\sin k\theta)(\xi_R + i\xi_I)) \\ &= 2(\alpha_R(\cos k\theta \xi_R - \sin k\theta \xi_I) - \alpha_I(\cos k\theta \xi_I + \sin k\theta \xi_R)) \\ &= 2(\alpha_R \xi_R - \alpha_I \xi_I)\cos k\theta - (\alpha_R \xi_I + \alpha_I \xi_R)\sin k\theta \end{aligned} \tag{4.17}$$

Here α_R and α_I are free and we can take $\alpha_I = 0$, $\alpha_R = \alpha$. Thus (4.17) becomes

$$u_k = \alpha(\xi_R \cos k\theta - \xi_I \sin k\theta).$$

In terms of an orbit and after scaling the time we have

$$u(t) = u_0 + \alpha(\xi_R \cos t - \xi_I \sin t) \tag{4.18}$$

as an asymptotic estimate.

Now, for compatibility with the pseudo arclength equation (4.13c), we take the estimate

$$\alpha^2 \int_0^{2\pi} |\xi_R \cos t - \xi_I \sin t|^2 dt - \delta s^2 = 0$$

or

$$\alpha = \frac{\delta s^2}{\sqrt{\pi(\xi_R^T \xi_R + \xi_I^T \xi_I)}}.$$

The last step in getting the asymptotic estimate is to find the initial τ. Consider

$$\psi_\lambda(u(t)) = u_0 + \alpha(\xi_R \cos(t+\tau) - \xi_I \sin(t+\tau)),$$

with ψ, ξ_R, ξ_I in R^2. Let j be the index governing the dimension of ψ_λ and $x_j(t) = \psi_{\lambda j}(u(t)) - u_{0j}$, $j=1,2$, and $\sigma = t+\tau$ we have

$$x_j(t) = \alpha(\xi_{Rj} \cos\sigma - \xi_{Ij} \sin\sigma)$$

or

$$x_j(t)(\sin^2 \tfrac{\sigma}{2} + \cos^2 \tfrac{\sigma}{2}) = \alpha(\xi_{Rj}(\cos^2 \tfrac{\sigma}{2} - \sin^2 \tfrac{\sigma}{2}) - \xi_{Ij}(2 \sin \tfrac{\sigma}{2} \cos \tfrac{\sigma}{2}))$$

or

$$(x_j(t) + \alpha\xi_{Rj}) \sin^2 \tfrac{\sigma}{2} + 2\alpha\xi_{Ij} \sin \tfrac{\sigma}{2} \cos \tfrac{\sigma}{2} + (x_j(t) - \alpha\xi_{Rj}) \cos^2 \tfrac{\sigma}{2} = 0$$

or

$$(x_j(t) + \alpha\xi_{Rj}) \tan^2 \tfrac{\sigma}{2} + 2\alpha\xi_{Ij} \tan \tfrac{\sigma}{2} + (x_j(t) - \alpha\xi_{Rj}) = 0,$$

which implies

$$\tan\frac{\sigma}{2} = \frac{-\alpha\xi_{Ij} + \sqrt{(\alpha\xi_{Ij})^2 - (x_j(t)+\alpha\xi_{Rj})(x_j(t)-\alpha\xi_{Rj})}}{x_j(t) + \alpha\xi_{Rj}}$$

and

$$\sigma = 2\tan^{-1}\frac{-\alpha\xi_{Ij} + \sqrt{(\alpha\xi_{Ij})^2 - (x_j(t)+\alpha\xi_{Rj})(x_j(t)-\alpha\xi_{Rj})}}{x_j(t)+\alpha\xi_{Rj}}$$

Since $\tan^{-1}$ has range $(-\frac{\pi}{2}, \frac{\pi}{2})$, lies in $(-\pi,\pi)$. If σ is in $(-\pi,0)$, it is equivalent to take it as $2\pi-\sigma$ and therefore σ in $[0,2\pi)$.

We note that for each t, we have four possible candidates for σ. Since theoretically two of these four candidates must be identical, we apply the following Algorithm 4.2 to take the average of the closest pair as the true σ. The case when the close pair has one value near zero and the other value near 2π is also considered. See Figure 4.2.

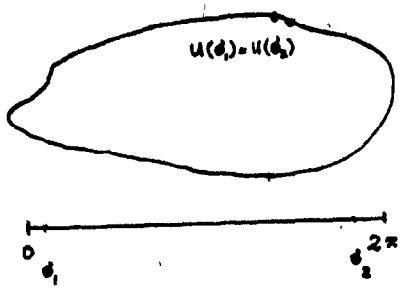

FIGURE 4.2

Algorithm 4.2

Let σ_1, σ_2, σ_3, σ_4 be the four possible values of σ.

(step 1). $d_{ij} = |\sigma_i - \sigma_j|$; $i \neq j$; $i=1,2$; $j=1,2$

(step 2). If $d_{ij} > \pi$ then $d_{ij} = 2\pi - d_{ij}$;

(step 3). Find the pair σ_i, σ_j which yields the smallest value of d_{ij};

(step 4). If $\sigma_j > \sigma_i + \pi$ then

$$\sigma_j = \sigma_j - 2\pi$$

Else

If $\sigma_j < \sigma_j + 2\pi$ then

$$\sigma_j = \sigma_j + 2\pi;$$

(step 5). $\sigma = (\sigma_i + \sigma_j)/2$

(step 6). If $\sigma > 2\pi$ then

$$\sigma = \sigma - 2\pi$$

Else

If $\sigma < 0$ then

$$\sigma = \sigma + 2\pi;$$

(step 7). output σ.

For each time step t_i, we have $\tau_i = \sigma - t_i$, $i=1,\ldots,2m+1$. As an initial approximation we take

$$\tau = \left(\sum_{i=1}^{2m+1} \tau_i\right) (2m+1)^{-1}.$$

4.6 Discussions on the computation method

In section 4.4, an invariant circle is represented by a truncated Fourier series. The reason for this choice is twofold. Firstly, the 2π-periodicity required by the invariant circle is built in a Fourier series a priori. Using a Fourier series representation we do not have to add other equations to the system to impose periodicity. Secondly, approximation using truncated Fourier series can attain very high accuracy in general. This is true especially when the computation is near the Hopf bifurcation point. For a comparison between the numerical results obtained by DSYS (using a Fourier series representation) and by iterating the map, see Figure 6.1, 6.4, 6.9 and 6.10. However, one drawback of using a truncated Fourier series to represent an invariant circle is that the Jacobian matrix of the corresponding system is full, and solving a full matrix system is an operation of order $O(n^3)$, where n is the order of the matrix. In the actual implementation, the Newton-Chord method is used so that unnecessary evaluation of the Jacobian matrix can be avoided.

One possible representation which can prevent the system of having a full Jacobian matrix is the piecewise polynomial representation. Using a piecewise polynomial representation for the invariant circles, the Jacobian matrix of the corresponding system has a special band structure (see the following section 4.7). It is well known that solving a

true band matrix system of order n is an operation of order O(n). A large varieties of existing computer software for solving true band matrix systems is also available. However, because of the special band structure, how to utilize the piecewise polynomial representation to compute the invariant circles is still not very clear to us (see section 4.7 for a more detailed discussion). Therefore due to its accuracy and ease to use, a Fourier series representation is still a very good choice for the computation scheme.

4.7 Cubic B-Splines representation

In the following, we consider the cubic B-splines [36] for the computation of an invariant circle. More precisely, let

$$P=\{t_i:\ i=0,\ldots,m;\ 0=t_0<t_1<\ldots<t_m<2\pi\}$$

be a partition on $[0,2\pi)$. Each t_i is called a knot. Adding six extra knots, $t_{-3},t_{-2},t_{-1},t_{m+1},t_{m+2},t_{m+3}$ we can define the normalized cubic B-splines as

$$B_i(t) = (t_{i+4}-t_i)[t_i,\ldots, t_{i+4}](s-t)^3 \text{ for all } t\in R,$$

where $[t_i,\ldots,t_{i+4}](s-t)^3$ denotes the 4-th divided difference of the function $(s-t)^3$ with s as the variable and t fixed. $B_i(t)$, $i=-3,-2,-1,\ldots,m-3,m-2,m-1$ has the following properties:

(1) $B_i(t)$ is C^2 for each $i=-3,-2,-1,\ldots,m-1$.

(2) $\sum_{i=-3}^{m-1} B_i(t)=1$ for all $t\in[t_0,t_m]$.

(3) $B_i(t)$ is identically zero outside the interval $[t_i,t_{i+4}]$, $i=-3,-2,-1,\ldots,m-1$.

See Figure 4.3 for the graphs of $B_i(t)$, $i=-3,-2,-1,\ldots,m-1$.

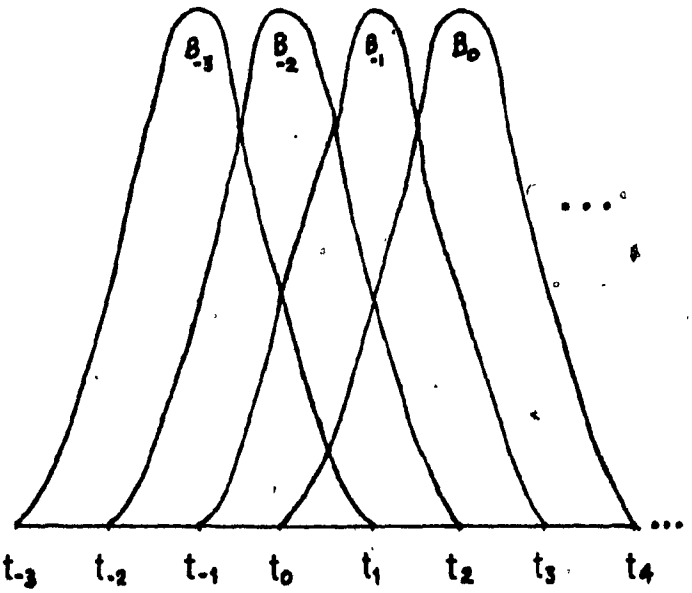

FIGURE 4.3

Using this sequence of m+3 B-splines, an invariant circle can be written as

$$u(t) = \sum_{i=-3}^{m-1} a_i B_i(t), \qquad (4.19)$$

with u,a_i in R^2, $i=-3,-2,-1,\ldots,m-1$.

The advantage of using (4.19) as the representation is that it is "piecewise local", i.e. $B_i(t)$ is identically zero outside the interval $[t_i,t_{i+4}]$, and the coefficient a_i is effective to the representation only inside the interval

$[t_i, t_{i+4}]$. The Jacobian matrix of the resulting system therefore has certain band structure and can be solved with considerably less effort than required to solve a full matrix.

The 2π-periodicity of $u(t)$ is not built into the representation (4.19). In order to have the 2π-periodicity, we impose the following conditions:

$$\begin{aligned} u(t_m) &= u(t_0) \\ u'(t_m) &= u'(t_0) \\ u''(t_m) &= u''(t_0). \end{aligned} \tag{4.20}$$

The three equations (4.20) are called <u>boundary conditions</u>. They are not separated as (4.6), in other words the first and last few unknowns both appear in these last few equations. Thus, with (4.20) the band structure of the corresponding Jacobian matrix is slightly distorted.

Suppose we have the (l-1)-st circle $(a_{-3}^{l-1}, a_{-1}^{l-1}, \ldots, a_{m-1}^{l-1}, \tau^{l-1}, \lambda^{l-1})$, to compute the l-th invariant circle $(a_{-3}^{l}, a_{-1}^{l}, \ldots, a_{m-1}^{l}, \tau^{l}, \lambda^{l})$ using these two ideas, instead of solving system (4.14), we need to solve the following $2(m+3)+2$ equations. In this case, one collocation point is chosen between each knot $t_0, \ldots, t_m$.

$$\psi_\lambda\left(\sum_{i=-3}^{m-1} a_i^l B_i(t_j)\right)-\sum_{i=-3}^{m-1} a_i^l B_i(t_j+\tau)=0,\quad j=1,\ldots,m \qquad (4.21a)$$

$$\sum_{i=-3}^{m-1} a_i^l B_i(t_m)-\sum_{i=-3}^{m-1} a_i^l B_i(t_0)=0,$$

$$\sum_{i=-3}^{m-1} a_i^l B_i'(t_m)-\sum_{i=-3}^{m-1} a_i^l B_i'(t_0)=0, \qquad (4.21b)$$

$$\sum_{i=-3}^{m-1} a_i^l B_i''(t_m)-\sum_{i=-3}^{m-1} a_i^l B_i''(t_0)=0,$$

$$\int_0^{2\pi}\left(\left(\sum_{i=-3}^{m-1} (a_i^l-a_i^{l-1})B_i(t)\right)^T \left(\sum_{i=-3}^{m-1} a_i^{l-1}B_i'(t)\right)\right)dt=0 \qquad (4.21c)$$

$$\int_0^{2\pi}\left(\left(\sum_{i=-3}^{m-1} (a_i^l-a_i^{l-1})B_i(t)\right)^T \left(a_i^l-a_i^{l-1})B_i(t)\right)\right)dt +$$

$$(\tau^l-\tau^{l-1})^2+(\lambda^l-\lambda^{l-1})^2-\delta s^2=0 \qquad (4.21d)$$

with a_i^l, a_i^{l-1} in R^2 $i=-3,-2,-1,\ldots,m-1$. Equation (4.21a) governs the invariance property. Equation (4.21b) is the boundary condition for the cubic B-splines representation. Equation (4.21c) is the anchor equation for the inherent non-uniqueness problem of the representation. Equation (4.21d) is the pseudo arclength equation.

Notice that with the same value of m, the order of system (4.21) is about the same of the order of system (4.13). Further, the Jacobian matrix of system (4.21) has a certain band structure; see Figure 4.4 for an illustration with m=10. When m=10, the Jacobian of system (4.21) is a matrix of 28x28 (2x(10+3)+2=28). The first twenty rows

Stand for the discretized system (4.21a). Row 21 to row 26 represent the imposed boundary conditions (4.21b). The last two rows stand for the anchor equation (4.21c) and the pseudo arclength equation (4.21d) respectively. Then each of the first twenty six columns contains the derivatives of the system with respect to a coordinate of a coefficient of the cubic B-splines representation (4.19). The last two columns contain the derivatives of the system with respect to τ and λ.

The three bands in the matrix are the results of the "piecewise local" property of the cubic B-spline representation. In the representation (4.19), $B_i(t)$ is identically zero outside the knot interval $[t_i, t_{i+4}]$. If m is small, the resulting Jacobian matrix is almost full. When m gets large, the one major and two minor bands in the matrix become more visible. In general, the band width of each band depends on the degree of the splines we employ. (In Figure 4.4, each band has width 7). The distance that the two minor bands separate from the major band is directly proportional to the value of τ which is one of the unknowns. Beside the three bands, the structures of the last columns and row 21 to row 28 of the matrix are fixed.

It is well known that true band matrix systems can be solved in order O(n), with n being the order of the system [11]. However, the particular structure of the Jacobian matrix of system (4.21) (i.e., the distance between the

bands depends on the unknown τ) makes it not quite evident to us how to utilize this band structure to improve the efficiency of the computation. When τ is small, the three bands are close together and a band matrix solver is useful. If τ is close to π mod n, then the two minor bands are in a significant distance with the major band and a sparse matrix solver is desirable provided that m is large also.

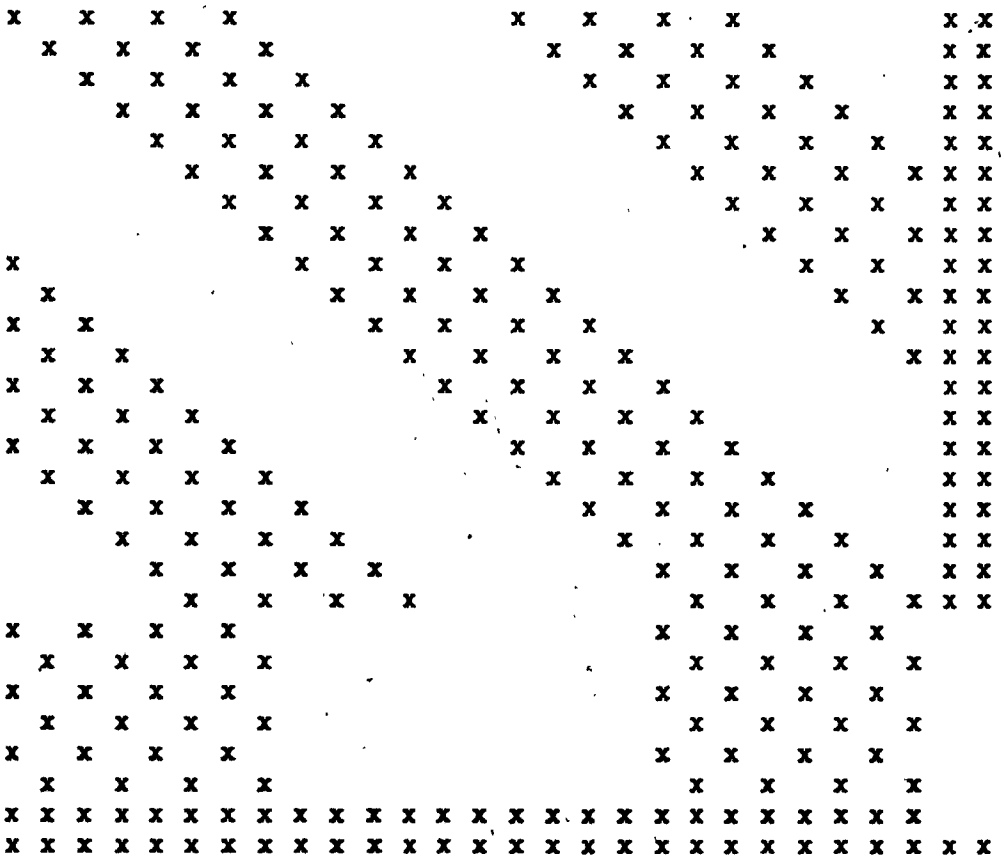

Figure 4.4

4.8 Summary

In this chapter, a numerical method to compute the bifurcating invariant circles for a general two dimensional diffeomorphism ψ_λ is described. The method uses Keller's psuedo arclength continuation technique and a Fourier series representation of an invariant circle. This method utilizes the property of ψ_λ being a rotation and the corresponding system is very simple. Solving the system doesnot only find the invariant circle but also its approximated rotation number. Thus a general idea about the dynamical behaviour of ψ_λ on the invariant circle is also obtained. Although in order to use this method some conditions on ψ_λ must be satisfied (ψ_λ' be continuous and of bounded variation, see Theorem (4.1)), we believe for most of the two dimensional diffeomorphisms these conditions can be met at least near the Hopf bifurcation point.

This method has been implemented and tested. Numerical results are shown in Chapter 6. As described in Chapter 3, bifurcation to invariant tori and bifurcation to invariant circles are closely related. A good method to compute the invariant circles can therefore serve as a foundation for computing invariant tori. A possibly more efficient representation scheme using cubic B-spline is also discussed. The latter has not been implemented.

CHAPTER FIVE

An Alternate Scheme for Computing the Invariant Circles

The numerical method introduced in Chapter 4 has been implemented and tested. In this chapter, we describe an alternate computation scheme for computing the invariant circles. The advantage of this method is that no conditions on ψ_λ are required. However, the discrete character of this method makes a continuous formulation of the corresponding system impossible.

In Chapter 4, the invariance property of an invariant circle is realized by the following equation

$$\psi_\lambda(u(t)) = u(t+\tau), \qquad (5.1)$$

if ψ_λ satisfies the conditions of Theorem 4.2. However, the invariance property of an invariance circle can also be enforced using the following equation

$$\psi_\lambda(u(t)) = u(\sigma(t)). \qquad (5.2)$$

Equation (5.2) simply enforce that every point on the invariant circle must again lie on the circle after the action of ψ_λ. It is more general than (5.1) in a sense that no conditions on ψ_λ are required for (5.2) to be satisfied as long as the invariant circles exist. Like τ, $\sigma(t)$ is

unknown a priori. The discrete system is then obtained by collocation using 2m+1 points t_i in the interval $[0,2\pi)$, $0 \leq i \leq 2m+1$, i.e.

$$\psi_\lambda(u(t_i)) - u(\sigma_i) = 0 \qquad (5.3)$$

where $\sigma_i = \sigma(t_i)$, $i=1,\ldots,2m+1$. Since (5.3) has $2(2m+1)$ equations and $3(2m+1)$ unknowns, there is indeterminacy in the system. In some cases, points on an invariant circle with equal time distance may in fact be very close to each other on the circle. In other words, with a parametrisation, time taken to travel from point 1 and point 2 on the circle may be very different from point 2 to point 3, although the physical distances between these points are the same. Therefore, if the parametrisation is not taken properly it may lead to difficulties when interpolating the invariant circle.

In order to circumvent the above stated problems, in this method, we choose the 2m+1 collocation time steps so that

$$|u(t_i) - u(t_{i-1})|^2 - d^2 = 0, \qquad (5.4)$$

$i=1,\ldots 2m+1$. By choosing a special set of collocation time steps, we enforce the points on the invariant circle (i.e. $u(t_i)$) corresponding to the time steps must be equally distanced according to the Euclidean norm. With $u(t_i)$, $i=1,\ldots,2m+1$, provided by the system and satisfy the

equations (5.4), interpolating the invariant circle is easy. In this method, the 2m+1 collocation time steps are fixed by Algorithm 5.1 and Algorithm 5.2 in the beginning of the computation and then remain unchange for all time.

Treating d as one of the unknowns, now (5.3) together with (5.4) have 3(2m+1) equations and 3(2m+1)+1 unknowns. Let $\hat{u}(t)$ denotes the previous circle that has been computed. The extra unknown can be compensated by the following "anchor" equation.

$$\int_0^{2\pi}(u(t) - \hat{u}(t))^T\hat{u}'(t)dt = 0. \qquad (5.5)$$

The next consideration is the continuation method. Again we can use Keller's psuedo arclength method (see section 4.2) and add the following psuedo arclength equation to the system.

$$\int_0^{2\pi}(u(t)-\hat{u}(t))^2dt+\sum_{i=1}^{2m+1}(\sigma_i-\hat{\sigma}_i)^2+(d-\hat{d})^2+(\lambda-\hat{\lambda})^2 = \delta s^2.$$

In Chapter 4, two different representation methods of an invariant circle are discussed. Both of them can be adopted for the method we described above. Since how to utilize the cubic B-splines representation is not quite evident to us, in our actual implementation of this method, we still use the Fourier series representation.

Again suppose we have the (l-1)-th invariant circle, to compute the l-th invariant circle we need to solve the following 3(2m+1)+2 equations for the unknowns a_0^l,

$$a_1^1,\ldots,a_m^1,b_1^1,\ldots\ ,b_m^1,\sigma_1^1,\ldots\ ,\sigma_{2m+1}^1,d^1,\lambda^1;$$

$$\psi_\lambda(a_0^1+\sum_{k=1}^{m}(a_k^1\sin kt_i+b_k^1\cos kt_i))-$$

$$(a_0^1+\sum_{k=1}^{m}(a_k^1\sin k\sigma_i+b_k^1\cos k\sigma_i))=0; \qquad (5.6a)$$

$$(\sum_{k=1}^{m}(a_k^1(\sin kt_i-\sin kt_{i-1})+b_k^1(\cos kt_i-\cos kt_{i-1})))^T$$

$$(\sum_{k=1}^{m}(a_k^1(\sin kt_i-\sin kt_{i-1})+b_k^1(\cos kt_i-\cos kt_{i-1})))-$$

$$(d^1)^2=0$$

$$i=1,2,\ldots 2m+1; \qquad (5.6b)$$

$$\sum_{k=1}^{m}k((a_k^{1-1})^T b_k^1-(b_k^{1-1})^T a_k^1)=0 \qquad (5.6c)$$

and

$$2\pi(a_0^1-a_0^{1-1})^T(a_0^1-a_0^{1-1})+$$

$$\pi\sum_{k=1}^{m}((a_k^1-a_k^{1-1})^T(a_k^1-a_k^{1-1})+(b_k^1-b_k^{1-1})^T(b_k^1-b_k^{1-1}))+$$

$$\sum_{i=1}^{2m+1}(\sigma_i^1-\sigma_i^{1-1})^2+(d^1-d^{1-1})^2+(\lambda^1-\lambda^{1-1})^2-\delta s^2=0. \qquad (5.6d)$$

System (5.6) has also been implemented in the computer program DSYS. In DSYS system (5.6) is again solved using Algorithm 4.1 and the Newton-Chord method. The initial approximation to the next invariant circle $w^1=(u^1(t),\sigma_1^1,\ldots,\sigma_{2m+1}^1,d^1,\lambda^1)$ is obtained by extrapolation from the two preceeding invariant circles.

To get started at the Hopf point, an asymptotic estimate of an invariant circle is again required (see section 4.5). In this case an asymptotic estimate of the form

$$u(t) = u_0 + \alpha(\xi_R \cos t - \xi_I \sin t) \qquad (5.7)$$

can be obtained using the method given in section 4.5. In (5.7), ξ is the corresponding eigenvector of the eigenvalue which is on the unit circle. ξ_R and ξ_I stand for the real part and imaginary part of ξ respectively. For the compatibility between (5.7) and (5.6d), again we take

$$\alpha = \frac{\delta s^2}{\sqrt{\pi(\xi_R^T\xi_R + \xi_I^T\xi_I)}}.$$

Next, we have to determine the 2m+1 time steps t_i, i=1,...,2m+1, and the corresponding d so that the 2m+1 equations (5.6b) are satisfied. This is done using the following two Algorithms which are based on the bisection method. Given time step t_i and d^*, Algorithm 5.1 uses the bisection method to locate time step t_{i+1}. Starting with

Algorithm 5.1 first locate a point r such that the distance between $u(t_i)$ and $u(r)$ is greater than d^*. Since

$$|u(t_i)-u(t_i)|^2-d^{*2}<0$$

and

$$|u(t_i)-u(r)|^2-d^{*2}>0,$$

using t_i and r as the initial guess, bisection method can be applied to locate t_{i+1} such that

$$|u(t_i)-u(t_{i+1})|^2-d^{*2}$$

is less than the prespecified tolerance ε.

Algorithm 5.1

$$p(s,r,d^*)=|u(s)-u(r)|^2-d^{*2}$$

(step 1). $s=t_i$; $r=s+\delta t$; $i=0$; Eval=true

(step 2). If $|p(t_i,r,d^*)|<\varepsilon$, $t_{i+1}=r$, Return

(step 3). If $p(t_i,r,d^*)<0$

$r=r+\delta t$

Until $p(t_i,r,d^*)>0$

(step 4). If (Eval) $p_1=p(t_i,s,d^*)$

(step 5). If $|p_1|<\varepsilon$; $t_{i+1}=s$; Return

(step 6). $i=i+1$; $q=s+(r-s)/2$

(step 7). $p_2=p(t_i,q,d^*)$

(step 8). If $|p_2|<\epsilon$; $t_{i+1}=q$; Return

(step 9). If $p_1p_2>0$ then

s=q

Eval=true

Else

r=q

Eval=false

(step 10). If I is less than a prespecified value then

go to (step 4)

Else

'method not successful'; stop

Given two initial approximation $d_1 < d < d_2$, Algorithm 5.2 uses Algorithm 5.1 to determine $t_1,\ldots,t_{2m+1}$ and d. In Algorithm 5.2, given t_1 and d the time steps $t_2,\ldots,t_{2m+1}$ are determined by Algorithm 5.1. From Algorithm 5.1 we know that equations

$$|u(t_i)-u(t_{i+1})|^2 - d^2 = 0,\ i=1,\ldots,2m$$

are true. However, whether $t_1,\ldots,t_{2m+1}$ and d taken together truely satisfy the equations of (5.6b) depends on whether

$$|u(t_1)-u(t_{2m+1})|^2 - d^2 = 0 \qquad (5.8)$$

is true. Therefore (5.8) serves as the criteria for the bisection method used in the algorithm. The initial guess

are $d_1 = \frac{l}{2m+1}$ and $d_2 = \frac{l}{2m+1}\frac{a}{10}$, where l is the length of the circumference and a is a constant depending on the two radii of the asymptotic estimate. Using d_1 and d_2 as the initial guess, bisection method is performed on d using (5.8) as the condition.

Algorithm 5.2

$$p(s,r,d^*) = |u(s)-u(r)|^2 - d^{*2}$$

(step 1). i=0; t_1=0.0; Eval=true

(step 2). If (Eval) then

given d_1 and t_1, use Algorithm 4.2 to locate

$$t_2,\ldots,t_{2m+1}$$

so that

$$p(t_{i+1},t_i,d_1)<\varepsilon \quad i=1,\ldots,2m$$

(step 3). $p_1 = p(t_{2m+1},t_1,d_1)$

(step 4). If $|p_1| < |\varepsilon|$ then Return

(step 5). i=i+1; $d = d_1 + (d_2 - d_1)/2$

(step 6). Given d and t_1, use Algorithm 4.2 to locate

$$t_2,\ldots,t_{2m+1}$$

so that

$$p(t_{i+1},t_i,d)<\varepsilon \quad i=1,\ldots,2m$$

(step 7). $p_2 = p(t_{2m+1},t_1,d)$

(step 8). If $|p_2|<\epsilon$ then Return

(step 9). If $p_1p_2>0$ then

$d_1=d$; Eval=true

Else

$d_2=d$; Eval=false

(step 10). If I is less than a prespecified value then

go to (step 2)

Else

'method not successful'; stop

The last step in getting the asymptotic estimate is to find the initial σ_i, $1\leq i\leq 2m+1$. Consider

$$\psi_\lambda(u(t)) = u_0+\alpha(\xi_R \cos\sigma-\xi_I\sin\sigma),$$

with ψ,ξ_R,ξ_I in R^2, using Algorithm 4.2 given in Chapter 4 we can solve for the initial estimate of σ's.

In the beginning of this chapter, we claimed that the method given in this chapter is more general than the method given in Chapter 4. However, we note that the method given in this chapter also has two disadvantages. The first disadvantage lies in the discrete character of equation (5.4) which makes a continuous formulation of system (5.6) impossible. In other words, obtaining a mathematical proof of convergence of system (5.6) is hopeless. The second disadvantage of the method lies in the

fact that the order of system (5.6) is almost one-third higher than the order of system (4.13). This implies solving system (5.6) requires more computer time than solving system (4.13).

CHAPTER SIX

Numerical Examples

and

Conclusion

The computation methods described in Chapter 4 and 5 based on a Fourier series representation have been implemented in a computer program DSYS. Given a two dimensional diffeomorphism Ψ_λ, the Jacobian of Ψ_λ, $\frac{\partial \Psi}{\partial x}$, a fixed point of Ψ_λ and a number of control parameters, DSYS has the following capabilities:

(1). Trace out branches of fixed points.

(2). Accurately locate fixed point bifurcations.

(3). Switch automatically onto bifurcating branches of fixed points.

(4). Compute past turning points on a fixed point branch without added difficulty.

(5). Compute the eigenvalues of $\Psi'_\lambda(u_0)$ where u_0 is a fixed point of Ψ_λ.

(6). Accurately locate Hopf bifurcation points on a branch of fixed points.

(7). Automatically start computing the invariant circles.

(8). Adaptive stepsize along a branch of invariant circles.

(9). Store plotting information in files. These files can be investigated by an interactive graphics program.

In this chapter, we use two examples to demonstrate the numerical results obtained using DSYS. They are the delay logistic equation and the Hénon map.

6.1 The delay logistic equation

The following delay logistic equation

$$g_\lambda \begin{bmatrix} x \\ y \end{bmatrix} = \begin{bmatrix} y \\ \lambda y(1-x) \end{bmatrix} . \qquad (6.1)$$

has been extensively studied by D.G.Aronson, M.A.Chory, G.R.Hall and R.P.McGehee [1]. (6.1) has two fixed points $x_1=y_1=0$ and $x_2=y_2=\frac{\lambda-1}{\lambda}$ which are the solutions of the following two algebraic equations:

$$\begin{cases} x - y = 0 \\ y - \lambda y(1-x) = 0. \end{cases}$$

The Jacobian matrix of (6.1) is

$$g_\lambda' = \begin{bmatrix} 0 & 1 \\ -\lambda y & \lambda(1-x) \end{bmatrix}$$

and the characteristic equation of (6.1) can be written as

$$\alpha^2 - \alpha\lambda(1-x) + \lambda y = 0. \qquad (6.2)$$

From the introduction of Chapter 4, we know that the fixed point $x_2=y_2=\frac{\lambda-1}{\lambda}$ is stable when $\lambda<2$. At $\lambda=2$, $g'_\lambda(x_2,y_2)$ has a pair of complex conjugate eigenvalues going out of the unit circle and as λ increases pass 2, invariant circles are developed. In this case, the invariant circles are attracting and the local dynamics of (6.1) is determined by these invariant circles.

However, the invariant circles only exist for those λ which lie in a neighbourhood of $\lambda=2$. For parameter values far from $\lambda=2$, the corresponding invariant set fails to be topologically a circle. In [1], based on iterating the map, the process by which the invariant circles dissolve is examined. This process is shown again in Figure 6.1.

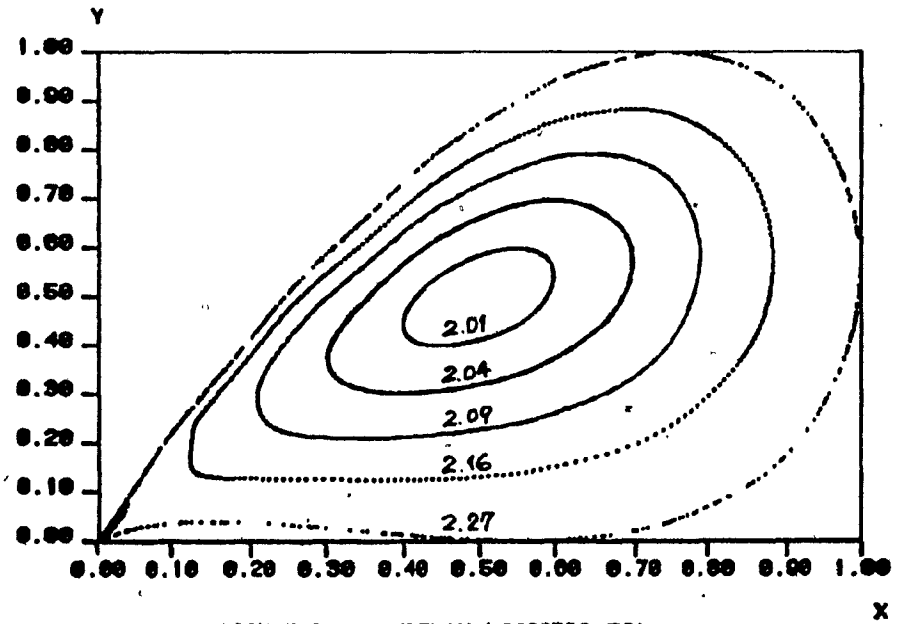

FIGURE 6.1 (DELAY LOGISTIC EQ)

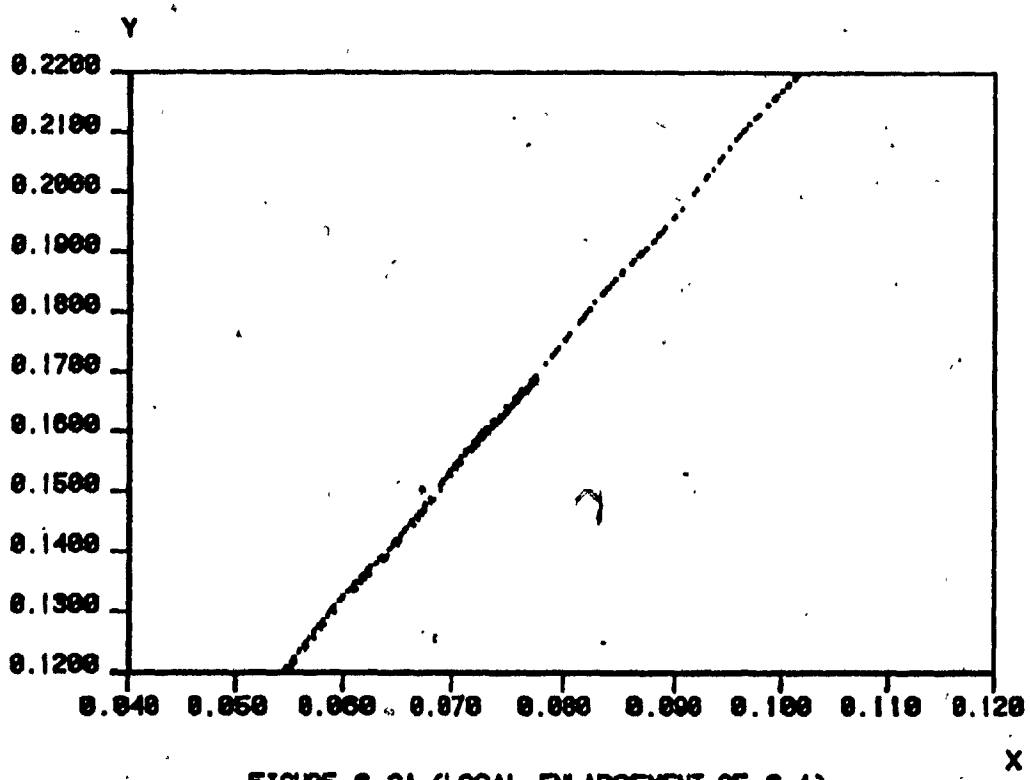

FIGURE 6.2A (LOCAL ENLARGEMENT OF 6.1)

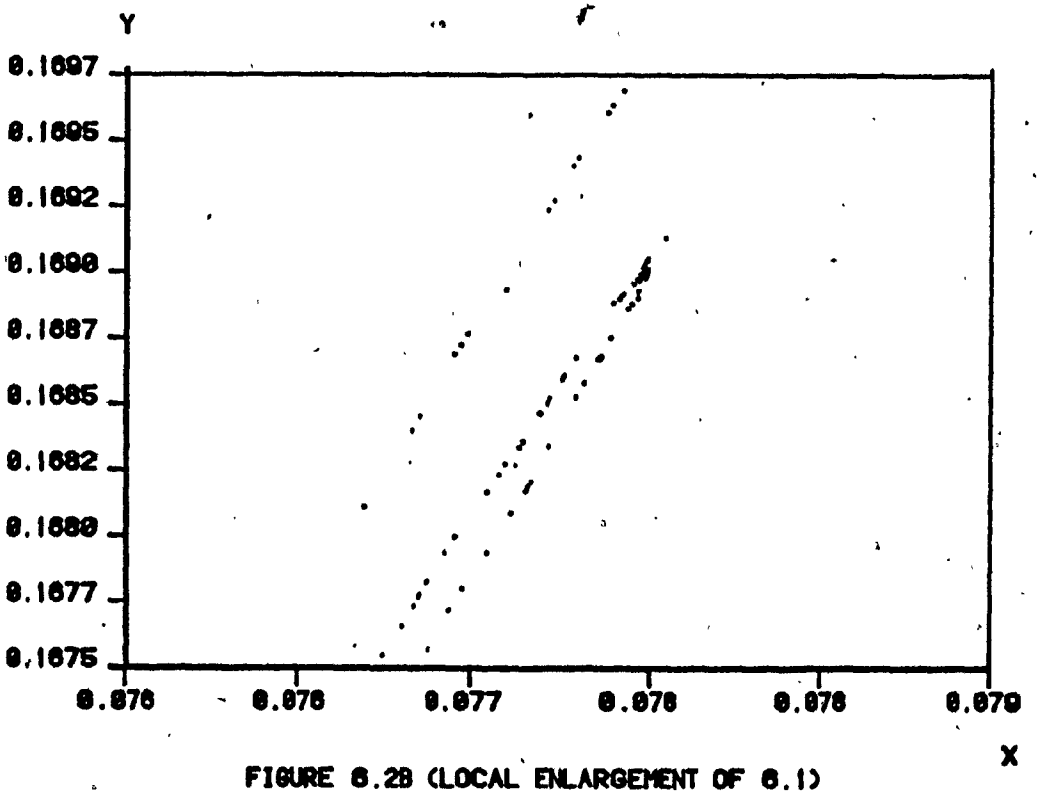

FIGURE 6.2B (LOCAL ENLARGEMENT OF 6.1)

Each invariant circle consists of the 1000-2500 iterates of the point (0.1,0.2). Transformation of the topological type of the invariant set seems to start at $\lambda=2.16$. At $\lambda=2.27$, we note that the invariant set is already a strange attractor. Various enlargements of a portion of the invariant set obtained at $\lambda=2.27$ are also shown in Figure 6.2.

Using DSYS, we compute the invariant circles of (6.1) again. A bifurcation diagram is given in Figure 6.3. Starting at $\lambda=-1$ the zero fixed point branch named branch 1 is traced. Along this branch, both the eigenvalues are real with one of them being identically zero and the other one equals to λ. Beside the value computed by DSYS, this can also be seen quite easily by substituting $x_1=y_1=0$ into the characteristic equation (6.2). After substituting $x_1=y_1=0$, (6.2) becomes

$$\alpha^2-\alpha\lambda = 0$$

which implies

$$\alpha = 0 \quad \text{or} \quad \alpha = \lambda.$$

At $\lambda=1$, an eigenvalue goes out of the unit circle through positive one when a fixed point bifurcation occurs. Branch 1 loses its stability at $\lambda=1$ and the fixed point $x_2=y_2=\frac{\lambda-1}{\lambda}$ appears. We note that $x_1=y_1=0$ remains a fixed point of (6.1) when $\lambda>1$, however it is unstable. The fixed points on the new fixed point branch, branch 2, remains

stable until at $\lambda=2$ when a Hopf bifurcation point is detected. At this point the two eigenvalues are a pair of complex numbers and they go out of the unit circle.

Invariant circles traced out by DSYS are shown in Figure 6.4. In the computation, 10 terms (m=10) are used in the Fourier series representation of an invariant circle,i.e.

$$u(t) = a_0 + \sum_{k=1}^{m=10} (a_k \sin kt + b_k \cos kt).$$

The order of the corresponding systems (4.13) and (5.6) are $2(2\times10+1)+2=44$ and $3(2\times10+1)+2=65$ respectively. They took a VAX 11/780 computer (running VAX/VMS operating system) approximately 40 and 60 minutes to complete the process of computing 100 invariant circles. In the parameter range $2\leq\lambda\leq2.16$, circles obtained by DSYS match the circles obtained by iterating the map. This can serve as an indication that the implementation in DSYS is sound. However, after $\lambda=2.16$, the circles given by DSYS become twisted and we know that the actual invariant set starts to deform from being topologically a circle.

It is obvious that the accuracy of the truncated Fourier series representation is higher when more terms are used in the series. When away from the Hopf bifurcation point, numerical results obtained by DSYS are quite sensitive to the value of m used. For $m<10$, the circles obtained by DSYS become twisted before $\lambda=2.16$. For $m\geq10$, the behaviour of

the computational result is more stable.

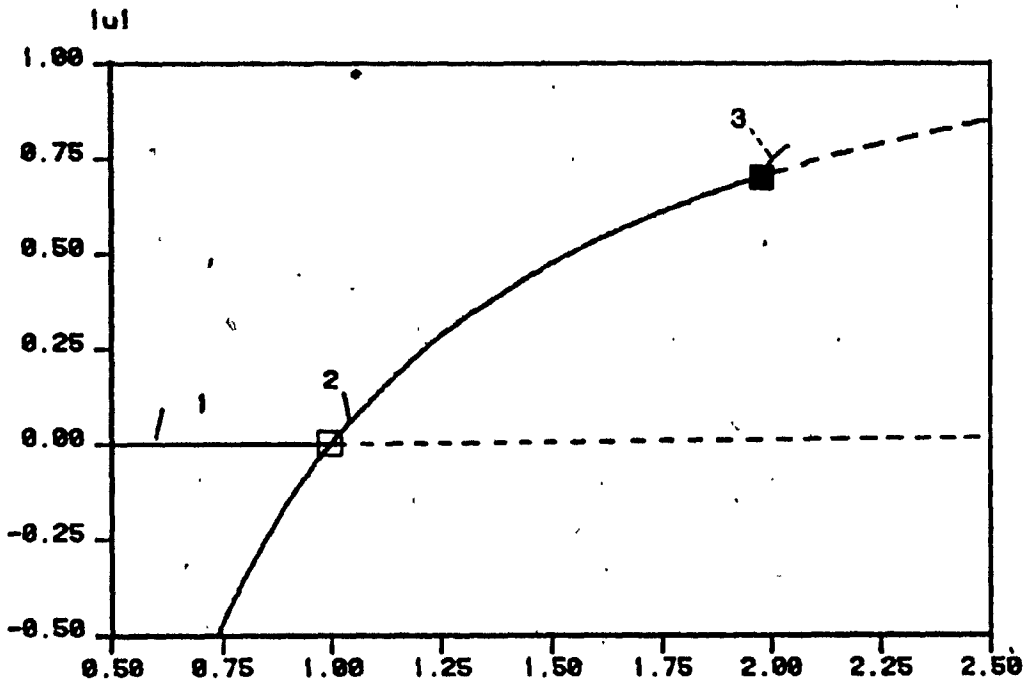

FIGURE 6. 3 (DELAY LOGISTIC)

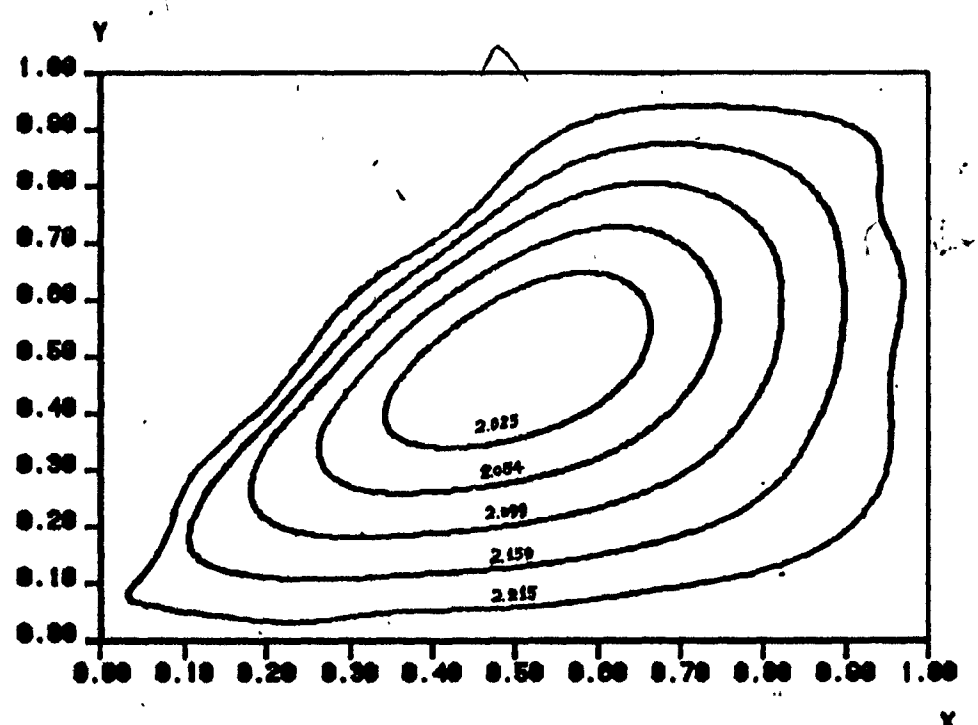

FIGURE 6.4 (INV CIR OF DELAY LOGISTIC)

6.2 The Hénon map

Much less numerical effort is required in studying a two dimensional map than studying a three dimensional differential equation. The computation can be more accurate since there are no integration errors. Also, with a simpler model there is more hope for applying techniques in mathematical analysis. For all the above stated reasons, M.Hénon [15],[16] constructed the following two dimensional map

$$T_{ab}\begin{bmatrix} x \\ y \end{bmatrix} = \begin{bmatrix} y+1-ax^2 \\ bx \end{bmatrix}, \qquad (6.2)$$

where a,b are parameters with $|b|<1$. (6.2) is now called the Hénon map. It contains the essential dynamics of a Poincaré map of the Lorenz system for high Rayleigh numbers. Therefore studying the Hénon map can add to the understanding of the dynamics of the Lorenz system. Inspired by numerical results on the Lorenz system, Hénon constructed the map (6.2) as follows [15]. First consider a region elongated along the x-axis as shown in Figure 6.5a. The region can be folded by the following transformation

$$T_1\begin{bmatrix} x \\ y \end{bmatrix} = \begin{bmatrix} x \\ y+1-ax^2 \end{bmatrix}$$

(by nunerically integrating the Lorenz system, Hénon observed that the flow of the Lorenz system is stretched in one direction but folded over itself). The folding is completed by a contraction along the x-axis

$$T_2 \begin{bmatrix} x \\ y \end{bmatrix} = \begin{bmatrix} bx \\ y \end{bmatrix} ,$$

see Figure 6.5b and 6.5c. Since T_2 is intended to be a contraction, b is required to be less than one in absolute value. Finally, the region is rotated along the x-axis by

$$T_3 \begin{bmatrix} x \\ y \end{bmatrix} = \begin{bmatrix} y \\ x \end{bmatrix} ,$$

see Figure 6.5d. Then map (6.2) is considered as

$$T_{ab} = T_1 \cdot T_2 \cdot T_3 .$$

It is easily seen that (6.2) has two fixed points

$$\begin{cases} x_1 = \dfrac{-(1-b)+\sqrt{(1-b)^2+4a}}{2a} \\ y_1 = bx, \end{cases} \qquad (6.3)$$

$$x_2 = \frac{-(1-b)-\sqrt{(1-b)^2+4a}}{2a}$$

$$y_2 = bx, \tag{6.4}$$

and these two points are real when $a > -(1-b)^2/4$. The characteristic equation of T'_{ab} is

$$\lambda^2 + 2ax\lambda - b = 0, \tag{6.5}$$

and the corresponding eigenvalues can be written as

$$\lambda = -ax \pm \sqrt{a^2x^2+b} \tag{6.6}$$

Substitute (x_2,y_2) into (6.6), we know that if $a > (1-b)^2/4$, one of the eigenvalues, namely

$$\lambda = \frac{(1-b)+\sqrt{(1-b)^2+4a}}{2} + \sqrt{\left\{\frac{(1-b)+\sqrt{(1-b)^2+4a}}{2}\right\}^2+b}$$

is always greater than 1. Therefore fixed point (x_2,y_2) is always unstable. Substitute (x_1,y_1) into (6.6) we have

$$\lambda = \frac{(1-b)-\sqrt{(1-b)^2+4a}}{2} \pm \sqrt{\left\{\frac{(1-b)-\sqrt{(1-b)^2+4a}}{2}\right\}^2+b} \tag{6.7}$$

and it is easily shown that (x_1,y_1) becomes unstable when

$$a > \frac{3(1-b)^2}{4}.$$

In [15], with a=1.4, b=0.3, Hénon found that map (6.2) has a "strange" attractor which appears to be the product of

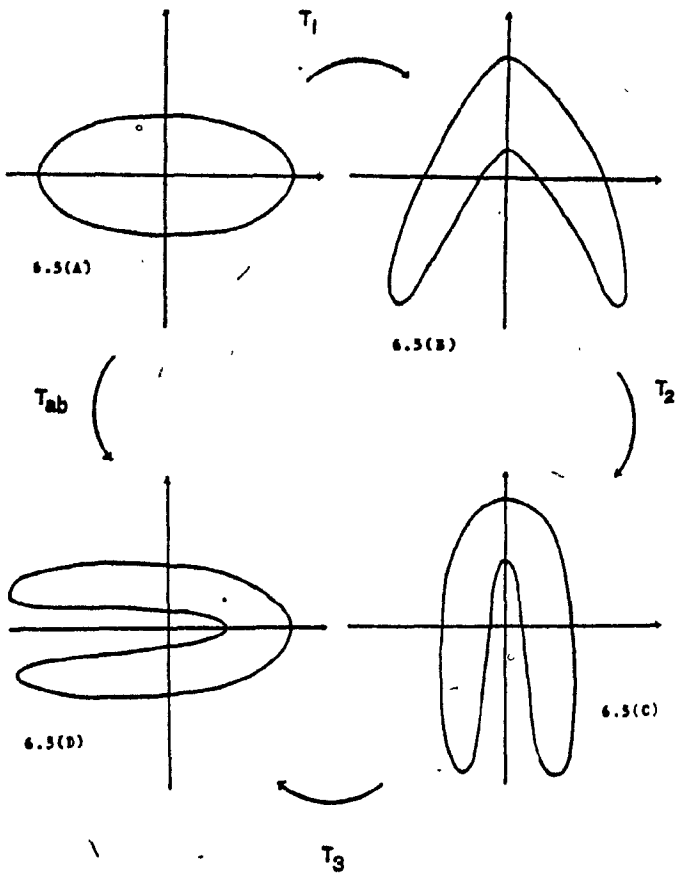

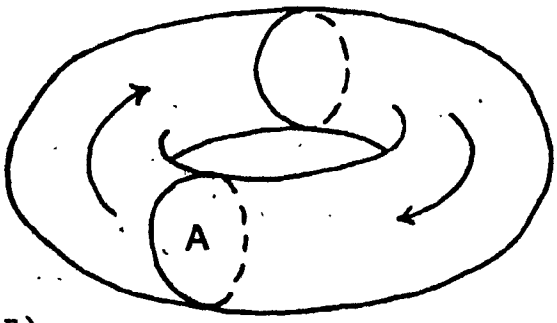

6.5(E)

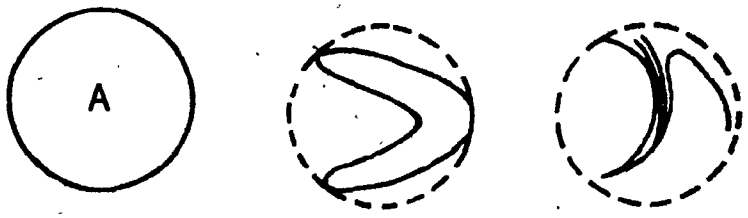

FIGURE 6.5

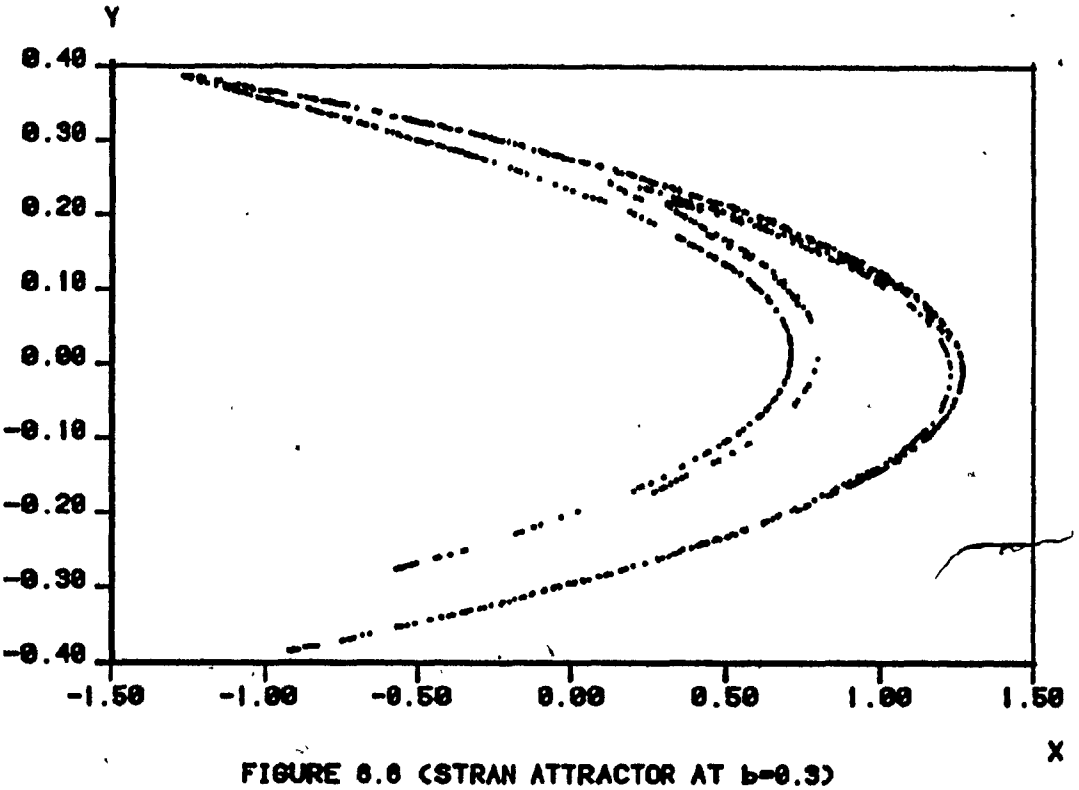

FIGURE 6.6 (STRAN ATTRACTOR AT b=0.3)

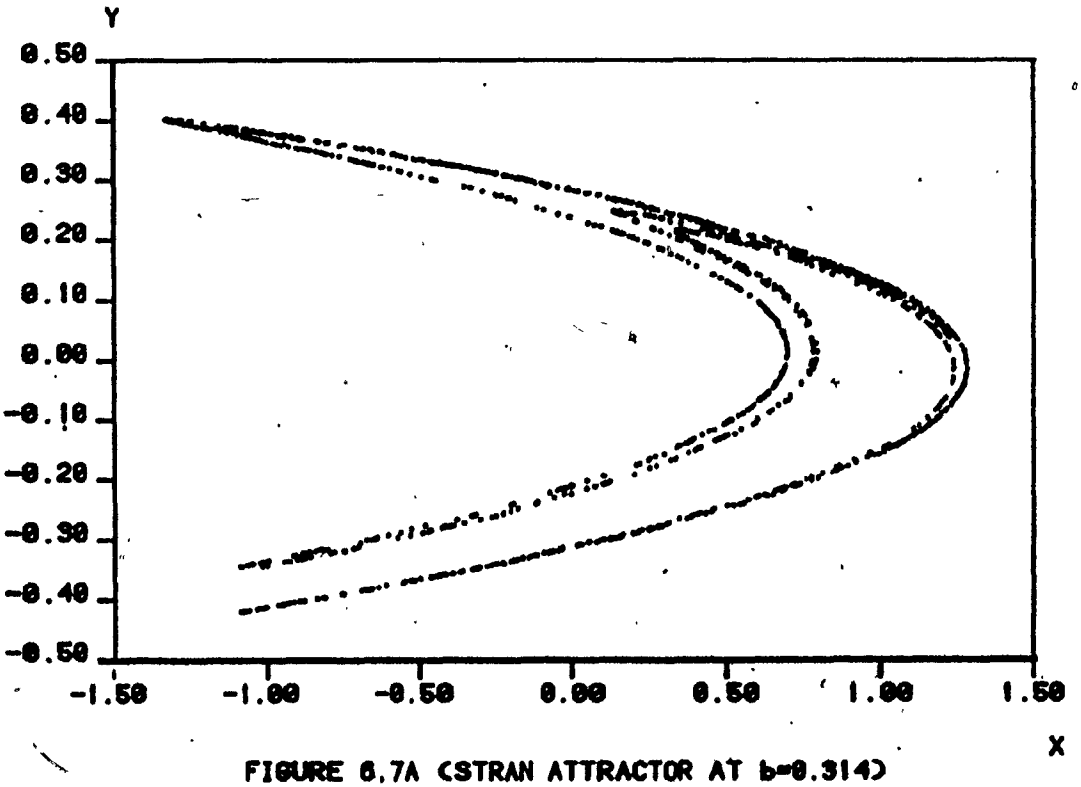

FIGURE 6.7A (STRAN ATTRACTOR AT b=0.314)

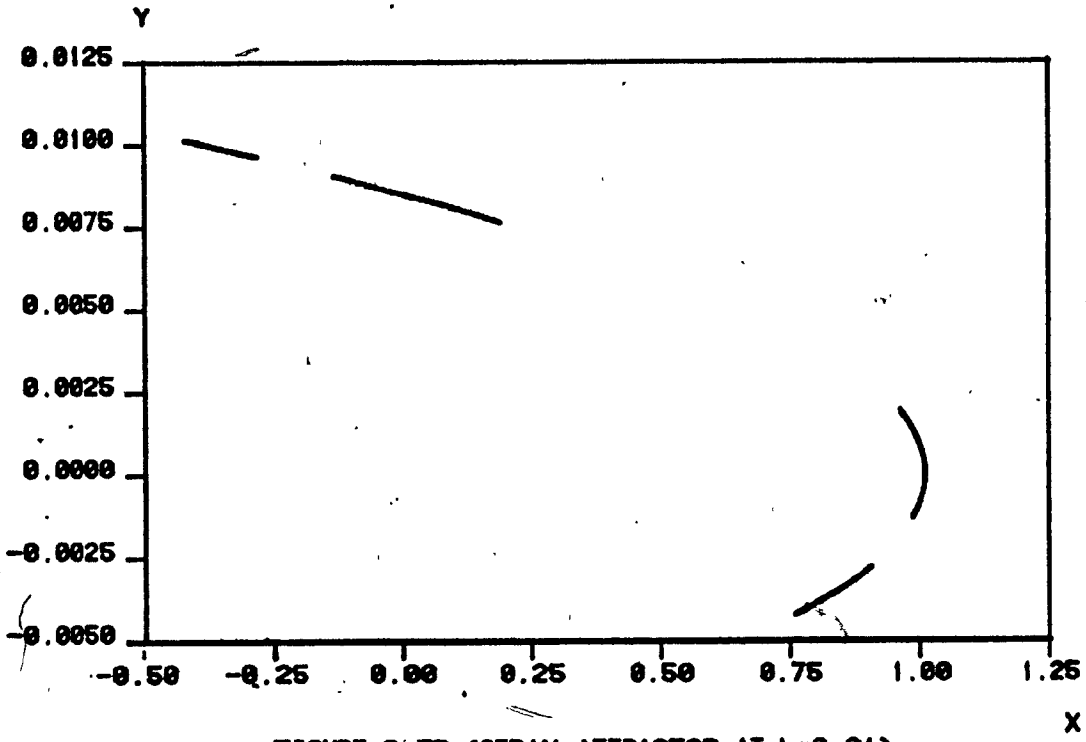

FIGURE 6.7B (STRAN ATTRACTOR AT b=0.01)

a one dimensional manifold by a Cantor set. This matches the observation we have on the Lorenz system. See Figure 6.6 for a diagram which contains the 1000-2500 iterates of the point (0.5,0.2). This attractor only exists in a small parameter range of b. For b>0.3, the attractor expands slightly and at b=0.314, part of the iterates of (0.5,0.2) escape to infinity. When b>0.315, iterates diverages very quickly. For b<0.3, the attractor contracts gradually to four parts when b is close to zero. See Figure 6.7 for the attractor at other parameter values. The layered structure of this strange attractor arises naturally from the folding nature of map T_{ab}. A simple explanation on the mechanism that lead to the existence of a similar layered strange attractor was given by O.E.Lanford in 1981 [27]. A pictorial form of the explanation is given in Figure 6.5e.

In Figure 6.5e, suppose the flow of a differential equation occurs in a toroidal region. If a return map takes a cross section A which transverse to the flow to a folded region, then a complex layered structure will be resulted from four iterations of such a Poincare map.

From (6.6) we know that with b>0, none of the eigenvalues given by (6.7) can be complex. Therefore no Hopf bifurcation can possibly occur when b>0. If we relax the original restriction on the parameter b a little, fixing a=1.4, DSYS located one Hopf bifurcation at b=-1. The

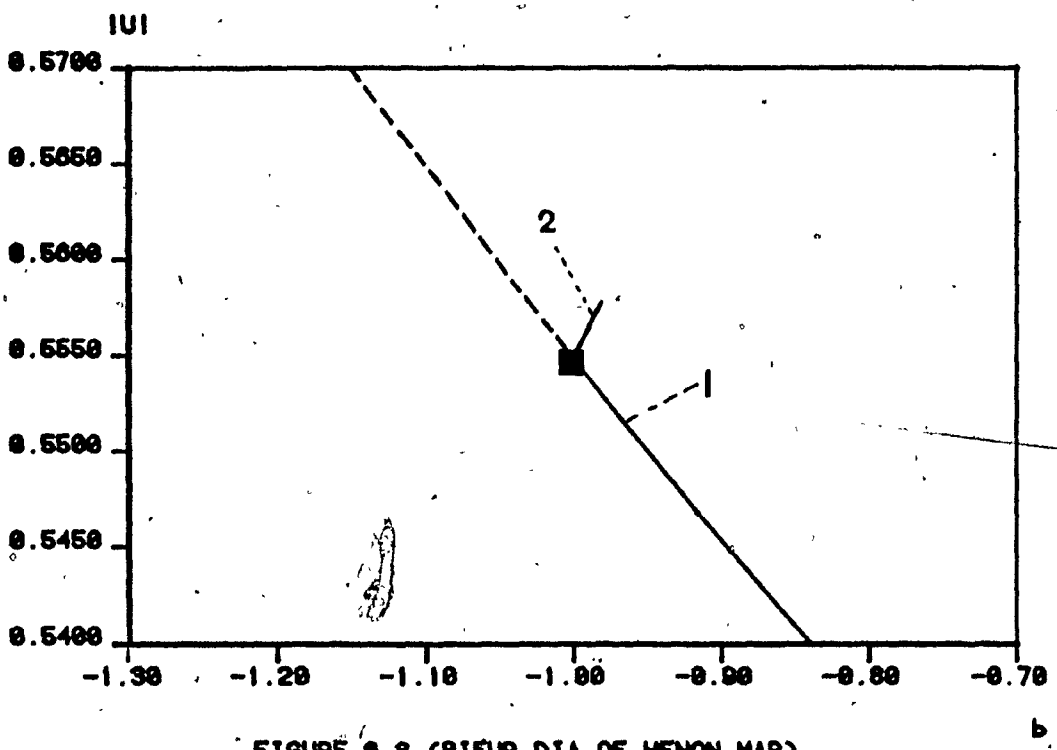

FIGURE 6.8 (BIFUR DIA OF HENON MAP)

corresponding bifurcation diagram is shown in Figure 6.8.

Starting with b=0 and the fixed point (x_1,y_1), a branch of fixed points named branch 1 is traced. In the parameter range $-0.302<b\leq 0$, branch 1 is unstable with one of the eigenvalues lies outside of the unit circle. At b=-0.302, the outside eigenvalue enters the unit circle through negative one and branch 1 becomes stable. Branch 1 remains stable until a Hopf bifurcation is detected at b=-1. At b=-1, the two eigenvalues become complex conjugates and go out of the unit circle. A family of invariant circles developes. Using DSYS, the bifurcating invariant circles

are traced and the results are shown in Figure 6.9.

From the numerical results given by DSYS, we observed that the branch of invariant circles is actually vertical to the fixed point branch 1. In other words, a whole family of invariant circles coexist at b=-1. Also the circles on the branch become twisted as soon as the continuation direction of the branch changes from being vertical to the fixed point branch 1. In order to confirm the result given by DSYS, we iterate the map (6.2) using different starting points and different values of parameter b. By fixing b=-1 and using different starting points we obtain Figure 6.10. The starting points used are indicated in the diagram. While testing the iterations using different starting points, we observed that no invariant circles seem to exist outside the circle labelled (0.45,-0.45) in Figure 6.10. The iterates of any starting points outside this region go to infinity very quickly.

Interesting dynamical behaviour is observed when the map is slightly perturbed from b=-1. Diagrams in Figure 6.11 to Figure 6.15 contain the 1000-2500 iterates of the point (0.4,-0.4) with different values of b. When b>-1, the fixed point (x_1,y_1) is asymptotically stable (both eigenvalues are inside the unit circle), and the local dynamics of map (6.2) is dominated by it. As b increases away from -1, the rate of convergence to (x_1,y_1) increases. The iterates in Figure 6.11 and Figure 6.12 are converging slowly to the

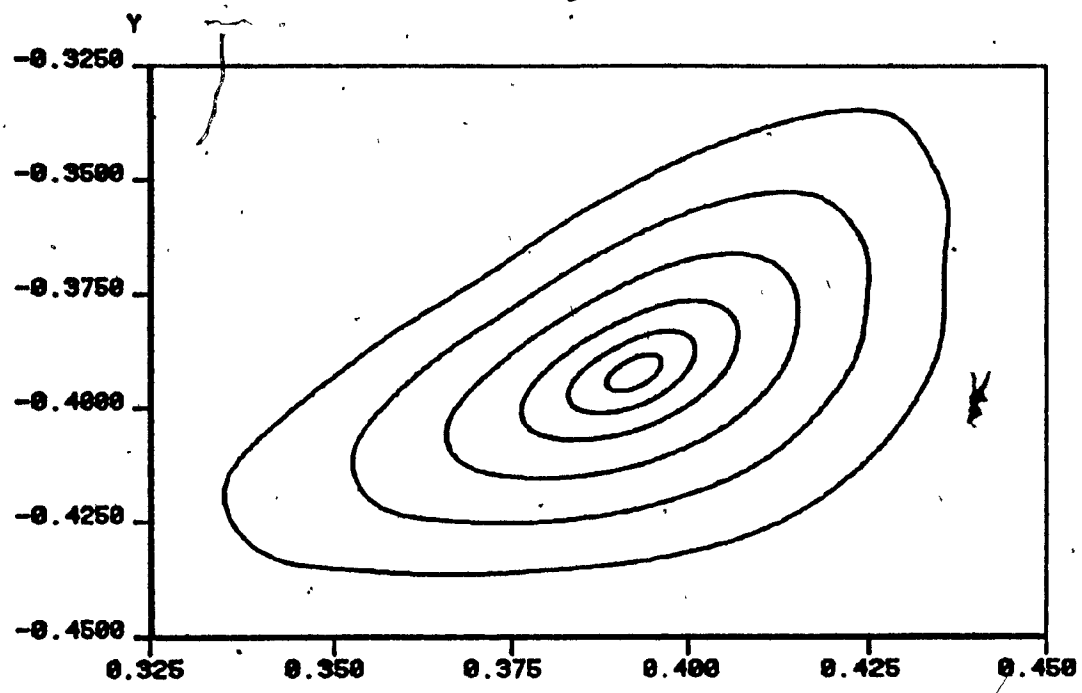

FIGURE 6.9 (INV CIR OF HENON MAP)

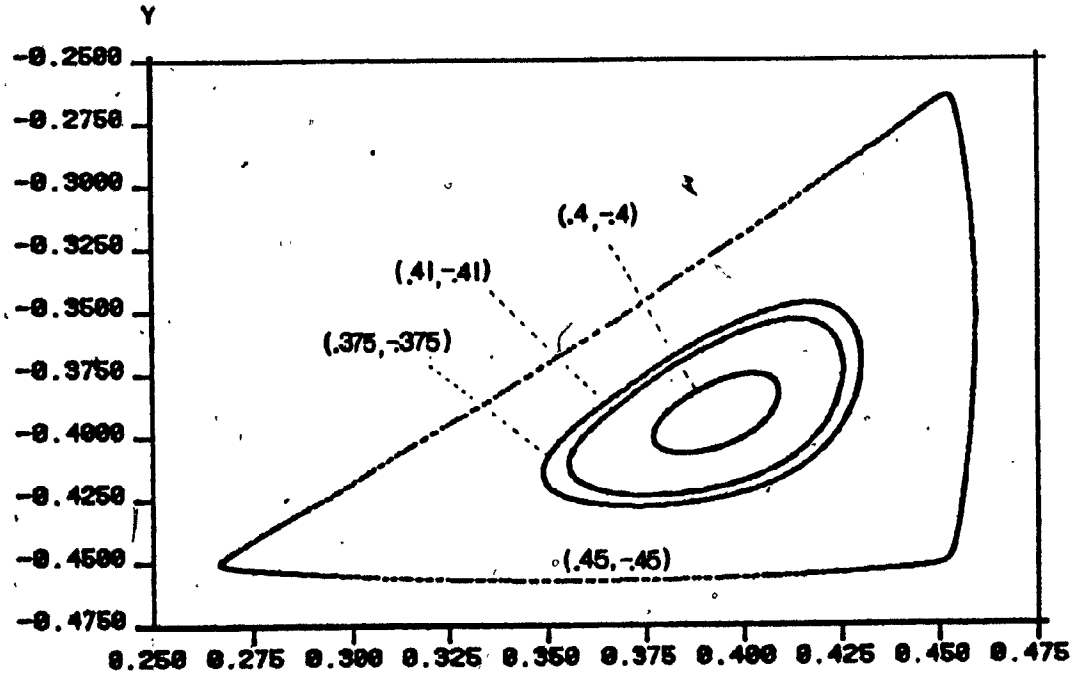

FIGURE 6.10 (INV CIR AT b=-1)

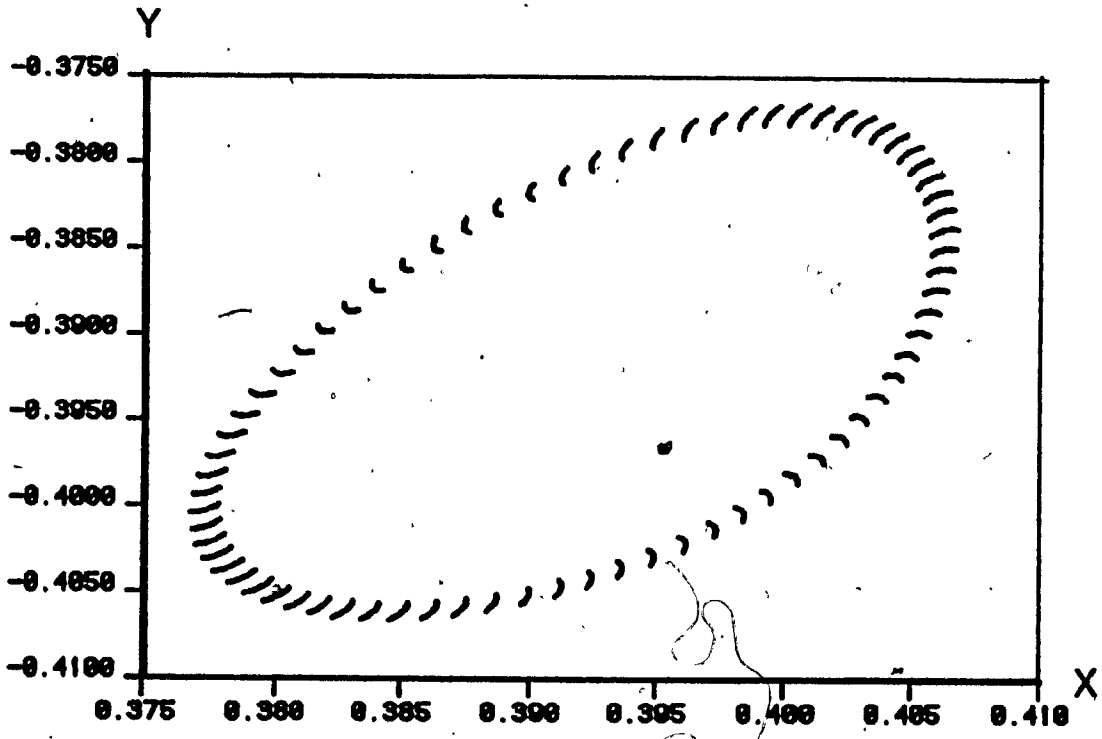

FIGURE 6.11 (b = -0.9999)

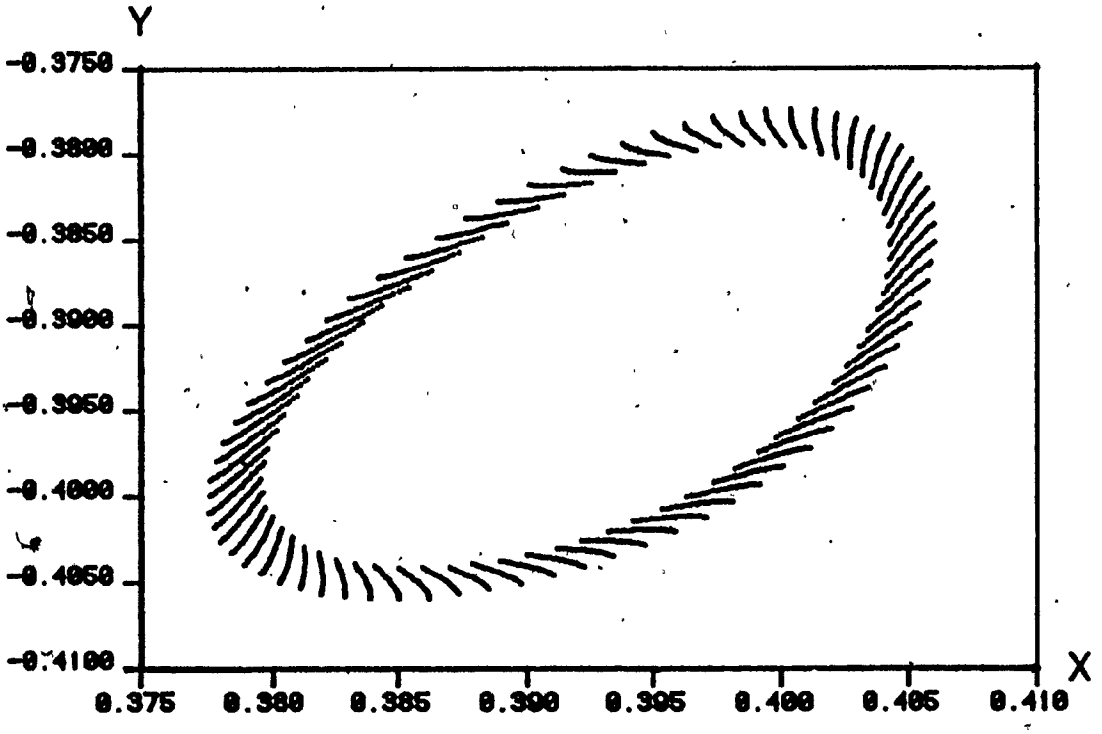

FIGURE 6.12 (b = -0.9998)

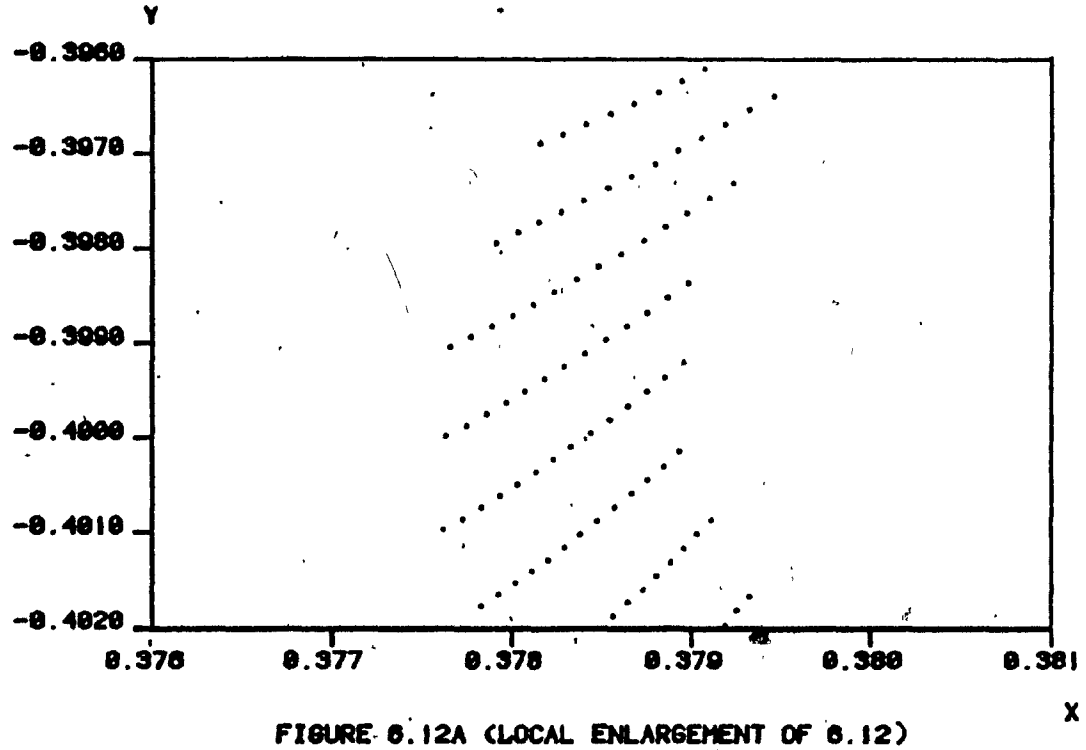

FIGURE 6.12A (LOCAL ENLARGEMENT OF 6.12)

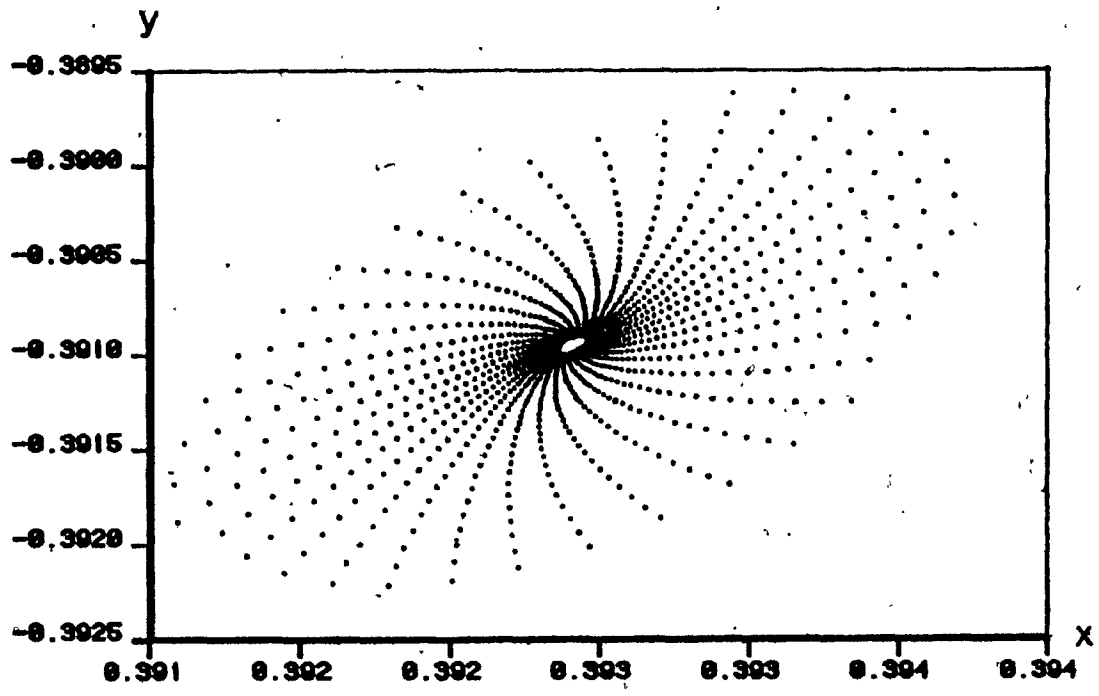

FIGURE 6.13 ($b = -0.995$)

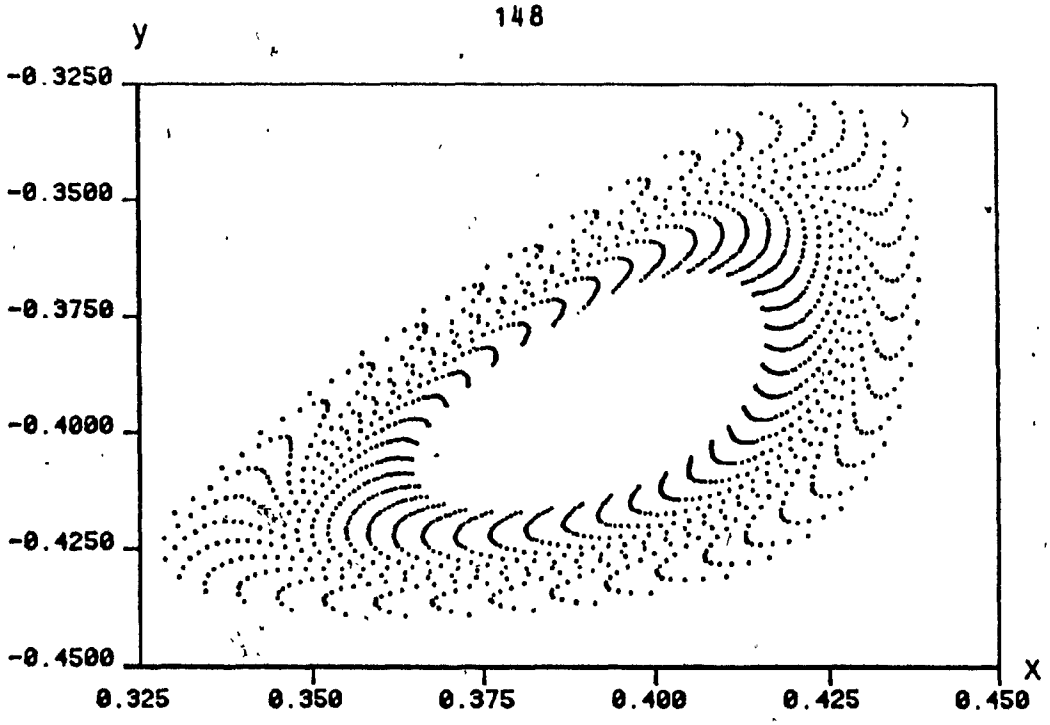

FIGURE 6.14 (b =-1.001)

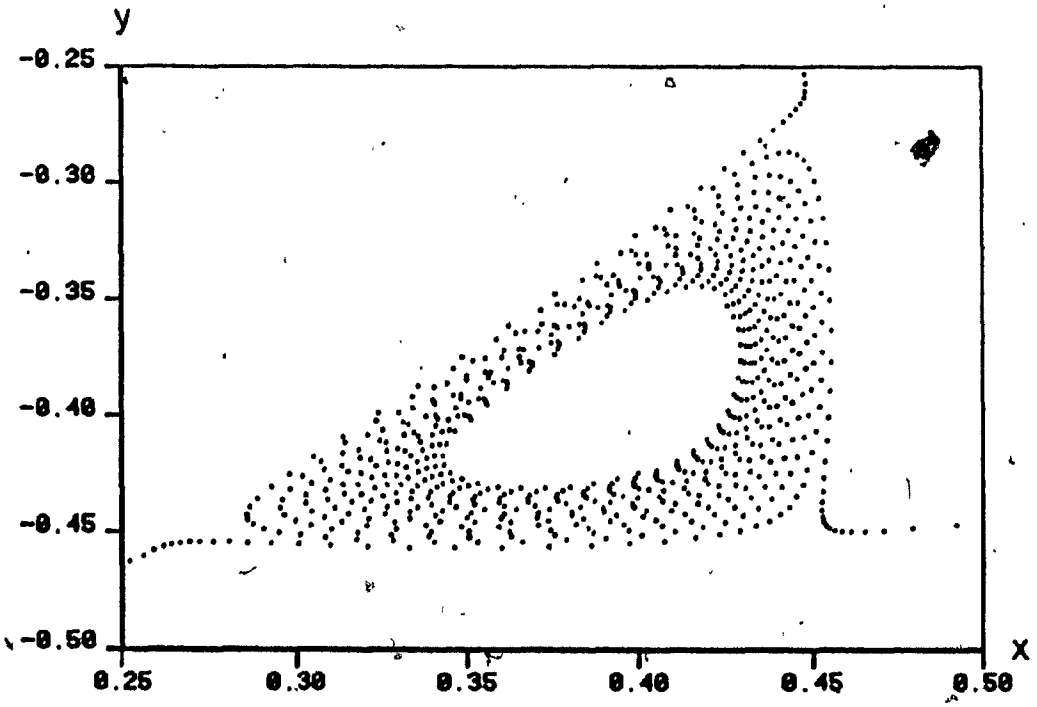

FIGURE 6.15 (b = -1.002)

stable fixed point. In Figure 6.13 the convergence is clearly seen. When $b<-1$, the fixed point (x_1,y_1) is unstable, and the iterates of map (6.2) are repelled from it. In this case, the rate of divergence increases as b decreases from -1. The diverging iterates form a beautiful pattern in the xy-plane as can be seen in Figure 6.14, 6.15.

6.3 Conclusion

In this thesis, we have reviewed the steady state bifurcation, Hopf bifurcation, period doubling bifurcation and bifurcation to invariant tori of a dynamical system. The three 3-dimensional systems discussed in Chapter 2 are examples showing how these bifurcation behaviours can occur and lead to a state of chaos. For the well known Lorenz system, six periodic solution branches including three period doubling bifurcation branches are traced. Some of these periodic solution branches lead to the location of several unstable periodic solutions inside the Lorenz attractor. Due to the unstable character of the solutions and many unstable solutions are being close together in the attracting region, these unstable periodic solutions in the Lorenz attractor would be very difficult to find using the generally adopted initial value technique. For the system arising from biochemistry, multiple cascading sequences of period doubling bifurcations are found. This implies many parameter regions that correspond to chaotic states of the system can exist in 3-dimensional systems. A strange attractor is also found in this system. From the numerical results obtained in the Lorenz system and the system from biochemistry, we observed that the existence of strange attractor often comes with many closely packed unstable periodic solutions in the attracting region. When a trajectory enters the attracting region, it is "push around"

by the unstable solutions and causes complicated dynamical behaviours. This observation may explain the mechanism that creates strange attractors.

Bifurcation behaviour of a periodic solution is an interesting topic in the theory of dynamical systems. Beside period doubling bifurcation, another bifurcation which can occur is the bifurcation to invariant tori. Through the idea of a Poincaré map and the center manifold theorem, the study of bifurcation to invariant tori of a dynamical system can essentially be reduced to the study of bifurcation to invariant circles of a two dimensional diffeomorphism. The relationship between bifurcation to invariant tori and bifurcation to invariant circles is described in Chapter 3. However, given a dynamical system, obtaining an explicit expression of a corresponding Poincaré map is generally recongized as an impossible task. A generally used method for computing the invariant circles is direct iteration of the map. This method is very easy to use but it fails when the invariant circles are repelling. Also direct iteration of the map cannot give a global bifurcation diagram of the system. For example, in the Hénon map, the bifurcating direction of the invariant circles is vertical to the original fixed point branch. Invariant circles fail to exist for parameter values in any neighbourhood of the Hopf bifurcation point. This phenomenon is not easily observed by directly iterating the

Hénon map.

In this thesis, we introduce a numerical method to compute the invariant circles of a general two dimensional diffeomorphism. The design objective of the computation scheme is two fold. Firstly, the computation scheme should work both for attracting and repelling invariant circles. Secondly, the computation scheme should be able to trace out fixed point branches of a general two dimensional diffeomorphism, detect Hopf bifurcations and automatically trace out the invariant circles. In other words, minimal requirement of user effort in the computation is important.

With the above stated objectives, two methods of computing the invariant circles are proposed in Chapter 4 and Chapter 5 respectively. A method involving the concept of a rotation number is described in Chapter 4. An alternate method is discussed in Chapter 5. These two methods have been implemented and tested in a computer program DSYS. The basic capabilities of DSYS are stated in Chapter 6. Numerical results obtained using DSYS indicated that the methods we propose are very efficient and accurate near the bifurcation point. However, once the topological type of the invariant circles start changing, the computation is not reliable anymore. In DSYS, an invariant circle is represented by a truncated Fourier series. However, using a truncated Fourier series representation, the corrsponding system has a full Jacobian matrix. Solving

a full matrix system is an operation of $O(n^3)$ and is rather expensive in terms of computer time. In Chapter 4, a possibly more efficient representation scheme for the invariant circles is also discussed. It is the cubic B-splines representation. These computation schemes can serve as a foundation for computing invariant tori of three dimensional differential equations.

For 2-dimensional diffeomorphisms, bifurcation to invariant circles from a fixed point is only one of the many types of dynamical behaviours that have been observed [14]. Other kinds of dynamical behaviours, say period doubling bifurcations, remain to be explored. Due to the fact that the dynamical behaviour of a dynamical system can be very complicated, numerical techniques are bounded to be necessary.

REFERENCES

[1]. Aronson, D.G., Chory, M.A., Hall, G.R. and McGehee, R.P., Bifurcations from an Invariant Circle for two parameter families of maps of the plane: a computer-assisted study, Comm. Math. Phys., 83, 1982, 303-354.

[2]. Aronson, D., Doedel, E.J. And Othmer, H.G., An Analytical and Numerical study of the Bifurcations in a canonical system of Coupled Oscillators, preprint, 1982.

[3]. Carr, J., Applications of Centre Manifold Theory, Springer Verlag, Appl. Math. Sc., 35, 1981.

[4]. Chillingworth, D.R.J., Differential topology with a view to applications, Pitman, 1976.

[5]. Coullet, P., Tresser, C. and Arneodo, A., Transition to stochasticity for a class of forced oscillators, Phys. Lett., 72A, no.4,5, 1979, 268-270.

[6]. Decroly, O. and Goldbeter, A., Birhythmicity, Chaos, and other patterns of temporal self-organization in a multiply regulated Biochemical system, Proc. Nat. Acad. Sci. USA, in press, 1982.

[7]. Doedel, E.J., AUTO: A program for the automatic bifurcation analysis of autonomous systems, Cong. Num., 30, 1981, 265-284.

[8]. Doedel, E.J. And Heinemann, R.F., Numerical computation of periodic solution branches and oscillatory dynamics of the stirred tank reactor with A-->B-->C reactions, MRC report 2353, Mathematics Research Center, University of Wisconsin, Madison, 1982.

[9]. Doedel, E.J., Jepson, A.D. and Keller, H.B., Branches of periodic solutions and their numerical computation, manuscript.

[10]. Doedel, E.J. and Leung, P.C., A numerical technique for bifurcation problems in delay differential equations, Cong. Num., 34, 1982, 225-237.

[11]. Dongarra, J.J., LINPACK: users' guide, Society for Industrial and Applied Math., 1979.

[12]. Feigenbaum, M.J., Quantitative universality for a class of nonlinear transformations, J. Stat. Phys., 19, 1978, 25-52, 21, 1979, 669-706.

[13]. Guckenheimer, J., Oster, G. and Ipaktchi, A., The dynamics of Density Dependent Population Models, J. Of Math. Biol., 4, 1977, 101-147.

[14]. Gumowski, I. and Mira, C., Recurrences and Discrete Dynamic Systems, Lecture Notes in Math., Springer-Verlag Berlin-Heidelberg, 809, 1980.

[15]. Henon, m., A two dimensional mapping with a Sstrange Attractor, Comm. Math. Phys., 50, 1976, 69-77.

[16]. Henon, M. And Pomeau, Y., Two strange attractors with a simple structure, Turbulence and Navier Stokes Equation, Lecture Notes in Math., Springer-Verlag, Berlin-Heidelberg-New York, 565, 1976, 30-68.

[17]. Hirsh, M,W. and Smale, S., Differential equations, Dynamical systems, and Linear algebra, Academic Press, 1974.

[18]. Hopf, E., Abzweigung einer Periodischen Losung eines Differentialsystems, Berichte der Mathematisch Physikalischen Klasse der Sachsischen Akademie der Wissenschaften zu Leipzig XCIV, 1942.

[19]. Iooss, G., Bifurcation of maps and applications, Math. Studies, North-Holland, 36, 1979.

[20]. Iooss, G., Arneodo, A., Coullet, P. and Tresser, C., Simple computation of bifurcating invariant circles for mappings, Lecture Notes in Math., Springer-Verlag, Berlin-Heidelberg-New York, 898, 1981.

[21]. Iooss, G. and Joseph, D.D., Elementary stability and bifurcation theory, Springer-Verlag, 1980.

[22]. Jepson, A.D., Numerical Hopf bifurcation, Thesis, part II, calif. Inst. of Tech., 1981.

[23]. Keller, H.B., Numerical solution of bifurcation and nonlinear eigenvalue problems, in: Applications of bifurcation theory, Ed. By P.H.Rabinowitz, Academic Press, 1977, 359-384.

[24]. Lorenz, E.N., Deterministic nonperiodic flow, J. Atmos. Sci, 20, 1963, 130-141.

[25]. Lorenz, E.N., On the prevalance of aperiodicity in simple systems, Global Analysis, Lecture Notes in Math., Springer-Verlag, Berlin-Heidelberg, 755, 1979, 53-75.

[26]. Lanford, O.E., Bifurcation of periodic solutions into invariant tori: the work of Ruelle and Takens, Lercture Notes in Math., Springer-Verlag Berlin-Heidelberg, 322, 1973, 159-192.

[27]. Lanford, O.E., Stranger attractors and turbulence, Hydrodynamic Instabilities and the Transition to Turbulence, Ed. By H.L. Swinney and J.P. Gollub, Springer-Verlag Berlin-Heidelburg, 1981.

[28]. Laudau, L.D. and Lifschitz, E.M., Fluid mechanics, Pergamon, Oxford, 1959.

[29]. Marsden, J.E. and McCracken, M., The Hopf Bifurcation and its applications, Springer-Verlag, New York, 1976.

[30]. May, R.M., Simple mathematical models with very complicated dynamics, Nature, 261, 1976, 459-467.

[31]. Nitecki, Z., Differentiable dynamics, an introduction to the orbit structure of diffeomorphisms, MIT Press, 1971.

[32]. Rossler, O.E., Horseshoe-map chaos in the Lorenz equation, Phys. Lett., 60A, no.5, 1977, 392-394.

[33]. Ruelle, D. and Takens, F., On the nature of turbulence, Comm. Math. Phys., 20, 1971, 167-192.

[34] Shimizu, T. and Morioka, N., Chaos and Limit cycles in the Lorenz model, Phys. Lett., 66A, no.3, 1978, 182-184.

[35] Sparrow, C., The Lorenz Equation: Bifurcations, chaos and strange attractors, Springer-Verlag, Berlin-Heidelberg-New York, 1982.

[36] Spath, H., Spline algorithms for curves and surfaces, Translated by W.D.Hoskins and H.W.Sager, Utilitas Math. Publ. Inc. Winnipeg, 1974.

[37] Swinney, H.L. and Gollub, J.P., Hydrodynamic instabilities and the transition to turbulence, Springer-Verlag Berlin Heidelberg, 1981.